# INFORMATION TO USERS

This manuscript has been reproduced from the microfilm master. UMI films the text directly from the original or copy submitted. Thus, some thesis and dissertation copies are in typewriter face, while others may be from any type of computer printer.

**The quality of this reproduction is dependent upon the quality of the copy submitted.** Broken or indistinct print, colored or poor quality illustrations and photographs, print bleedthrough, substandard margins, and improper alignment can adversely affect reproduction.

In the unlikely event that the author did not send UMI a complete manuscript and there are missing pages, these will be noted. Also, if unauthorized copyright material had to be removed, a note will indicate the deletion.

Oversize materials (e.g., maps, drawings, charts) are reproduced by sectioning the original, beginning at the upper left-hand corner and continuing from left to right in equal sections with small overlaps.

Photographs included in the original manuscript have been reproduced xerographically in this copy. Higher quality 6" x 9" black and white photographic prints are available for any photographs or illustrations appearing in this copy for an additional charge. Contact UMI directly to order.

Bell & Howell Information and Learning
300 North Zeeb Road, Ann Arbor, MI 48106-1346 USA
800-521-0600

# Zero energy quasiparticle conduction in unconventional superconductors

May Chiao

Department of Physics

McGill University

May 1999

A thesis submitted to the Faculty of Graduate Studies and Research in partial fulfillment of the requirements of the degree of Doctor of Philosophy.

# Acknowledgments

Although my lone name appears on the titlepage, I cannot honestly claim all the credit for this work, as I have benefitted tremendously from others over the years. I feel very fortunate to have worked with Prof. Louis Taillefer, who has not only provided guidance throughout my PhD work but opportunities for my future.

Initiated into lab life by Brett Ellman and Benoit Lussier, it was a great learning experience to work between such bipolar attitudes towards research. Also, I owe a lot to Robert Gagnon, whose sample growth and characterization has shaved years from my thesis. ATTENTION. Without Christian Lupien, both friend and fellow fridge technician, everything would have been infinitely more difficult. Furthermore, things would not be running so smoothly had it not been for the timely arrival of Rob Hill. I am also grateful for help from Stéphane, Bojana, Patrik and Etienne.

I consider as our extended group that of Prof. Peter Grütter, for there has been a constant—mostly uni-directional—flow of equipment and other gadgets between our labs. Moreover, I have really enjoyed all the discussions with Prof. Grütter, as well as with other professors in the department. I do apologize for the excessive noise escaping from room 437!

During my years at McGill, I have received a tremendous amount of help from the technicians. I am very grateful to Steve Kecani for putting up with my haunting of the shop. Moreover, lots of help came from Michel Champagne, the "Dutch boys" and Frank van Gils. The support staff has been indispensible, in particular Paula Domingues, Lynda Corkum and Joanne Longo.

Now what is physics without collaborations? Considering my own fruitless battle with our evolving crystal growth facility, it was extremely helpful to have received single crystals of $UPd_2Al_3$ from Prof. Noriaki Sato. Furthermore, several theoreticians have taken an active interest in this work, and I would like to thank Profs. Peter Hirschfeld and Patrick Lee for our many discussions. Useful exchanges with the UBC group, in particular Profs. Doug Bonn and Walter Hardy, and meetings with Profs. John Berlinsky and Catherine Kallin at McMaster are also gratefully acknowledged. Also, I thank Dr. Kamran Behnia for his suggestions and encouragement, plus all his philosophical musings. I have pestered several colleagues of my own generation, such as Bill Atkinson, Ahmad Hosseini, Chris O'Donovan, Jeff Sonier and Ilya Vekhter. Here I would like to express my gratitude for the Canadian Institute for Advanced

Research, which is responsible for initiating me into the strong network of superconductivity researchers from across Canada and around the world. I am also grateful for the warm welcome I received from my temporary homes, the Department of Physics at the University of Toronto and le Centre de Recherches sur les Très Basses Températures, Grenoble, France, especially the latter for providing sanctuary before my "trial" at McGill.

None of this would have been possible without the financial support of

- Department of Physics, McGill University
- Alexander McFee Foundation
- Natural Sciences and Engineering Research Council
- Walter C. Sumner Memorial Foundation
- Carl Reinhardt Foundation.

A million thanks to Christoph Bergemann for sharing his LaTeX genius and for providing so much support, on-line and otherwise. Other LaTeX guidance came from Mikko Karttunen, from whom several templates have leached my way over the years.

Finally, I would like to thank my biggest supporters: family and friends. But for the constant emotional and financial backing of my family and relatives in Vancouver, I might have gone insane—thanks for believing in the family nerd! Local sustenance, especially during Prelim madness, came from Alex, André, Andrea (*cool* Andrea), Bonnie, Christine, Claude, Graham, Jake, Jeremy, Martin, Mikko, Nicolas, Philippe, Rahma, Sean, Tiago, Valérie, Wai... Lastly, to Erica and Kim: long live the physics babes!

To my grandparents, parents and sister.

# Statement of Originality

The work presented in this dissertation has made a noticeable contribution to scientific knowledge. Here is a brief summary of my original research:

- The systematic study of magnetic field effects on quasiparticle transport in an unconventional superconductor provides important information on the superconducting gap. In particular, the low temperature experiments probe the local area around a node in the gap function, and provide a *quantitative* measure of the parameters which dictate quasiparticle properties. Furthermore, the study of the role of impurities in a magnetic field has revealed that universal transport is lost in the presence of a field, and that treatment of Zn impurities in the strong scattering limit is indeed the right one. These results unambiguously verify the population of extended quasiparticle states predicted five years ago. This study was performed at the same time as the development of the $d$-wave theory of quasiparticle transport in a magnetic field, with far-reaching mutual benefits.

- In zero field, I have found that the low temperature anisotropy in the heat conduction of $YBa_2Cu_3O_{7-\delta}$ is smaller than that in charge conduction. This discovery has led to several theories of transport anisotopy between the planes and the chains.

- As for $UPd_2Al_3$, the theory has so far only reached a qualitative level. Still, there is evidence for a residual normal fluid at $T = 0$. Moreover, on the basis of my measurements on single crystals, it is already possible to eliminate several order parameter candidates.

A number of publications are associated with this thesis, which I list below:

- May Chiao, Benoit Lussier, Brett Ellman and Louis Taillefer, *Heat conduction in the heavy fermion superconductor $UPd_2Al_3$*, Physica B **230-232**, 370 (1997).

- May Chiao, R. W. Hill, Christian Lupien, Bojana Popic, Robert Gagnon and Louis Taillefer, *Quasiparticle transport in the vortex state of $YBa_2Cu_3O_{6.9}$*, Phys. Rev. Lett. **82**, 2943 (1999).

- May Chiao, Brett Ellman, Robert Gagnon and Louis Taillefer, *Anisotropy of low temperature heat transport in $YBa_2Cu_3O_{6.9}$*, in preparation.

# Résumé

À basse température, nous avons utilisé la technique de la conductivité thermique pour effectuer une étude de quasiparticules électroniques dans les supraconducteurs non-conventionnels, centrée sur $UPd_2Al_3$ (un fermion lourd) et $YBa_2Cu_3O_{7-\delta}$ (un cuprate à haute température critique). Nous présentons aussi une revue des expériences qui peuvent sonder la densité d'états.

Nous avons réalisé des mesures de l'anisotropie entre les axes $b$ et $c$ d'$UPd_2Al_3$. Pour les deux cas, nous avons l'évidence des quasiparticules résiduelles. En comparant nos résultats à des calculs, on trouve trois candidats possibles pour la symétrie du gap, de symétrie $A_{1g}$, $E_{2u}$ ou $E_{1g}$.

Le paramètre d'ordre de symétrie $d_{x^2-y^2}$ est bien établi pour $YBa_2Cu_3O_{7-\delta}$. Une étude de l'anisotropie entre les axes $a$ et $b$ à basse température démontre un terme de nature électronique, prévue par la théorie, en accord avec les mesures de la longeur de pénétration. Le valeur de l'anisotropie, $1.3\pm0.3$, est plus faible que l'anisotropie dans l'état normal. Ceci indique que la conductivité à basse température est supprimée par la diffusion par des impuretés ou par les effets de localisation.

Nous avons effectué des mesures de conductivité thermique sur des monocristaux d'$YBa_2(Zn_xCu_{1-x})_3O_{7-\delta}$ en fonction d'un champ magnétique. Pour les cas $x = 0$, 0.006 et 0.03, le terme électronique $\kappa_0/T$ augmente avec le champ magnétique, ce qui démontre l'existence d'états étendus de quasiparticules à cause de vortex. En comparant avec l'échantillon pur, l'augmentation de $\kappa_0/T$ en fonction du champ appliqué est supprimée pour les échantillons dopés avec Zn. L'ordre de grandeur de la réduction est en accord avec la théorie. Nos résultats confirment la validité d'une approche "diffusion résonnante par les impuretés". Aussi, notre excellent accord avec les mesures de la chaleur spécifique renforce la théorie de l'effect Doppler dans l'état de vortex.

# Abstract

At low temperature, we have used thermal conductivity as a directional probe of the residual normal fluid in two superconductors. $UPd_2Al_3$ (a heavy fermion) and $YBa_2Cu_3O_{7-\delta}$(a high-$T_c$ cuprate). By extrapolating our measurements to zero temperature, we can shed light on zero energy quasiparticles and the structure of the superconducting gap.

For both superconductors, we review measurements pertaining to the density of states. In the case of the heavy fermion superconductor $UPd_2Al_3$, we have found a finite anisotropy between $b$ axis and $c$ axis heat conduction, which excludes those gap structures with only zeroes along $c$ or in the equatorial plane of a spherical Fermi surface; however, our results are consistent for two line nodes equidistant from the equatorial plane, as in the $A_{1g}$ gap. Comparisons to theory developed for $UPt_3$ show qualitative agreement with two hybrid gaps with strong spin-orbit coupling, of $E_{2u}$ and $E_{1g}$ symmetry.

For $YBa_2Cu_3O_{7-\delta}$, because the gap symmetry has been established as $d_{x^2-y^2}$, we can go much further as regards a quantitative analysis. The anisotropy in the thermal conductivity was measured along both high symmetry directions. A residual $T$-linear term in $\kappa(T)$ was observed in both directions. In the $CuO_2$ planes (**J**||**a**) the magnitude of the residual normal fluid conduction is perfectly consistent with the temperature dependence of the penetration depth, within the theory for a $d$-wave superconductor. The value for J||b is slightly larger, yielding an anisotropy ratio of 1.3±0.3. This is considerably weaker than that observed in the normal state resistivity, pointing to a suppressed heat conduction by quasiparticles in the chains, either due to strong defect scattering or a gapped excitation spectrum.

With the application of an external magnetic field (up to 8 T), we can study the effect of vortices on quasiparticle transport. The residual linear term increases with field, directly reflecting the occupation of extended quasiparticle states. A study for different Zn impurity concentrations reveals a good agreement with recent calculations for a $d$-wave gap. The magnitude of the suppression indicates that Zn impurity scattering needs to be treated in the resonant impurity scattering limit, until now an unverified assumption. Together with specific heat measurements, we obtain a quantitative measure of the gap near the nodes.

# Contents

# List of Figures

# List of Tables

# 1 Introduction

The study of superconductivity involves a collective effort on the part of physicists, chemists and materials engineers alike. The technological stalwarts of superconductivity are Onnes' (1911) discovery of zero electrical resistance in Hg below some critical transition temperature $T_c$ (Fig. 1.1) and Meissner and Ochsenfeld's (1933) observation of complete magnetic field exclusion below some critical magnetic field $H_c$. Then came the type-II superconductors, through which magnetic flux can penetrate by means of flux tubes, from $H_{c1}$ up to an upper critical field $H_{c2}$ above which there is no superconductivity (see Fig. 1.2). Furthermore, the flux tubes each carry a quantum of flux $\Phi_0 = \frac{hc}{2e}$ and are arranged in a lattice predicted by Abrikosov (1957). Within each unit cell of the flux lattice, there is a vortex of supercurrent which concentrates the flux at the centre. Since type-II superconductors can carry high critical currents, several applications were realized after their discovery, such as superconducting magnets which can produce constant fields up to 23 tesla. Another important application is the use of superconducting quantum interference devices (SQUIDs) to measure small changes in magnetic fields ($\sim 10^{-6}\Phi_0$). SQUIDs are actively employed in a number of fields requiring extreme sensitivity, from brain imaging to materials research. Although the search for room temperature superconductivity has somewhat given way to pure scientific interest in a complex problem, higher values of the critical transition temperature $T_c$ remain a tantalizing goal.

Within half a decade of its discovery, there was a coherent understanding of superconductivity thanks to the successful microscopic theory of Bardeen, Cooper and Schrieffer (1957) (BCS) based on electron pairs with zero net momentum (Cooper pairs) which undergo condensation below some critical temperature $T_c$. In the BCS model (a specific form of the more general BCS theory), the attractive interaction between electrons is mediated by phonons: one electron interacts with the lattice and deforms it, so when another electron comes along, it takes advantage of the deformed lattice by adjusting itself and lowering its energy (see figlattice. This leads to a ground state separated from the excited states by an energy gap $\Delta$, where $2\Delta$ is the energy required to break a Cooper pair and create two quasiparticles.

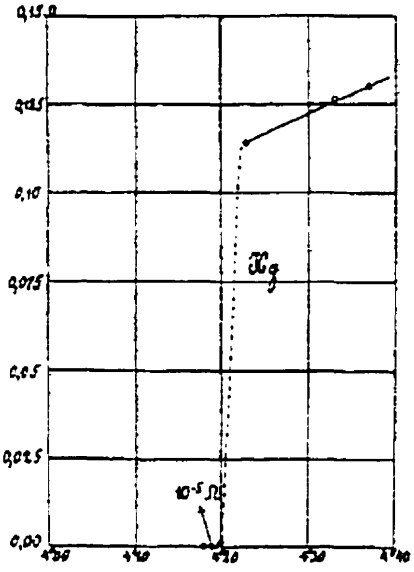

Figure 1.1: Resistivity of Hg as a function of temperature showing the transition to the superconducting state first measured by Onnes (1911).

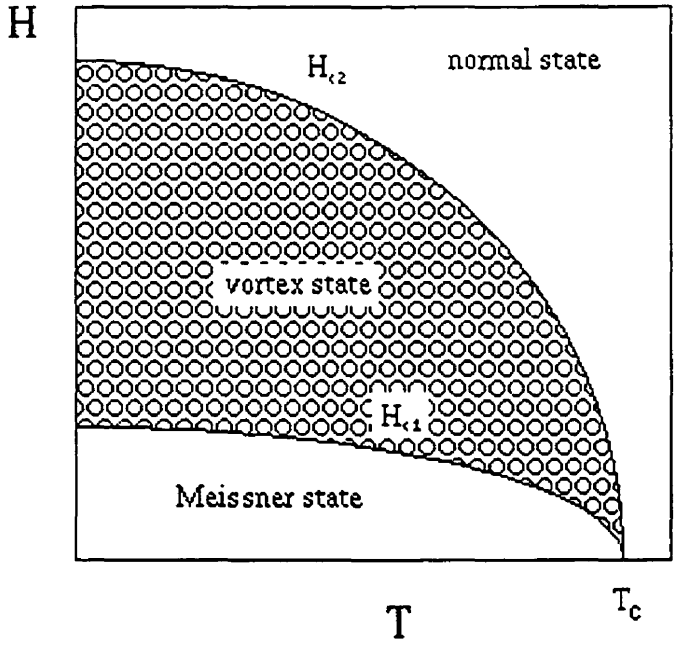


Figure 1.2: Magnetic field phase diagram showing the Meissner state in which there exists flux expulsion, the vortex state in which flux can penetrate through flux tubes and the normal state in which magnetic flux can fully penetrate.

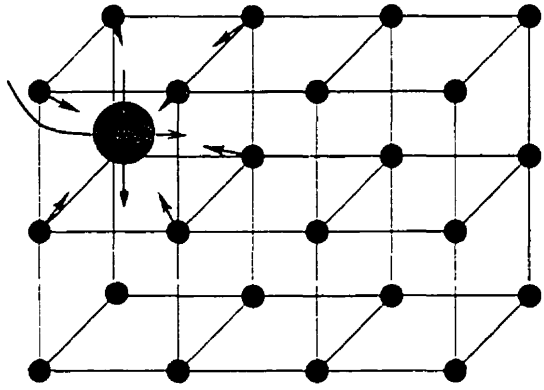

**Figure 1.3:** A cartoon of the e-ph interaction via the lattice that leads to the formation of a Cooper pair.

A more phenomenological approach, the earlier theory of Ginzburg and Landau (1950), was found to be a limiting case of BCS near $T_c$ by Gor'kov (1959). This macroscopic theory was more suitable for problems involving spatial inhomogeneities. For a time it seemed as though superconductivity were well understood, until the discovery of $CeCu_2Si_2$, a heavy fermion superconductor (Steglich *et al.* 1979). Normally, magnetic ions with $f$ electrons act as pair breakers and hence destroy superconductivity. However, in this case, the itinerant $f$ electrons are responsible for a linear specific heat term orders of magnitude larger than in other metals, implying carriers of enormous mass $\sim 1000\, m_e$.

Heavy fermions are particularly intriguing owing to their proximity to magnetic instabilities. Superconductivity also exists in $UBe_{13}$, $UPt_3$, $URu_2Si_2$, $UNi_2Al_3$ and $UPd_2Al_3$, whose normal states can all be described by Fermi liquid theory. However, other heavy fermions have been discovered which challenge our understanding of metals. $CeIn_3$, $CePd_2Si_2$ and $CeNi_2Ge_2$ are all superconductors, although the first two only undergo a superconducting transition under pressure. By tuning the magnetic interactions with pressure, it is possible to suppress the antiferromagnetic transition (or Néel) temperature $T_N$ to 0 K, at which point a quantum critical transition occurs and superconductivity can exist (Julian *et al.* 1998, Mathur *et al.* 1998, Grosche *et al.* 1998). At this critical pressure, the temperature dependence of both resistivity and specific heat display non-Fermi liquid characteristics, namely $\rho$ is closer to linear than quadratic and $c$ is logarithmically divergent rather than linear. These fascinating metals will continue to play a major role in research in the years to come.

That superconductivity is magnetically mediated is highly suggestive, and in

| Compound | maximum $T_c$ | |
|---|---|---|
| $La_{2-x}Sr_xCuO_4$ | 38 K | |
| $YBa_2Cu_3O_{7-\delta}$ | 92 K | not perfectly tetragonal — oxygen chains in $CuO_{1-\delta}$ layers |
| $Bi_2Sr_2Ca_{n-1}Cu_nO_{2n+4-\delta}$ | 110 K | |
| $Tl_2Ba_2Ca_{n-1}Cu_nO_{2n+4+\delta}$ | 122 K | |
| $HgBa_2Ca_{n-1}Cu_nO_{2n-2+\delta}$ | 133 K | highest $T_c$ known so far — up to 164 K under pressure |
| $Nd_{2-x}Ce_xCuO_{4-\delta}$ | 25 K | *electron* doped cuprate superconductor |

**Table 1.1:** Basic properties of several families of high-$T_c$ cuprate superconductors. In the bismuth, thallium, and mercury compounds, the number $n$ of $CuO_2$ planes per unit cell can take on any value between 1 and 4, where the highest $T_c$ is reached for $n = 3$ in all three cases. The data are from Maple (1998), Waldram (1996, p. 223), and references therein.

fact this may well extend to other strongly correlated systems as well, such as the high temperature superconductors, which exploded onto the field with the discovery of high-temperature oxide superconductors by Bednorz and Müller (1986), which increased the highest known $T_c$ by about 12 K. A year later, the discovery of $YBa_2Cu_3O_{7-\delta}$ (Wu *et al.* 1987, Hikami *et al.* 1987, Zhao *et al.* 1987), with a $T_c$ accessible by liquid nitrogen (77 K) cooling (rather than expensive $^4$He at 4 K), revolutionized the field. The Y (yttrium) can be substituted by other rare earths such as La, Nd, Sm, Eu, Gd, Ho, Er and Lu; carrier concentration can be adjusted by oxygen doping from 6.0 to 7.0, with $YBa_2Cu_3O_{6.0}$ an insulator. Each unit cell of $YBa_2Cu_3O_{7-\delta}$ contains two copper oxide ($CuO_2$) planes stacked along the $c$-axis, with CuO chains running along the $b$-direction (see Fig. 4.1). The superconducting properties are thought to be dominated by the planes, with the chains acting as charge reservoirs to control the carrier density in the planes (Tinkham 1996). Table 1.1 lists some of the other high-$T_c$ materials which are commonly studied.

Currently, the central question in both heavy fermion and high-$T_c$ superconductivity concerns the nature of the superconducting pairing mechanism. There are many parallels, in fact, between these seemingly different materials. Considering that high-$T_c$ research has been extremely intense, and that the order parameter symmetry in the cuprates is believed to be known, the remainder of this introduction will focus

on the high-$T_c$ systems.

So far, we know high-$T_c$ superconductivity involves Cooper pairs since the usual flux quantum $\Phi_0$ is observed (Gough *et al.* 1987), as well as the ac Josephson effect frequency of $\frac{2eV}{h}$ (Esteve *et al.* 1987). During the first few years of investigation, it seemed as if $s$-wave pairing (gap has full symmetry of underlying crystal) could describe high-$T_c$ in addition to conventional (BCS) superconducting properties. However, as higher quality crystals emerged, the evidence for $d$-wave pairing (gap has lower symmetry than underlying crystal) has become more and more compelling. For instance, measurements of the penetration depth $\lambda$, which gives the superfluid density $\rho_s$ via $\lambda^{-2} \propto \rho_s$, show that $\rho_s$ has a linear rather than exponential temperature dependence at low temperature (Hardy *et al.* 1993); such a strong dependence on temperature indicates low energy states consistent with a $d$-wave gap. Further evidence comes from the nuclear magnetic resonance (NMR) relaxation rate $1/T_1$ (Pennington and Slichter 1990). Rather than having an exponential temperature dependence at low temperature, a power law once again prevails. Both of these techniques involve an indirect measurement of the symmetry of the pairing state by measuring the density of states, which can easily be affected by sample quality. Perhaps the strongest evidence to date for $d$-wave comes from measurements of trapped flux in double Josephson junction dc SQUID rings combining $s$- and $d$- wave superconductors (e.g. Pb and YBCO) (Tsuei *et al.* 1994, Mathai *et al.* 1995). These experiments are sensitive to the phases of the superconductors, and the data have been very impressive and will be described in Chapter 4.

In the last few years, the technique of thermal conductivity has risen above its reputation as a rather mundane measurement. Being highly directional, thermal conductivity $\kappa$ is an extremely powerful bulk probe of quasiparticle excitations. At low temperature, heat propagation along the direction of a node gives us a measure of the low energy excitations. In conventional BCS superconductors, a finite excitation gap $\Delta(k)$ exists over the entire Fermi surface so that $\kappa$ goes exponentially to zero below $0.2T_c$ and is therefore not terribly illuminating at low temperature. However, high-$T_c$ (and heavy fermion) superconductors have zeroes in the energy gap so that quasiparticles in the neighbourhood of the nodes are easily excitable. In general, high-$T_c$ superconductors are thought of as stacks of weakly coupled $CuO_2$ planes, so the problem becomes two dimensional (2D). All low temperature transport properties are dominated by the gap zeroes, and we can further simplify the problem if we assume a

linearized gap at each node: the density of states also vanishes linearly at the Fermi surface. The signature of a linear density of states is power law $T$-dependence in charge and heat transport, specific heat, penetration depth and nuclear magnetic relaxation, which is measurably different from the exponential behaviour in pure $s$-wave states.

Impurities slightly alter the picture. An impurity can be thought of as smearing out the node such that more than just a point on the Fermi surface becomes exposed. This gapless region then behaves exactly like a normal fluid and we can use familiar Fermi liquid (Landau 1958) language to describe the local quasiparticle excitations within this region. As for a normal metal, one expects the quasiparticle term in $\kappa$ to be linear. It turns out that adding impurities (up to a certain level) has no effect on low temperature transport. This is a consequence of the *exact* compensation between the loss in mean free path due to the impurities and the gain in the residual normal fluid density. Lee (1993) was the first to propose this *universal* behaviour in quasiparticle charge transport for a $d$-wave superconductor.

Recently, universal heat conduction in $YBa_2Cu_3O_{7-\delta}$ was observed by Taillefer *et al.* (1997). By varying the impurity concentration using Zn doping, they found that the residual linear term $\kappa_0/T$ (the value of $\kappa(T)/T$ as $T \rightarrow 0$) stayed roughly constant despite a 40-fold increase in the scattering rate. Furthermore, the value of $\kappa_0/T$ was in *quantitative* agreement with calculations for a $d$-wave superconductor.

We note that calculations have only been made for a heat current applied along the $a$-axis. Conduction along $b$ can occur through another channel: the CuO chains. For optimally-oxygenated crystals of high purity ($\delta \simeq 0.1$), the anisotropy in electrical resistivity $\rho_a/\rho_b$ can be as high as 2.3 (Gagnon *et al.* 1997). This is similar to the anisotropy in the plasma frequency determined by far infrared reflectance and in the DC conductivity, both quoted as 2.2±0.2 (Basov *et al.* 1995).

Previous attempts to measure the anisotropy of transport in the superconducting state of $YBa_2Cu_3O_{7-\delta}$ have been somewhat inconclusive. The real part of the charge conductivity, $\sigma_1$, estimated from microwave measurements of the surface impedance and of the London penetration depth combined with infrared measurements of the plasma frequency, exhibits an anisotropy of 2.4 in the normal state which decreases to approximately 1.6 as $T \rightarrow 0$ (Zhang *et al.* 1994). The uncertainty is on the order of 50%. Thermal conductivity measurements have also been unsuccessful because they have not been measured at low enough temperature in order to clearly

identify the linear electronic term: in fact, above 200 mK, there is no indication of any *ab* anisotropy (Gold *et al.* 1994, Behnia *et al.* 1995, Wand *et al.* 1996). It is extremely puzzling that the anisotropy in $\kappa$ does not appear to agree with that in other transport measurements. We propose to measure several samples of both *a* and *b* axis crystals to determine the anisotropy, if any, well below 200 K. This would help us understand the role of the chains, and perhaps address the issue of whether superconductivity exists in the chains.

Regardless of this question of anisotropy, measurements of $\kappa_a$ (Taillefer *et al.* 1997) strongly validate current transport theory in a high-$T_c$ system. The observation of universal heat conduction in $YBa_2Cu_3O_{7-\delta}$ has made a very strong impact on the community, spawning several predictions and calculations of properties beyond zero temperature. Since the electronic contribution to $\kappa$ in $YBa_2Cu_3O_{7-\delta}$ is dominated by phonons, finite temperature studies are difficult, if not impossible, to interpret in any reliable sense. Therefore, we use the application of an external magnetic field to probe the quasiparticle states away from zero energy and to further test the *d*-wave theory.

In the presence of a magnetic field, the supercurrent flow around the vortices introduces a Doppler shift to the quasiparticle energy spectrum. Thus certain quasiparticle states fall below the Fermi level and extended quasiparticle states can be populated. In conventional superconductors, the field leads to localization of quasiparticles in the vortex cores which do not contribute to transport. It was shown by Volovik (1993) that extended states increase the *d*-wave density of states as $\sqrt{H}$. Of course the specific heat should reflect this field dependence, but it measures both localized and extended states, and has a huge low temperature upturn due to nuclear moments. Furthermore, measurements of conventional superconductors have also shown a $\sqrt{H}$-dependence for totally different reasons (Sonier *et al.* 1998). Thus thermal conductivity is a more reliable diagnostic tool of extended quasiparticle states in the presence of a magnetic field.

Calculations by Kübert and Hirschfeld (1998b), which ignore vortex scattering, show that the field dependence of the residual linear term in $\kappa$ follows a function which roughly resembles $\sqrt{H}$, but rises less steeply. However, in a magnetic field, $\kappa_0(H)/T$ is *dependent* on the impurity concentration. The expected enhancement of $\kappa$ is in direct opposition to *s*-wave behaviour in a field. In Nb, a conventional superconductor, the thermal conductivity actually *decreases* with applied field be-

cause vortex scattering is important. In a $d$-wave superconductor, impurity scattering dominates vortex scattering at low temperature and field.

In this work, we wish to test the theory, in particular, the *increase* in $\kappa$ with applied field. Moreover, by studying Zn-doped samples, we can observe whether the effect of the increase is actually *suppressed* by impurities, as predicted by the theory. If these effects are observed, together with all the other evidence so far, there would remain very little doubt about $d$-wave pairing in high-$T_c$. We hope to shed light on the nature of scattering, by impurities and by vortices and to obtain a *quantitative* measure of the gap near the nodes. As regards the heavy fermions, we show that we are still in the process of eliminating particular gap structures, and not uniquely identifying the correct ones for various matericals.

This dissertation is organized as follows: Chapter 2 describes the theory of thermal conductivity, covering transport in both zero and finite magnetic fields, comparing metals, conventional and unconventional superconductors; Chapter 3 introduces the normal and superconducting states of the heavy fermion superconductor $UPd_2Al_3$; Chapter 4 discusses general properties of the high-$T_c$ superconductor $YBa_2Cu_3O_{7-\delta}$ including descriptions of several other measurement techniques in the normal, superconducting and vortex states; Chapter 5 covers the experimental details (cryogenics, measurements, analyses); Chapter 6 deals with the thermal conductivity of $UPd_2Al_3$, presenting sample details, results and comparison with theory; Chapter 7 reviews the current status of heat transport in $YBa_2Cu_3O_{7-\delta}$, describes the samples, the anisotropy and the magnetic field dependence; Chapter 8 concludes the dissertation with a brief recapitulation of the main results.

# 2 Thermal Conductivity

Thermal conductivity is a directional probe of the bulk and as such, is ideal for investigating the gap structure of unconventional superconductors. The existence of nodes in the superconducting energy gap allows us to study excitations on very small energy scales in the neighbourhood of these nodes. This means that heat propagates more easily along a nodal direction where there is no gap in the excitation spectrum. Several other techniques, such as microwave conductivity, suffer complications from surface effects since electromagnetic fields can only penetrate as far as the London penetration depth (order 1000 Å). Unfortunately, besides the electronic carriers we wish to study, phonons and magnons can also carry heat, as well as scatter the electrons. Thus a complete interpretation of heat conduction must take into account all the different carriers and their associated scattering mechanisms.

## 2.1 Heat Transport in Zero Magnetic Field

### 2.1.1 Metals

Before tackling superconductors, it is worth while understanding basic heat transport in metals. We start with a simple picture based on a metal rod which is heated at one end, and we consider only the heat which is carried by electrons. Intuitively, we expect the heat to flow toward the cold end, against the temperature gradient. The magnitude of the thermal current density $\mathbf{j}_Q$ is the thermal energy per unit time per unit area perpendicular to the flow. Then Fourier's law, applicable to a small temperature gradient $\nabla T$, gives:

$$\mathbf{j}_Q = -\kappa \nabla T. \tag{2.1}$$

where the positive proportionality constant $\kappa$ is the thermal conductivity, in general a tensor. Following the derivation in Ashcroft and Mermin (1976) using the free

electron model of Drude, the expression for the electronic thermal conductivity is

$$\mathbf{j}_Q = \frac{1}{3}v^2\tau c_v(-\nabla T) \tag{2.2}$$

from which we see that

$$\kappa = \frac{1}{3}v^2\tau c_v = \frac{1}{3}c_v v\ell \tag{2.3}$$

where $v$ is the mean velocity, $\tau$ the relaxation time (mean time between collisions), $c_v$ the specific heat and $\ell$ the mean free path.

For this simple kind of electron gas picture, the thermal and charge conductivities are closely related. To show this, we would like to find a similar expression for charge conductivity. An electric field $\mathbf{E}$ at a point in a metal induces a current density $\mathbf{j}$, so that

$$\mathbf{E} = \rho\mathbf{j} \tag{2.4}$$

where the proportionality constant $\rho$ is the resistivity of the metal. For $n$ electrons per unit volume moving with velocity $\mathbf{v}$, in time $dt$ they travel a distance of $vdt$ parallel to $\mathbf{v}$. The number of electrons passing a cross-sectional area $A$ in time $dt$ is $n(vdt)A$, so that the total charge is $-nevAdt$. Hence the current is $-nevA$, yielding a current density of

$$\mathbf{j} = -ne\mathbf{v}. \tag{2.5}$$

Immediately after a collision, an electron emerges with velocity $\mathbf{v}_0$ plus an additional term $-e\mathbf{E}\tau/m$ due to the electric field. However, since we have assumed that the electron is going in a random direction, $\mathbf{v}_0$ averages to zero, leaving $\mathbf{v}_{avg} = -e\mathbf{E}\tau/m$, or

$$\mathbf{j} = (\frac{ne^2\tau}{m})\mathbf{E}. \tag{2.6}$$

In terms of the conductivity $\sigma = 1/\rho$, we now have

$$\mathbf{j} = \sigma\mathbf{E}; \sigma = \frac{ne^2\tau}{m}, \tag{2.7}$$

a well-known result.

Thus far, we have used a classical treatment of the electrons which works amazingly well for $\sigma$ since it only depends on the kinetic properties of the conduction electrons, which do behave as a gas of non-interacting particles. However, the free electron model gives $c_v = \frac{3}{2}nk_B$, which is not material dependent. To calculate the specific heat of a metal, it is necessary to include the Pauli exclusion principle and use Fermi-Dirac statistics for the density of states. Now we can only have two electrons, of opposite spin, in each energy level up to an energy called the Fermi energy $\varepsilon_F$. Thus in $k$-space, all the ground state electrons lie within the Fermi surface. Excitations out of the ground state will have a velocity $v_F$. Using this model, we get

$$c_v = \frac{\pi^2}{3}k_B^2 N_F T \tag{2.8}$$

where $N_F$ is the DOS at the Fermi surface.

Now we can write down the Sommerfeld value of the Lorenz number, $L_0$, using the Wiedemann-Franz law (WFL) relating heat and charge conductivities. This intimate relationship between that two quantities we later wish to test in the superconducting state. First we must first replace the mean electron velocity $v$ used above with the Fermi velocity $v_F$:

$$\begin{aligned}\frac{\kappa}{\sigma T} &= \frac{\frac{1}{3}v_F^2 \tau c_v}{ne^2\tau/m} \\ &= \frac{\pi^2}{3}\left(\frac{k_B}{e}\right)^2 \\ &= 2.45 \times 10^{-8}\ \mathrm{W\Omega K^{-2}}\end{aligned} \tag{2.9}$$

which is accurate for many metals such as Au, Cd and Pb (Kittel 1986). Departure from the WFL is usually due to e-ph scattering.

So far, we have only covered electronic heat conduction. Phonons also carry heat so they must be taken into consideration. We will concern ourselves with the low temperature characteristics when $T \ll \Theta_D$, where $\Theta_D$ is the Debye temperature within the Debye model of lattice vibrations. The basic assumption of the Debye model is that there is a cut-off frequency to the phonon dispersion $\omega = v_{ph}k$ (we reserve the more common $v_s$ for superflow velocity later on), so modes above some Debye wavevector $k_D$ are not allowed. This makes the density of states easy to

calculate, and the well-known total phonon energy is given by

$$U = 9Nk_BT(\frac{T}{\Theta_D})^3 \int_0^{x_D} dx \frac{x^3}{e^x - 1} \tag{2.10}$$

where $N$ is the number of atoms in the specimen and $x_D = \Theta_D/T$. From this expression, the specific heat (at constant volume) is easily obtained:

$$c_{ph} = 9Nk_BT(\frac{T}{\Theta_D})^3 \int_0^{x_D} dx \frac{x^4 e^x}{(e^x - 1)^2}. \tag{2.11}$$

At very low temperature, $x_D \to \infty$ and the integral in Eq.(2.10) becomes $\frac{\pi^4}{15}$ so that the phonon specific heat becomes

$$c_{ph} = \frac{12}{5}\pi^4 Nk_B(\frac{T}{\Theta_D})^3 \simeq 1944(\frac{T}{\Theta_D})^3 \mathrm{Jmol^{-1}K^{-1}}. \tag{2.12}$$

This expression is usually valid up to at least 10 K in metals, and since we work well below this temperature, we need not worry about higher energy phonon modes.

If we consider the phonons as a gas diffusing through a material, our earlier expression for electrons still holds, and so for phonons, the thermal conductivity is given by

$$\kappa_{ph} = \frac{1}{3} c_{ph} v_{ph} \Lambda_{ph} \propto \lambda_{ph} T^3 \tag{2.13}$$

where now the relevant parameters are the sound velocity $v_{ph}$ and phonon mean free path $\Lambda_{ph}$. This $T^3$ dependence occurs when phonons are limited by a temperature-independent mean free path, such as grain size or sample size.

### 2.1.2 Conventional Superconductors

Before we start talking about unconventional superconductors, we had better define what a conventional superconductor is. In fact, the basic assumptions of the BCS theory are general and have been applied to heavy fermion and high-$T_c$ superconductors as well. At the heart of BCS theory lie the Cooper pairs—pairs of electrons of opposite spin and momentum, k↑ and -k↓. The pairing of the electrons and their condensation to the ground state occur simultaneously at $T_c$, with all pairs going into

a wavefunction of the same phase. [1] As Cox and Maple (1995) put it, "rather than performing a 'tango' in the superconducting state, the electron pairs participate in a 'square dance', exchanging partners on a time scale of order $\tau_c = \hbar/(k_B T_c)$". The coherence length $\xi_0 = v_F \tau_c$ is of order 1000 Å in Al and 15 Å in $YBa_2Cu_3O_{7-\delta}$.

Below $T_c$, all electrons are bound in pairs, in identical two-electron states. Thus there are $\frac{N}{2}$ pair wavefunctions $\phi(rs, r's')$ constructing the total wavefunction $\Psi(r_1 s_1, \ldots, r_N s_N) = \phi(r_1 s_1, r_2 s_2) \cdots \phi(r_{N-1} s_{N-1}, r_N s_N)$. These electron pairs should not be considered as independent particles, for the stability of the state depends on their spatial interlocking. In order for the wavefunction $\Psi$ to obey the Pauli exclusion principle, i.e. $\Psi$ changes sign under exchange of spin and orbital labels, it must be explicitly antisymmetrized. The superconducting gap function $\Delta(k)$ is related to $\Psi(r)$ by a Fourier transform. Thus an isotropic $\Psi(r)$, as in $s$-wave pairing, gives an isotropic gap $\Delta(k)$.

Now the BCS *model* is a specific form of the theory, where the e-e correlation is mediated by phonons and the pair wavefunctions are singlet states $\uparrow\downarrow$. Furthermore, the energy gap is assumed to be isotropic. Without getting into details, we write down the famous BCS ground state wavefunction and then show the results for a weak-coupling superconductor. We begin with the wavefunction:

$$|\Psi\rangle = \prod_{\mathbf{k}} (u_{\mathbf{k}} + v_{\mathbf{k}} c^{\dagger}_{\mathbf{k}\uparrow} c^{\dagger}_{-\mathbf{k}\downarrow})|0\rangle \tag{2.14}$$

where $|u_{\mathbf{k}}|^2 + |v_{\mathbf{k}}|^2 = 1$. The probability of a pair $(\mathbf{k}\uparrow, -\mathbf{k}\downarrow)$ being occupied is $|v_{\mathbf{k}}|^2$, and unoccupied is $|u_{\mathbf{k}}|^2 = 1 - |v_{\mathbf{k}}|^2$. Thus the ground state, whose energy is lowered if the states $(\mathbf{k}\uparrow, -\mathbf{k}\downarrow)$ are both occupied or both unoccupied, is completely characterized by $\{u_{\mathbf{k}}, v_{\mathbf{k}}\}$.

Excitations out of the ground state behave as fermionic quasiparticles with energy $E_{\mathbf{k}} = \sqrt{\varepsilon_{\mathbf{k}}^2 + \Delta_{\mathbf{k}}^2}$, where $\varepsilon_{\mathbf{k}}$ is the kinetic energy above the Fermi energy $\varepsilon_F$ and

$$\Delta_{\mathbf{k}} = -\sum_{\mathbf{k}'} V_{\mathbf{k}\mathbf{k}'} u_{\mathbf{k}'} v_{\mathbf{k}'}. \tag{2.15}$$

[1] The reason all pairs go into the same phase is that the phase $\phi$ and electron number $N_e$ obey an uncertainty relation just like the conjugate variables position and momentum, i.e. $\Delta\phi \Delta N_e \geq 1$. When the system undergoes a superconducting transition which requires that $\Delta\phi$ be small, forcing $\Delta N_e$ to be large, charge conservation is violated in the superconducting state (Tinkham 1996).

where $V_{kk'}$ is the interaction strength. When this term is negative (attractive interaction), it is energetically favourable for pairing to occur, so the BCS model sets

$$V_{\mathbf{k}\mathbf{k}'} = \begin{cases} -V & \text{if } |\varepsilon_{\mathbf{k}}| \text{ and } |\varepsilon_{\mathbf{k}'}| \leq \hbar\omega_c \\ 0 & \text{otherwise} \end{cases} \tag{2.16}$$

where $\hbar\omega_c$ is a cut-off energy. (Similarly, $\Delta_{\mathbf{k}} = \Delta$ is isotropic.) In the weak-coupling limit, $N_0 V \ll 1$, $\Delta \approx 2\hbar\omega_c e^{-1/(N_0 V)}$ where $N_0$ is the DOS at the Fermi level. At $T = 0$, the value of the gap is given by

$$\Delta_0 = 1.764 k_B T_c. \tag{2.17}$$

The presence of a finite gap over the Fermi surface means that for $E < \Delta$, there are no states, or

$$N(E) = \begin{cases} N_0 \frac{E}{\sqrt{E^2 - \Delta^2}} & (\mathrm{E} > \Delta) \\ 0 & (\mathrm{E} < \Delta). \end{cases} \tag{2.18}$$

In Fig. 2.1, we see the effect of the DOS (left) on the specific heat (right). The specific heat jump at $T_c$ is 1.43 times the size of the normal state specific heat at $T_c$. $c(T)$ exhibits activated low temperature behaviour, as $e^{-\Delta/(k_B T)}$. Since $\kappa \sim \int dE\, N(E)\tau(E)$, it also dies exponentially at temperatures much below $T_c$. As $T \to 0$, the scattering time diverges since there are fewer and fewer states into which to scatter, but since the DOS is zero, $\kappa$ goes to zero.

The theory of Bardeen, Rickayzen and Tewordt (1959) describing thermal conductivity in conventional superconductors, based on the BCS model, very well describes the interplay of electrons and phonons. We show in Fig. 2.2 aluminum data which closely follow the calculation of Bardeen, Rickayzen and Tewordt (1959), demonstrating the success of BCS theory. Since these superconductors are generally metals, the electronic contribution to $\kappa$ dominates near $T_c$. By about $0.2T_c$ or $0.3T_c$ the phonon contribution dominates. Such are the qualitative features of a two-fluid model, in which the normal electrons carry heat and scatter phonons but whose numbers decrease exponentially with temperature (in the superconducting state). With the reduction of normal electrons comes the growth in $\kappa_{ph}$. For high quality samples, phonons are mainly limited by electron scattering (at higher temperature)

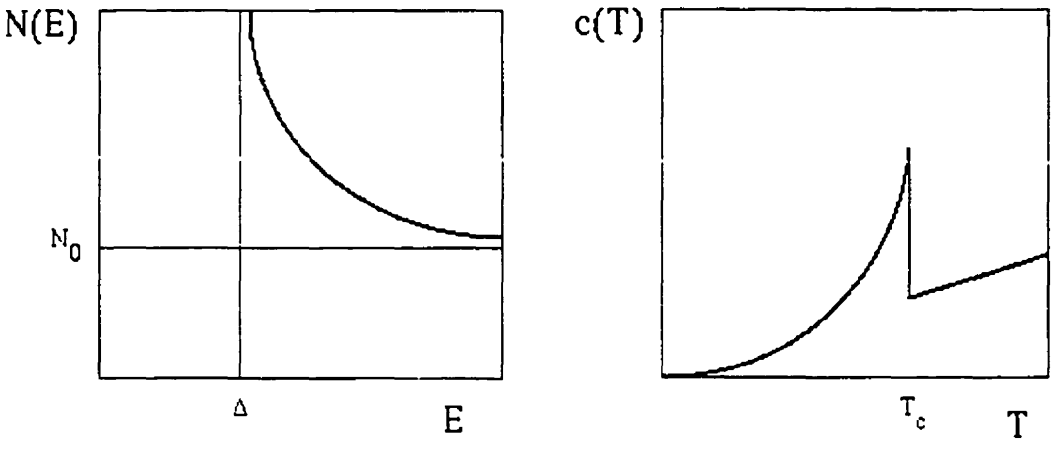


**Figure 2.1:** Density of states (left) and specific heat (right) of a classic BCS superconductor. The presence of the gap leads to activated specific heat at low temperature.

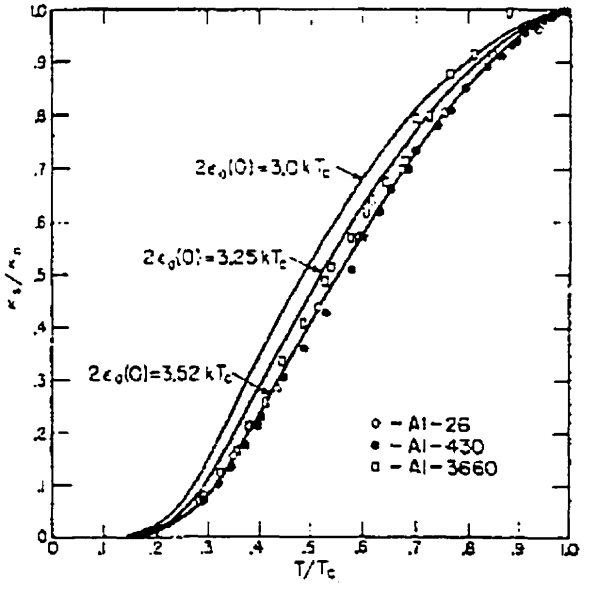


**Figure 2.2:** Normalized thermal conductivity of three samples of Al (after Satterthwaite (1962)). Despite the differences in purity, where RRR goes from 26 to 3660, all three data sets lie close to the $\Delta = 1.76 k_B T_c$ curve.

and boundary scattering (at lower temperature). In impure samples, the data in Fig. 2.2 show that the thermal conductivity is not sensitive to impurity concentration, even when $\rho_0$ is decreased by a factor of 100. This is because the presence of a non-magnetic impurity in a conventional superconductor has no effect on the gap. Such impurities do not break pairs. We will see in the following section that this is not the case for unconventional superconductors.

### 2.1.3 Unconventional Superconductors

In classic superconductors, the order parameter can be expressed as $\Delta_k = \Phi_k e^{i\phi}$ where $\Phi_k$ has the full symmetry of the lattice. When $\phi$ is fixed, as when all the electrons collapse into the same ground state with the same phase, symmetry is broken. By unconventional, we mean that $\Delta_k = \eta_k e^{i\phi}$ where $\eta_k$ has a lower symmetry than the lattice, i.e. there are additional broken symmetries. We sketch various gaps for $UPt_3$ (in Fig. 2.3), from which we see the presence of nodes in all but the isotropic $s$-wave gap in the top left. In $UPt_3$, the simplest candidate gap structures are based on an ellipsoidal Fermi surface (Norman and Hirschfeld 1996a, Norman 1996b). A polar gap has a line of nodes along the equator, an axial gap point nodes at the poles, a tropical gap two line nodes equidistant from the equator and a hybrid gap both line and point nodes with the gap approaching zero at the poles either with a linear (type I) or quadratic (type II) $k$-dependence.

When the superconducting gap has zeroes, there are important consequences for quasiparticles with momentum in the vicinity of these nodes. The signature of an order parameter having nodes is power law $T$-dependence in charge and heat transport, specific heat, penetration depth and nuclear magnetic relaxation, which is very different from the activated behaviour in pure $s$-wave states. In fact, the observation of non-exponential behaviour first alerted researchers to unconventional gap structures with reduced order parameter symmetry.

For a superconductor with an order parameter having a line of nodes on the Fermi surface, the simplest example of which is the polar gap, the DOS is *linear* in the excitation energy, i.e. states exist for $E < \Delta$—previously unallowed! Such is believed to be the case for $UPt_3$, with a line of nodes in the basal plane $p_{Fz} = 0$ and also point nodes at the poles $p_{Fx} = p_{Fy} = 0$; point nodes which are linear in $k$ give a DOS $N(E) \propto E^2$ while point nodes which are quadratic in $k$ give $N(E) \propto E$. For $UPd_2Al_3$, there has not been much theoretical analysis, though NMR measurements

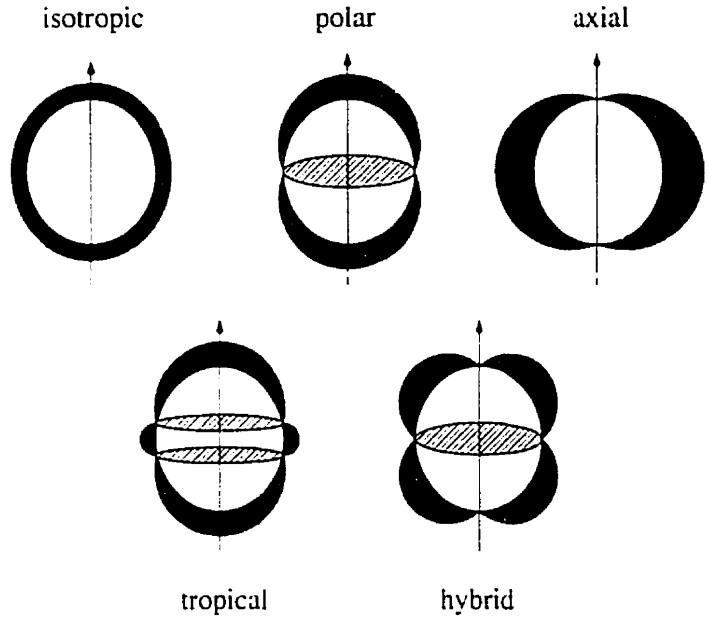


**Figure 2.3:** A few gap candidates for $UPt_3$ (and $UPd_2Al_3$). From the clockwise from the top left, we have an isotropic gap, a polar gap, an axial gap, a hybrid (of polar and axial) gap and a tropical gap (so-called since in $UPt_3$ the line nodes occur at $\pm 23$ degrees, i.e. at the tropics instead of the equator). There are two types of hybrid gaps under consideration, whose difference lies in the $k$-dependence of the polar nodes. The hybrid-I gap, of $E_{1g}$ symmetry, approaches the Fermi surface with a linear $k$-dependence, whereas the hybrid-II, of $E_{2u}$ symmetry, does so as $k^2$.

suggest a line of nodes (Kyogaku *et al.* 1993): we will need to modify slightly the $UPt_3$ calculations. In the case of $YBa_2Cu_3O_{7-\delta}$, the gap is thought to vanish at four points on the two-dimensional Fermi surface (see Fig. 2.4). Quasiparticle excitations at these nodes should also have a linear dispersion: hence the DOS is linear in energy near the Fermi surface.

Impurities alter the low temperature DOS by introducing an impurity band whose width $\gamma$ is a new energy scale relevant to all low-energy thermodynamic and transport properties in superconductors with gap zeroes (Hirschfeld *et al.* 1986, Schmitt-Rink *et al.* 1986, Graf *et al.* 1996). $\gamma$ grows with the impurity scattering rate $\Gamma$, in a way which depends strongly on whether impurities act as Born or resonant scatterers. It is convenient to define the notion of "clean" and "dirty", because in the historical sense, clean refers to $\ell > \xi$ and dirty refers to $\ell < \xi$; thus extreme type-II superconductors at low temperature are always in the clean limit (e.g. $\ell \sim 10000$ Å $\gg \xi \sim 10$ Å for $YBa_2Cu_3O_{7-\delta}$). A more relevant definition of the clean limit is when $\gamma < T \ll \Delta$, where $N(E) \sim E$ and calculations do not need to be done self-consistently. This means that at very low temperature, we are in the dirty limit $T < \gamma$ where

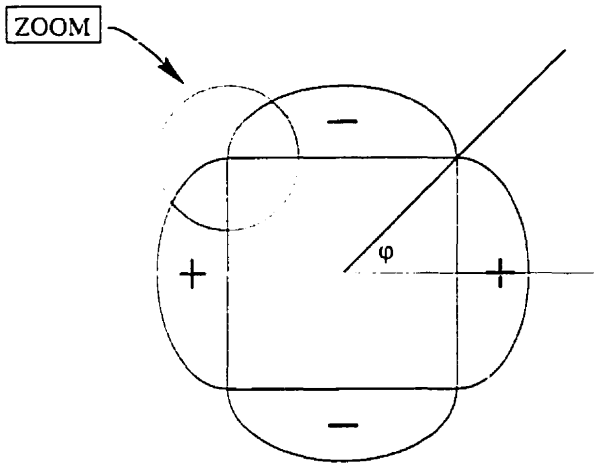


**Figure 2.4:** The two-dimensional tetragonal $d$-wave gap $\Delta_0 \cos(2\phi)$, with zeroes at $\pm\pi/4$ and $\pm 3\pi/4$. At low temperature, we effectively zoom in at a node where the gap is linear in $k$.

"dirt" breaks pairs and the DOS departs from linearity below $\gamma$ and remains roughly constant as $T \to 0$, as demonstrated in Fig. 2.5. This finite DOS at $T = 0$ produces a residual normal fluid of zero-energy quasiparticles deep in the superconducting state. The properties of this residual fluid are like those of a normal Fermi liquid, in that the thermal conductivity of these quasiparticles is expected to be linear in temperature.

From here, we take the 2D $d$-wave gap as our basis for the following development of the theory, since our aim is to *quantitatively* explain $YBa_2Cu_3O_{7-\delta}$ data (a quantitative description of heavy fermions lags far behind). Quasiparticle relaxation time $\tau$ has been calculated for different scattering strengths $\cot\delta_0 \sim 1/U$ where $\delta_0$ is the scattering phase shift and $U$ is the impurity interaction. For $\delta_0 = 0$, which is known as Born scattering, we have

$$\frac{1}{\tau} \simeq \begin{cases} \Gamma\omega & \text{clean} \\ \gamma \sim \Gamma e^{-\Delta_0/\Gamma} & \text{dirty} \end{cases} \tag{2.19}$$

where the very small impurity band in the dirty limit means that impurity effects do not affect the DOS until very low energy scales (see Fig. 2.6). When $k_B T < \gamma$, we call this the "gapless" regime. For maximum scattering phase shift $\delta_0 = \pi/2$, also

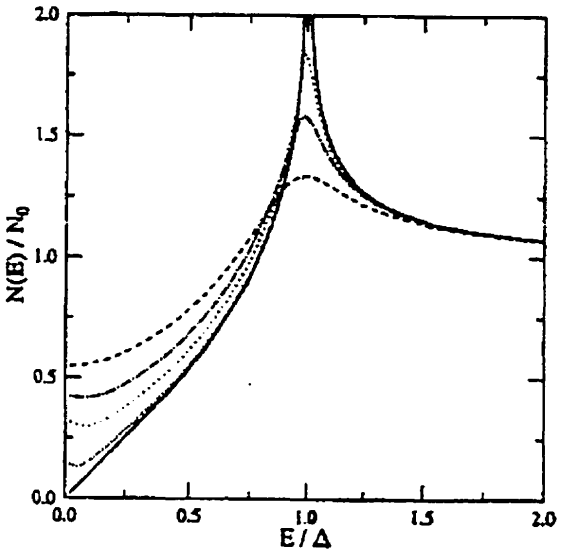


**Figure 2.5:** The density of states $N(E)/N_0$ as a function of reduced energy $E/\Delta_0$ (see Sun and Maki (1995)). For $\Gamma = 0$ (solid line), we have the clean limit result, but when $\Gamma$ is finite, the DOS increases, up to 50% of the normal state value when $\Gamma \simeq 0.4T_c$. Although unmarked, $\gamma$ corresponds to the energy scale below which the DOS curves away from linearity and remains finite down to $T = 0$.

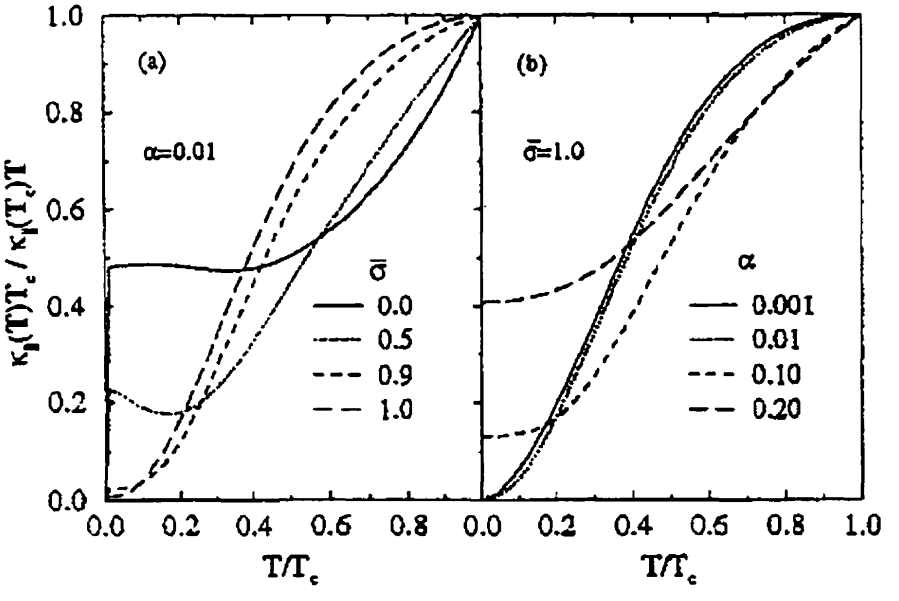


**Figure 2.6:** Normalized in-plane thermal conductivity $\kappa_{||}/T$, after Graf *et al.* (1996), for (a) fixed scattering rate $\alpha = 0.01$ ($\Gamma = 0.03T_c$) and varying scattering cross-section $\bar{\sigma} = \sin^2\delta_0$. Born scattering corresponds to $\bar{\sigma} = 0.0$ and resonant to $\bar{\sigma} = 1.0$, for (b) fixed phase shift $\delta_0 = \pi/2$ and varying scattering rates, showing an increase in $\kappa_{||}/T$ with scattering rate.

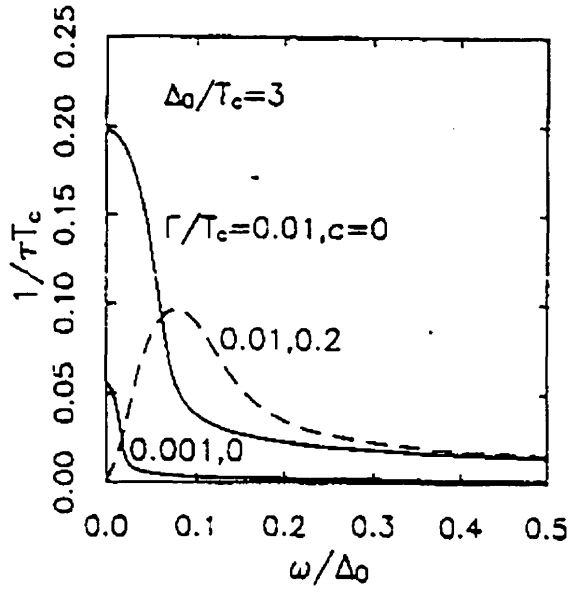


**Figure 2.7:** Impurity scattering rate $1/(\tau T_c)$ vs reduced frequency $\omega/\Delta_0$ for $\Gamma/T_c = 0.01, 0.001$ and $c = 0$ ($\delta_0 = \pi/2$) (solid lines) and $\Gamma/T_c = 0.01$, $c = 0.02$ ($\delta_0 = \pi/6$) (dashed line) (from Hirschfeld, Putikka and Scalapino (1994)). For energy less than $\gamma$, $1/\tau \sim \omega$ for weak scattering and $1/\tau \sim 1/\omega$ for strong, resonant scattering.

called resonant or unitarity scattering, we have (Kübert and Hirschfeld 1998b)

$$\frac{1}{\tau} \simeq \begin{cases} \Gamma/(\omega \ln^2 \omega) & \text{clean} \\ \gamma \simeq 0.61\sqrt{\Delta_0 \Gamma} & \text{dirty} \end{cases} \tag{2.20}$$

where now gapless behaviour occurs over a larger temperature/energy range. In Fig. 2.7, the solid lines represent the impurity relaxation rate in the unitarity limit $c = \cot\delta_0 = 0$ and the dashed line represents a weaker phase shift $\delta_0 = \pi/6$. Taking $\Delta_0 = 3k_B T_c$ simulates strong coupling (weak-coupling BCS gives $\Delta_0 = 2.14 k_B T_c$).

When the gap approaches zero with a linear $k$-dependence, we can concentrate on the linear nodal region and forget about the structure of $\Delta_k$ away from the node. In other words, we linearize the gap, as depicted on the left-hand side of Fig. 2.8. Quasiparticle excitations can then be described by the Dirac spectrum $E(k) = \sqrt{\varepsilon_k^2 + \Delta_k^2} = \hbar\sqrt{(v_f k_1)^2 + (v_2 k_2)^2}$ where $(k_1, k_2)$ defines a coordinate system whose origin is at the node, with $k_1$ a vector normal to the Fermi surface and $k_2$ tangential; the slope of the energy gap $S = d\Delta/dk = \hbar k_F v_2$ (Lee 1993). Thus the quasiparticle energies are confined to a cone, as shown on the right-hand side of

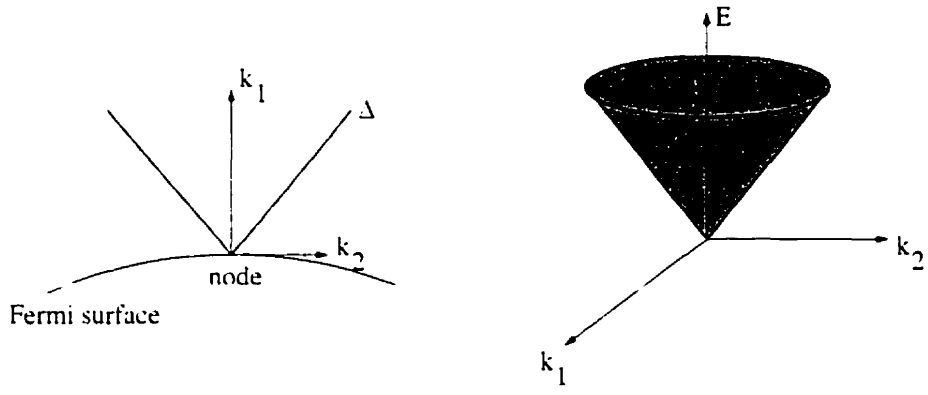


**Figure 2.8:** On the left, the linearized gap $\Delta \sim k$, whose slope $d\Delta/dk \sim v_2$. On the right, the quasiparticle energies lie on a cone, defined by $E(k) = \sqrt{\varepsilon_k^2 + \Delta_k^2} = \hbar\sqrt{(v_f k_1)^2 + (v_2 k_2)^2}$.

Fig. 2.8.

In the clean limit, we have already mentioned that $N(E) \sim E$; the full expression for $N(E)$, in terms of $v_f$ and $v_2$, is

$$N(E) = \frac{2}{\pi\hbar^2}\frac{E}{v_F v_2}. \tag{2.21}$$

Since we want to describe the zero temperature regime in which impurity scattering dominates, the quantity of interest is the residual density of states in the presence of impurities, which is approximately constant for $T < \gamma$:

$$N_0 = \frac{\gamma}{\pi^2\hbar v_F v_2}. \tag{2.22}$$

This finite DOS leads to *universal* (independent of impurity concentration) charge transport in the basal plane at $T = 0$, since the growth in the residual normal fluid density exactly compensates the decrease in mean free path as the scattering rate increases (Lee 1993). Very roughly, we have

$$\sigma_{00} = N_0(ev_F)^2\tau \tag{2.23}$$

which is the just the number of residual carriers times the energy transported times the lifetime. Putting the last two expressions together, we get the charge conductivity

per plane:

$$\sigma_{00} = \frac{e^2}{2\pi\hbar}\frac{2}{\pi}\frac{v_F}{v_2}. \tag{2.24}$$

Note that universality in transport is a consequence of the $d$-wave gap being linear at a node, and depends only on the ratio $v_F/v_2$.

Since the pioneering work of Lee, others have investigated universality in both charge and heat transport (Sun and Maki 1995, Norman 1996b, Graf *et al.* 1996). In the work of Graf and co-workers, they have used a combination of the microscopic theory of superconductivity of Bardeen, Cooper and Schrieffer (1957) and the Fermi liquid theory of Landau (1958), coined the *quasiclassical theory of superconductivity* by Larkin and Ovchinnikov (1968). Then using linear response equations for $\kappa$ and $\sigma$ (in the long wavelength limit $q \to 0$) at $T \to 0$, it was found that the residual normal fluid obeys the Wiedemann-Franz law, i.e. deep in the superconducting state a simple relationship between $\kappa$ and $\sigma$ is recovered. Hence the thermal conductivity as $T \to 0$ in a $d$-wave superconductor should also be universal, and given by:

$$\frac{\kappa_{00}}{T} = L_0\sigma_{00} = \frac{k_B^2}{3\hbar}\frac{v_F}{v_2}n. \tag{2.25}$$

where $\sigma_{00}$ is the universal charge conductivity per conducting plane, $L_0 = (\pi^2/3)(k_B/e)^2$ is the Sommerfeld value of the Lorenz number and $n$ is the number of $CuO_2$ planes stacked along the $c$-axis per unit cell. Now we have another handle on the ratio $v_F/v_2$.

While we have used $d$-wave language in our description, the theory is general, and has been applied to both $YBa_2Cu_3O_{7-\delta}$ and $UPt_3$ extensively; in fact, the theory was originally developed to explain heavy fermion superconductors. It was only later applied to the cuprates, and has since been going strong because the highly two-dimensional nature of these materials make the calculations simpler. Moreover, the gap structure of $YBa_2Cu_3O_{7-\delta}$ is known to be primarily $d$-wave (with possible admixtures of $s$), whereas in $UPt_3$ for example, there is much less evidence for one gap over another. Nevertheless, the so-called hybrid-II gap with a line of nodes on the equator and quadratic point nodes at the poles of an ellipsoidal Fermi surface (see Fig. 2.3) is the current front-runner (more on this in Chapter 3). In calculating the in-plane thermal conductivity $\kappa_{||}/T$ for both $UPt_3$ and $YBa_2Cu_3O_{7-\delta}$ in the limit

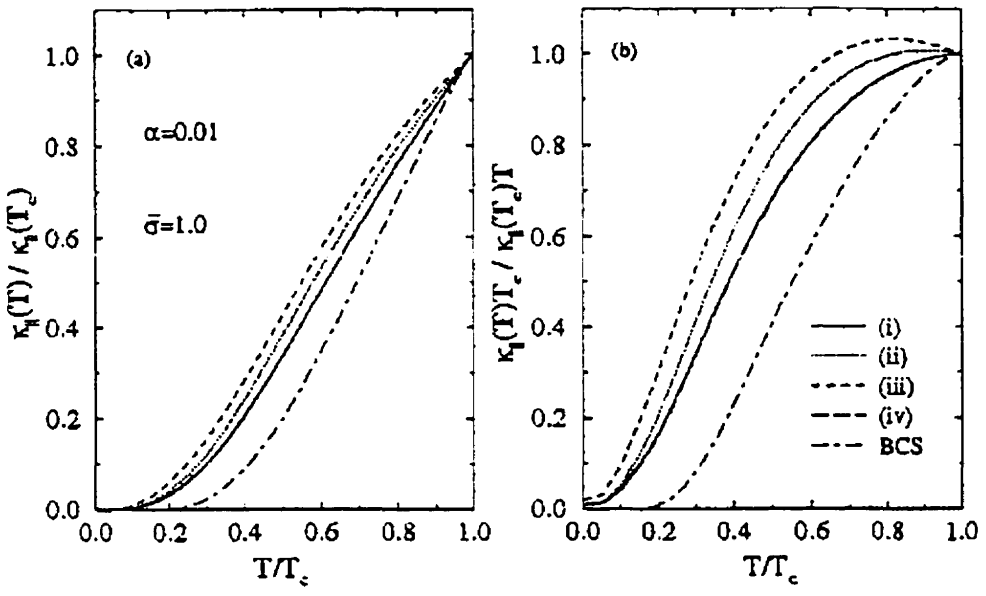


**Figure 2.9:** Normalized thermal conductivity vs reduced temperature for $\delta_0 = \pi/2$ ($\bar{\sigma} = \sin^2\delta_0$) and $\Gamma = 0.03T_c$ ($\alpha = \Gamma/(\pi T_c)$) calculated by Graf *et al.* (1996). On the left, we have the in-plane $\kappa_{ll}$. On the right, we have the in-plane $\kappa_{ll}/T$, showing that the 2D $d_{x^2-y^2}$ and the 3D hybrid-II gaps give the same $T$-linear behaviour.

$\delta_0 = \pi/2$. Graf *et al.* (1996) found the normalized $\kappa_{ll}/T$ to be essentially *identical* for the 2D $d_{x^2-y^2}$ and 3D hybrid-II gaps, shown in Fig. 2.9. Although this result may at first seem reasonable considering there are line nodes with a linear $k$-dependence for both of these gaps, there are also line nodes in the other $UPt_3$ candidates, the hybrid-I and polar gaps.

More recently, others have reinvestigated localization due to disorder (Senthil *et al.* 1998) using a non-linear sigma model. In this treatment, they specify *spin* conductivity $\sigma_s$, and not *charge* conductivity, as being related to the thermal conductivity by the Wiedemann-Franz law. This is one major distinction between the quasiparticles in a superconductor and those in a normal metal: in a superconductor, quasiparticle charge is not a conserved quantity, therefore, it cannot be transported by diffusion. However, quasiparticle spin is conserved, since the condensate does not carry spin in a singlet superconductor. Moreover, quasiparticle energy is also a conserved quantity due to the inability of the condensate to carry entropy. Thus in the field theory to describe quasiparticle localization in a superconductor, Senthil *et al.* have adopted a single dimensionless coupling constant, the *spin* conductance.

In two dimensions, they have found quasiparticle localization, robust in the pres-

ence of either an orbital or Zeeman field but not both. In three-dimensions, i.e. by the inclusion of interlayer coupling, a quantum phase transition from an extended *spin metal* to a localized *spin insulator* becomes possible. The properties of the novel spin metal include a non-zero spin diffusion constant, spin susceptibility and spin conductivity all at zero temperature. Given enough interlayer coupling, it is possible to suppress the effects of localization found in 2D. Then at zero temperature there would be quasiparticle transport just as in the $d$-wave theory we have been discussing.

As for the thermal conductivity within this field theory, a self-consistent treatment gives

$$\frac{\kappa}{T} = \frac{2}{3}\frac{k_B^2}{\hbar}\frac{v_F^2 + v_2^2}{v_F v_2}. \tag{2.26}$$

from the Wiedemann-Franz law:

$$\frac{\kappa}{\sigma_s T} = \frac{4\pi^2}{3}. \tag{2.27}$$

where the factor 4 difference from the usual form is due to the replacement of $e^2$ by $(spin\ \frac{1}{2})^2$. Since the claim that microwave conductivity and thermal conductivity are not related by the Wiedemann-Franz law is such a radical break from conventional wisdom, it is worth examining the breakdown of the WFL in another way. Consider scattering within (inter-) and between (intra-) nodes. According to Lee (1998), only intra-node scattering would transport charge, as inter-node scattering would not carry any momentum out of the node. Heat transport, however, could be accomplished by either mechanism. Thus heat and charge transport would have different scattering times and there would not be a cancellation leading to the simple WFL. Calculations are currently underway.

## 2.2 Heat Transport in an Applied Magnetic Field

We are interested in quasiparticle transport by a type-II superconductor in a magnetic field, for we expect that the presence of vortices will have a profound effect on both quasiparticle number and scattering behaviour. In fact, unconventional gaps which contain nodes give rise to vastly different properties from BCS superconductors. Both will be described in this section.

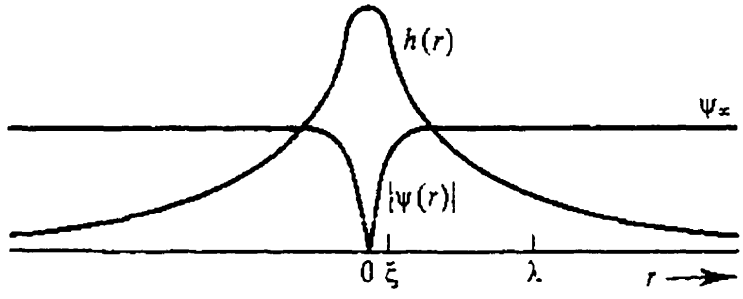


**Figure 2.10:** The spatial variation of the order parameter $|\Psi(r)|$ and the field $h(r)$ within a vortex core (after (Tinkham 1996)). Thus the core size is of order $2\xi$ and is less than the penetration depth $\lambda$.

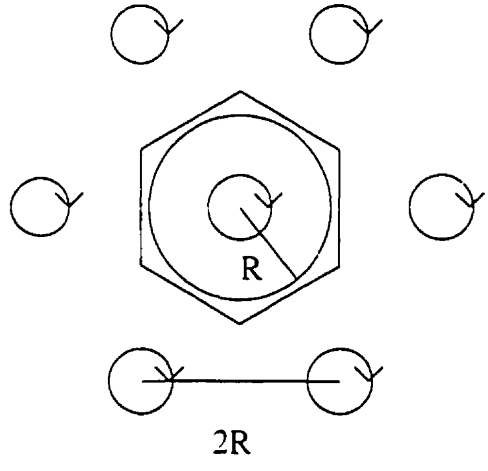


**Figure 2.11:** Vortices arranged in a triangular lattice, with hexagonal unit cells (only one shown). The intervortex distance is $2R$.

### 2.2.1 Conventional Superconductors

For a type-II superconductor in an applied magnetic field, induced vortices are arranged in a vortex lattice. Magnetic flux penetrates the superconductor through the cores, and the superconducting order parameter $|\Psi(r)|$ is zero at the centre of the core and rises with distance $r$ from the core, as in Fig. 2.10.

Using Fig. 2.11, which depicts a triangular arrangement of cores separated by a distance of $2R$, with $R = 1/(a\sqrt{\pi})\sqrt{\Phi_0/H}$ where $a$ is some vortex lattice parameter [2], we describe the vortex state of a type-II $s$-wave superconductor (Hirschfeld 1998b).

[2] $a$ is introduced to account for the effective vortex unit cell whose area is $a^2\pi R^2$, equal to $\Phi_0/H$. For a circular unit cell, $a \equiv 1$, and for a hexagonal unit cell, Tinkham (1996, p.146) gives $a = 1.05$.

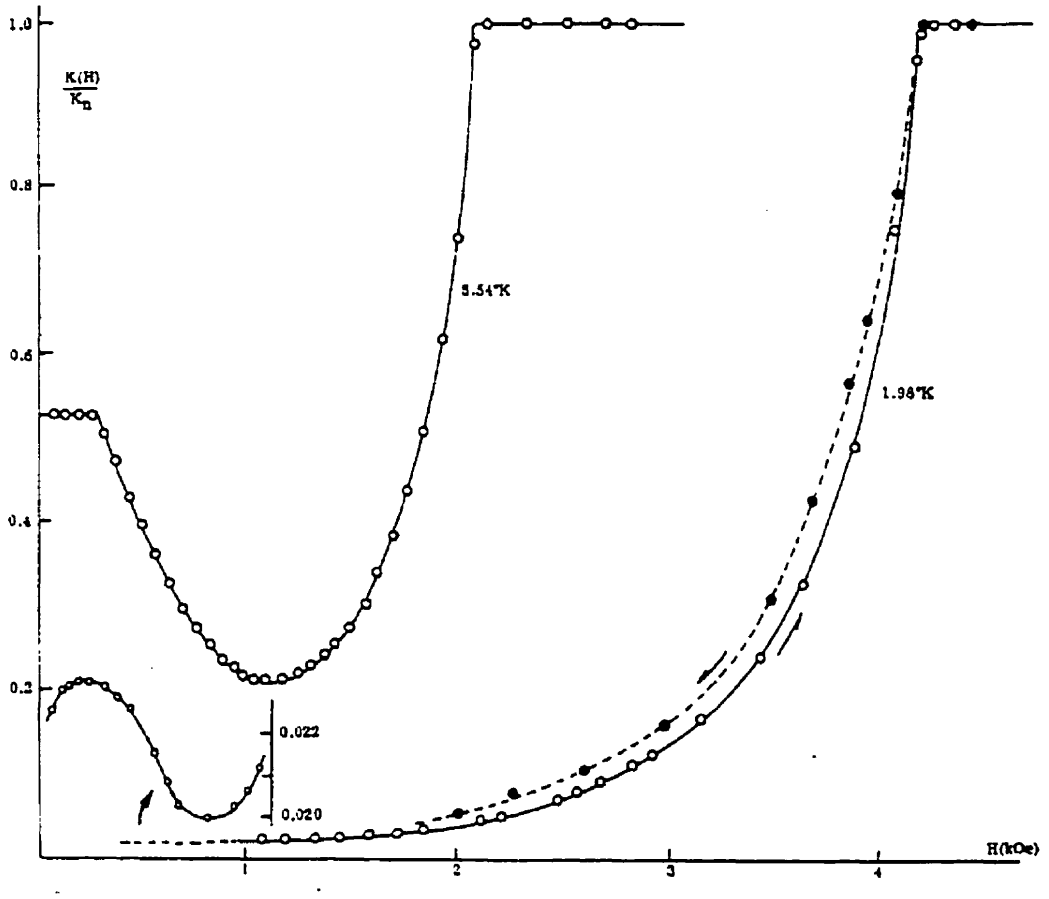


**Figure 2.12:** Normalized thermal conductivity $\kappa(T)/\kappa_N$ of Nb in field $H$ up to 4 kOe (0.4 T) obtained by Lowell and Sousa (1970).

Within the cores, the order parameter $\Delta(r)$ is suppressed, and quasiparticles can be thought of as obeying Schrödinger's equation in a potential $\Delta(r)$. The eigenstates are bound states with spacing $\Delta^2/\varepsilon_F$, contributing to the DOS $N_0$ in the cores. Extended states are fully gapped, so make no contribution to the DOS. Since the number of excitations goes as the number of cores ($\sim H$), the enhancement to the core DOS can be expressed as

$$N(0; H) \sim N_0 T \frac{H}{H_{c2}}. \tag{2.28}$$

Specific heat measurements can detect these states within the vortex cores. However, thermal conductivity is not sensitive to these bound states, only extended states, which are gapped. So while $c(T; H)$ is expected to increase with magnetic field $H$,

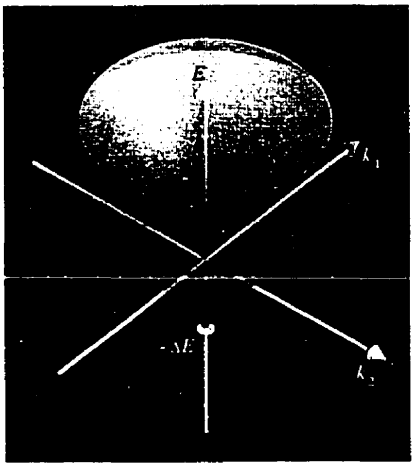

**Figure 2.13:** The effect of the Doppler shift due to a superfluid flow on the quasiparticle energy spectrum. Now the vertex of the energy cone is below the Fermi energy by an amount $\Delta E$.

$\kappa$ should not. In fact, at low fields, $\kappa(H)$ drops rapidly with $H$! This phenomenon is generally attributed to vortex scattering, as the coherence length is much longer than the intervortex spacing. At high fields, pair-breaking effects dominate $\kappa(H)$ since the order parameter is strongly suppressed as the field approaches $H_{c2}$ (in other words, the energy $2\Delta$ required to break a pair decreases). Thus $\kappa(H)$ grows rapidly up to its normal state value as $H \rightarrow H_{c2}$. A good example is Nb, shown in Fig. 2.12, where nothing changes until vortices appear above $H_{c2}$.

### 2.2.2 Unconventional Superconductors

In the presence of an external magnetic field, quasiparticle states outside the vortex cores are Doppler shifted due to the superfluid flow around the vortices. Certain states will then have energy which is negative with respect to the Fermi energy, and so will be accessible to quasiparticle excitations (see Fig. 2.13). For those quasiparticles within the vortex cores, Volovik (1993) has shown that their contribution to the density of states is much smaller than that due to the delocalized quasiparticles occupying the extended states, by a factor of order $\ln\frac{min\{R,\lambda\}}{\xi_0}$. Since the extended states dominate the DOS, we will concentrate on the quasiparticles outside the vortex cores. The superfluid flow shifts the quasiparticle spectrum by $E \rightarrow E - v_s \cdot k$ or

$$E(\mathbf{k}, \mathbf{A}) = E(\mathbf{k}) - \frac{e}{c}\mathbf{v}_k \cdot \mathbf{A}, \tag{2.29}$$

where $\mathbf{v}_k$ is the normal state velocity (Lee and Wen 1997) and $\mathbf{A}$ is the vector potential satisfying $\Phi_0 = \oint \mathbf{A} \cdot d\ell$, with $\Phi_0$ the flux quantum; thus, $A = \Phi_0/(2\pi r)$. The magnitude of the Doppler shift is characterized by its average, $E_H$, obtained by integrating over a vortex-lattice unit cell of radius $R$. Within each vortex unit cell, its area times the field should be equal to one flux quantum. The field induced energy shift is given by

$$\begin{aligned} E_H &= \frac{e}{c}\langle|\mathbf{v}_k \cdot \mathbf{A}|\rangle \\ &= \frac{e}{c}\frac{\int_0^R dr\ r\int_0^{2\pi} d\phi\ v_F \cdot A|\cos\phi|}{\int_0^R dr\ r\int_0^{2\pi} d\phi} \\ &= \frac{e}{c}\frac{\int_0^R dr\ r\int_0^{2\pi} d\phi\ v_F\Phi_0/(2\pi r)|\cos\phi|}{R^2/2\cdot 2\pi} \\ &= \frac{e}{c}\frac{v_F\Phi_0}{2\pi}\frac{4}{\pi R} \\ &= \sqrt{\frac{2}{\pi}}\hbar a v_F\sqrt{\frac{H}{\Phi_0}} \end{aligned} \tag{2.30}$$

since $aR = \sqrt{\Phi_0/(\pi H)}$ (from previous section) and $\Phi_0 = hc/(2e)$. Note also that $|v_k| = \sqrt{v_F^2 + v_2^2} \approx v_F$ because $v_F \sim 10v_2$, which we will later show.

Volovik (1993) was the first to calculate the DOS due to a Doppler shifted energy spectrum. We expect, from inspecting the zero field expression for $N(0)$ (Equation (2.21)), that $N(0; H)$ averaged over a vortex cell should look something like

$$\langle N(0; H)\rangle \sim \frac{2}{\pi\hbar^2}\frac{E_H}{v_F v_2}. \tag{2.31}$$

Substituting Equation (2.30) in the above, we get

$$\langle N(0; H)\rangle \sim \frac{a}{\hbar v_2}\sqrt{\frac{H}{\Phi_0}}. \tag{2.32}$$

In fact, the correct calculation (Kübert and Hirschfeld 1998b) gives

$$\begin{aligned}\langle N(0;H)\rangle &= \sqrt{\frac{8}{\pi}}a\sqrt{\frac{H}{H_{c2}}}N_0 \\ &= \sqrt{\frac{8}{\pi}}a\sqrt{2\pi}\xi_0\sqrt{\frac{H}{\Phi_0}}N_0 \\ &= 4a(\frac{m}{\pi\hbar^2})(\frac{\hbar v_F}{\pi\Delta_0})\sqrt{\frac{H}{\Phi_0}} \\ &= \frac{4}{\pi^2\hbar}amv_F(\frac{2}{\hbar k_F v_2})\sqrt{\frac{H}{\Phi_0}} \\ &= \frac{8}{\pi^2\hbar}\frac{a}{v_2}\sqrt{\frac{H}{\Phi_0}}\end{aligned} \tag{2.33}$$

since $E_H$ can also be expressed as $a\Delta_0\sqrt{H/H_{c2}}$, via the relations $H_{c2} = \Phi_0/(2\pi\xi_0^2)$ and $\xi_0 = \hbar v_F/(\pi\Delta_0)$. We have also used $2\Delta_0 = \hbar k_F v_2$, $\hbar k_F = mv_F$ and $N_0 = \frac{m}{\pi\hbar^2}$. The latter is included in calculations because a probe of the nodes should also be sensitive to the normal state DOS near the nodes.

For low field and temperature, quasiparticles in a $d$-wave superconductor are predicted to have a thermal conductivity $\kappa^{el}/T$ which increases with applied field, reflecting the occupation of extended states. Recall that this is in contrast to conventional type-II superconductors such as niobium, in which the quasiparticle mean free path is set by the vortices (since impurities do not break pairs). However, in a $d$-wave superconductor where impurity scattering is important, the impurity mean free path is smaller than the intervortex spacing. Thus Kübert and Hirschfeld (1998b) assume that impurities remain the dominant scattering centres at low temperature. Comparison to experiments will verify whether this assumption is correct.

Because thermal conductivity involves the transport scattering time, it is complicated to calculate. A simple way to view heat conduction parallel to the vortex cores is as follows: since $\kappa_0(H)/T \propto N(\omega)\tau(\omega)$ (where $N \sim 1/\gamma \sim \tau$ for $\delta_0 = \pi/2$), and the superfluid velocity $v_s = \hbar/(2m_e r)$, we have, as $(\omega, T) \to 0$ (and so the Doppler

shift $\omega - v_s \cdot k \rightarrow v_s \cdot k$)

$$\begin{aligned} \frac{\kappa_0(H)}{T} &\propto N(v_s)\, \tau(v_s) \propto \langle v_s \cdot v_s \rangle_H \\ &\propto \frac{1}{\pi R^2} \int_{\xi_0}^{R} dr\, r\left(\frac{1}{r^2}\right) \propto \frac{1}{R^2} \log \frac{R}{\xi_0} \\ &\propto H \log H. \end{aligned} \tag{2.34}$$

This "hand-waving" approach already highlights two important results, namely that the field is expected to contribute to the thermal conductiviy and that the increase does not go as $\sqrt{H}$.

Putting in the full details for $J \perp H$ and $H \perp c$ is more involved. Fortunately, the calculation has been done, by treating transport with the same semi-classical approach as in zero-field. Kübert and Hirschfeld (1998b) have found that at $T$=0, the field dependence for $\mathbf{H} \parallel \mathbf{c}$ and $\mathbf{J} \perp \mathbf{c}$ follows

$$\frac{\kappa(0; H)}{T} = \frac{\kappa_0}{T} \frac{\rho^2}{\rho\sqrt{1+\rho^2} - \sinh^{-1}\rho} \tag{2.35}$$

where $\rho$ is essentially the ratio of the two relevant energy scales, $\gamma$ and $E_H$: in the dirty limit where $\gamma > E_H$,

$$\rho = \sqrt{\frac{6}{\pi}} \frac{\gamma}{E_H} \propto \frac{\gamma}{a v_F \sqrt{H}} \tag{2.36}$$

where $\kappa_0/T$ is the universal value of $\kappa/T$ at both $T$=0 and $H$=0. While this function qualitatively resembles $\sqrt{H}$, the rise with $H$ is not as steep and it does not saturate so quickly.

Since vortex scattering is so important in conventional superconductors such as Nb (see Fig. 2.12), it is fair to ask how vortices would affect transport in $d$-wave superconductors. Franz has shown that a disordered vortex lattice in a $d$-wave superconductor can result in quasiparticles scattering off the superflow (Franz 1999). The reduction in mean free path then compensates the increase in $N(E)$, producing a field-independent *universal* $\kappa/T$ at fields large enough that vortices are the dominant scattering process. The theory demonstrates a drop in $\kappa$ with field which then reaches a plateau, consistent with measurements in BSCCO and underdoped YBCO (see Section 7.5). At low temperature, a decreasing $\kappa$ would be in contrast

with calculations assuming impurity scattering to be the dominant scattering process (Kübert and Hirschfeld 1998b).

Besides the Doppler shift in the quasiparticle spectrum, there are also contributions from the Zeeman effect. When a field is applied parallel to the $CuO_2$ planes, spin up state energies are lowered by $\mu H$; spin down states are increased by the same amount. Near the nodes, where the gap $\Delta_k$ is small, arbitrarily small values of an applied magnetic field can produce a Zeeman energy larger than the local gap, creating spin polarized normal electrons, i.e. spin degeneracy is lifted.

Yang and Sondhi (1998) have shown that for a two-dimensional $d$-wave superconductor in a magnetic field, orbital effects are negligible for $\mathbf{H} \perp \mathbf{c}$. However, in real superconductors, orbital effects become important in the presence of interplane coupling. For $YBa_2Cu_3O_{7-\delta}$, the spin-orbit scattering time has been estimated to be about 100 times shorter than impurity scattering times of about $10^{-12}$ s, so orbital effects can probably be safely ignored. We can estimate the order of magnitude of the Zeeman contribution to the specific heat by

$$\frac{N(0;H)}{N_0} = \frac{\delta\gamma(H)}{\gamma_N} \approx \frac{\mu_B H}{\Delta_0} \tag{2.37}$$

where $\delta\gamma(H)$ is the increase in the $\sqrt{H}$ coefficient in the specific heat and $\gamma_N$ is the normal state Sommerfeld $T$-linear coefficient. In a field of 8 T, $\mu_B H = 5.4$ K. Compared to the Doppler shift energy $E_H = 45$ K (using $a = 1$ and taking the Fermi velocity estimated by tight-binding band structure calculations (Lee and Wen 1997) $v_F = 1.2\times10^7$ cm/s), the Zeeman energy is much smaller.

# 3 The Heavy Fermion Superconductor $UPd_2Al_3$

In this thesis, the heavy fermion we study is $UPd_2Al_3$, discovered by Geibel *et al.* (1991). It exhibits co-existing antiferromagnetism and superconductivity at ambient pressure, with the highest $T_c$ (2 K) and magnetic moment ($0.85\mu_B$/U, $T_N$ = 14 K) of all the known heavy fermion superconductors. The ordered moments lie within the basal plane, in which they are coupled ferromagnetically; along $c$, the planes are coupled antiferromagnetically. The sheer size of the magnetic moment suggests that the interplay between superconductivity and antiferromagnetism is stronger than in the other heavy fermion superconductors. Comparisons will be made with $UPt_3$, which has been the most actively studied heavy fermion to date, so we now outline the salient features of $UPt_3$ (for further details, see review by Taillefer *et al.* (1991) and references therein).

There are a number of reasons why $UPt_3$ has been an ideal system to study. It is relatively easy to grow high purity samples, and the low $T_c$ of 0.5 K, compared to the Debye temperature $\Theta_D \sim 300$ K, ensures the absence of phonons in the superconducting state. In addition, it shares many properties with $UPd_2Al_3$, such as the coexistence of superconductivity and antiferromagnetism ($T_N$ = 5 K with moment $0.02\mu_B$). However, like $^3$He, it has multiple superconducting phases, shown in Fig. 3.1, first discovered in the double transition of the specific heat (Fisher *et al.* 1989). The two transitions merge under hydrostatic pressure of about 3-4 kbar (Hayden *et al.* 1992). Moreover, neutron scattering shows that the decreasing amplitude of the magnetic moment with applied pressure also disappears at around 3-4 kbar, suggesting that the magnetic moment is responsible for the splitting, i.e. no magnetic order beyond 4 kbar, no phase multiplicity.

## 3.1 Phase Diagram

For $UPd_2Al_3$, there is only one superconducting phase. There are, however, several magnetic phases: three with the applied field in the basal plane and one perpen-

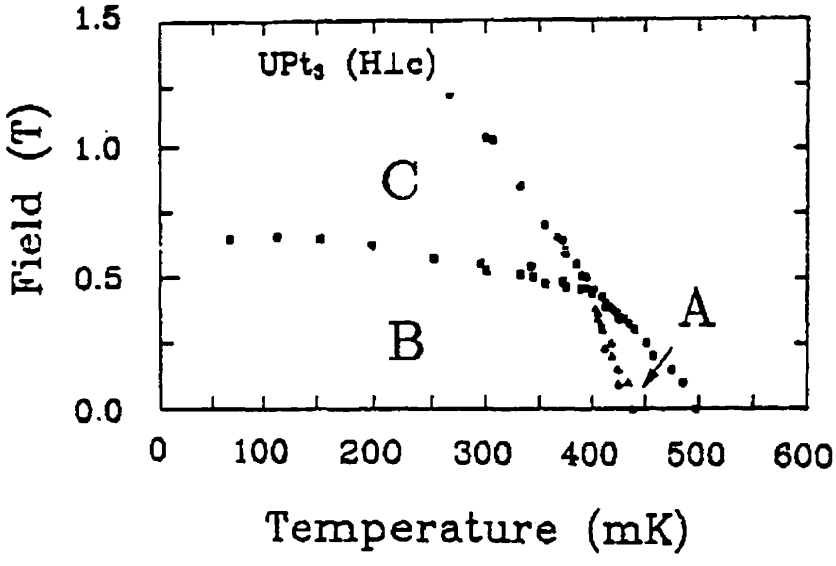


**Figure 3.1:** Magnetic field and temperature phase diagram of $UPt_3$ determined from sound velocity measurements of Adenwalla *et al.* (1990). *A*, *B* and *C* refer to distinct superconducting phases, with *A* and *B* accessible at ambient pressure and zero magnetic field.

dicular. We show the magnetic field and temperature phase diagram for an applied magnetic field in the hexagonal plane Fig. 3.2. For $H = 0$, there are the antiferromagnetic (AF.$T < T_N$) and paramagnetic (PM.$T > T_N$) phases, and it is possible to cross the antiferromagnetic phase boundary into the paramagnetic phase by the application of 18 T (de Visser *et al.* 1992).

## 3.2 Crystal Structure

$UPd_2Al_3$ crystallizes in a hexagonal crystal structure ($PrNi_2Al_3$, as in Fig. 3.3) and has lattice parameters $a = b = 5.365$ Å and $c = 4.186$ Å (Geibel *et al.* 1991). Thus the volume of a unit cell is $(\sqrt{3}/2)a^2c = 104.3$ Å$^3$ and the density is 8.464 g/cm$^3$.

## 3.3 Normal State

The resistivity of $UPd_2Al_3$ is shown in Fig. 3.4. From room temperature down to about 80 K, $\rho$ increases much like in other heavy fermions and systems containing isolated magnetic impurities, suggestive of a Kondo scattering mechanism. As we go lower in temperature, the resistivity drops as many-body effects develop. At the Néel transition (14 K), spin-disorder scattering drops rapidly as the spins order themselves

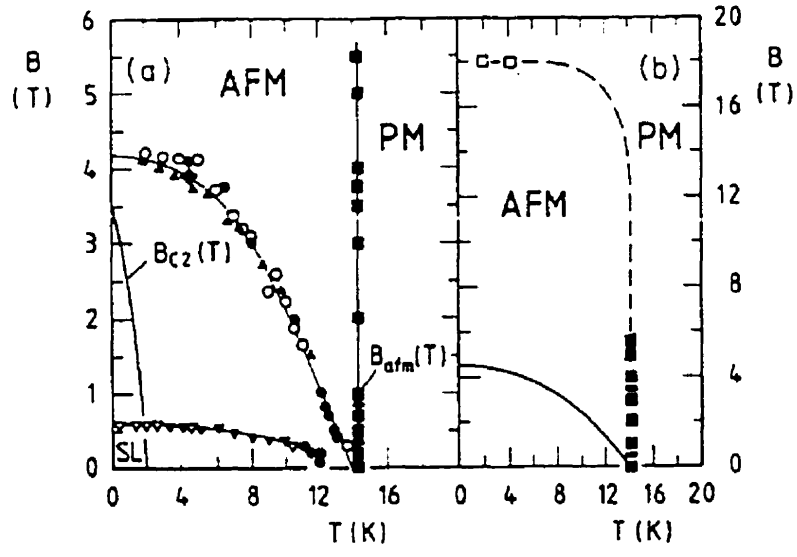


**Figure 3.2:** Magnetic field (in plane) and temperature phase diagram of $UPd_2Al_3$ obtained by Grauel *et al.* (1992). On the left is the low field region showing $H_{c2}$ (or $B_{c2}$) as a solid line and on the right, the field axis is expanded to show the metamagnetic transition (dashed line).

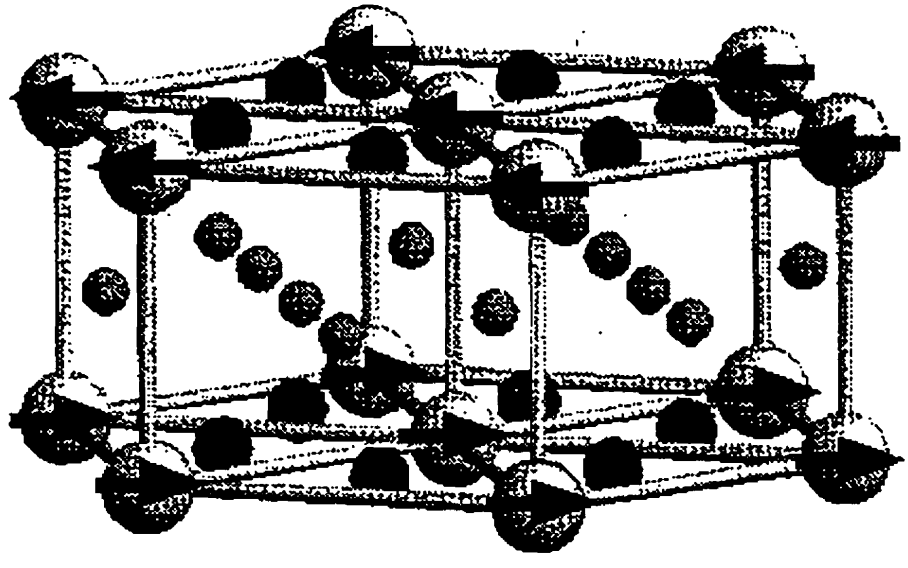

**Figure 3.3:** Crystal structure of $UPd_2Al_3$ (after Sato *et al.* (1992)). Large spheres at the corners represent U atoms (with magnetic moments denoted by arrows), which are surrounded by Pd atoms in the basal plane. The smallest spheres represent Al atoms between the planes.

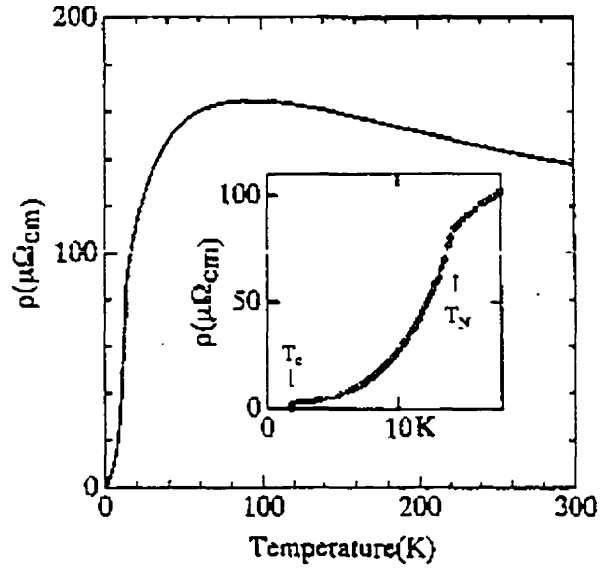


**Figure 3.4:** Temperature dependence of the electrical resistivity $\rho$ of $UPd_2Al_3$ along the $b$ axis (after Hiroi *et al.* (1997)). Inset: Low temperature scale showing antiferromagnetic order at the Neél temperature ($T_N$) and superconductivity at $T_c$.

antiferromagnetically, and $\rho$ falls roughly as $T^2$, characteristic of the Fermi liquid state. Moreover, the normal state specific heat follows $c(T) = \gamma_0 T + \beta T^3$, with the Sommerfeld coefficient $\gamma_0 = 145$ mJ $K^{-2}mol^{-1}$ (Caspary *et al.* 1993). The $T^3$ coefficient is attributed to phonons.

## 3.4 Superconducting State

In the superconducting state, there is evidence for both conventional and unconventional behaviour. The nuclear magnetic relaxation rate $1/T_1$ shows a power law temperature dependence suggestive of a gap with a line of zeroes on the Fermi surface, as does the absence of a coherence peak (or Hebel-Slichter peak) below $T_c$ (Kyogaku *et al.* 1993). However, the $T$-dependence of the penetration depth determined from muon spin relaxation is quite close to that expected for an s-wave gap (Amato *et al.* 1992, Feyerherm *et al.* 1994). There are further inconsistencies to come.

From de Haas-van Alphen (dHvA) measurements, we can determine quasiparticle masses and scattering times. The observation of quantum oscillations in $UPd_2Al_3$ by Inada *et al.* (1994) confirms the presence of a Fermi surface, and also the itinerant nature of the $5f$ electrons. Five main branches were detected, giving a range of

$10m_0$-$33m_0$ for the effective cyclotron masses. Using the Dingle temperature $T_D = \hbar/(2\pi k_B \tau)$ of 169±3 mK for the $\gamma$ branch, we find a scattering rate $\Gamma = 1/(2\tau) = 0.25T_c$.

As for the specific heat, $c(T)$ has been a widely-used probe of heavy electron nature: for instance, the huge jump at $T_c$ in $CeCu_2Si_2$ first demonstrated that the heavy electrons formed the Cooper pairs, the double transition in $UPt_3$ revealed multiple superconducting phases and the power laws observed at low temperature pointed to order parameters with nodes on the Fermi surface.

In $UPd_2Al_3$, the specific heat measured by Caspary *et al.* (1993) shows a single jump at $T_c$ of size $\Delta c/(\gamma_0 T_c) \approx 1.48$, which is not far from the weak-coupling BCS value of 1.43, suggesting that there is nothing very unconventional going on. For $0.3 < T < 1$ K, $c(T)$ (shown in Fig. 3.5) fits $c(T) = \gamma T + bT^3$. The first term, also seen in $CeCu_2Si_2$, $UPt_3$ and $URu_2Si_2$, is attributed to residual electrons since the coefficient $\gamma$ increases with the $T_c$ transition width, indicating that defects are responsible for pair-breaking. Below about 0.3 K, an upward curvature appears. The $T^3$ term is compatible with calculations for a linear point node, since in this case the density of states $N(E) \sim E^2$ and $c/T \sim T^2$. Thus the $H = 0$ temperature dependence of the specific heat seems to favour a gap with linear point nodes.

With an applied field, we need to add a hyperfine term to the specific heat, due to the Zeeman splitting of the local $5f$ moments on $^{27}Al$ (see inset of Fig. 3.5). Moreover, the coefficients are field dependent, so that $c(T;H) = a(H)/T^2 + \gamma(H)T + b(H)T^3$ (Caspary *et al.* 1993). Below $H_{c2}$, $\gamma(H) \sim H$, consistent with normal excitations in the vortex cores. So far, our analysis has been mostly qualitative: indeed, quantitative comparisons are premature since the Fermi surfaces are complicated, with several sheets, so one uses the simplest spherical Fermi surfaces in calculations. Still, we can conclude from specific heat measurements, both in field and in zero field, that there is evidence for linear point nodes.

A recent study of the pairing state was performed by Jourdan, Huth and Adrian (1999) using tunneling spectroscopy in a superconductor-insulator-superconductor (SIS) tunneling junction, with $UPd_2Al_3$-$AlO_x$-Pb, with aluminum oxide as the insulating barrier. The differential conductivity, which depends on the bias voltage, of an SIN (N=normal metal) junction gives a measure of the thermally smeared density of states of the superconductor. Additional structures in the differential conductivity outside of the gap region is a sign of strong-coupling superconductivity, for

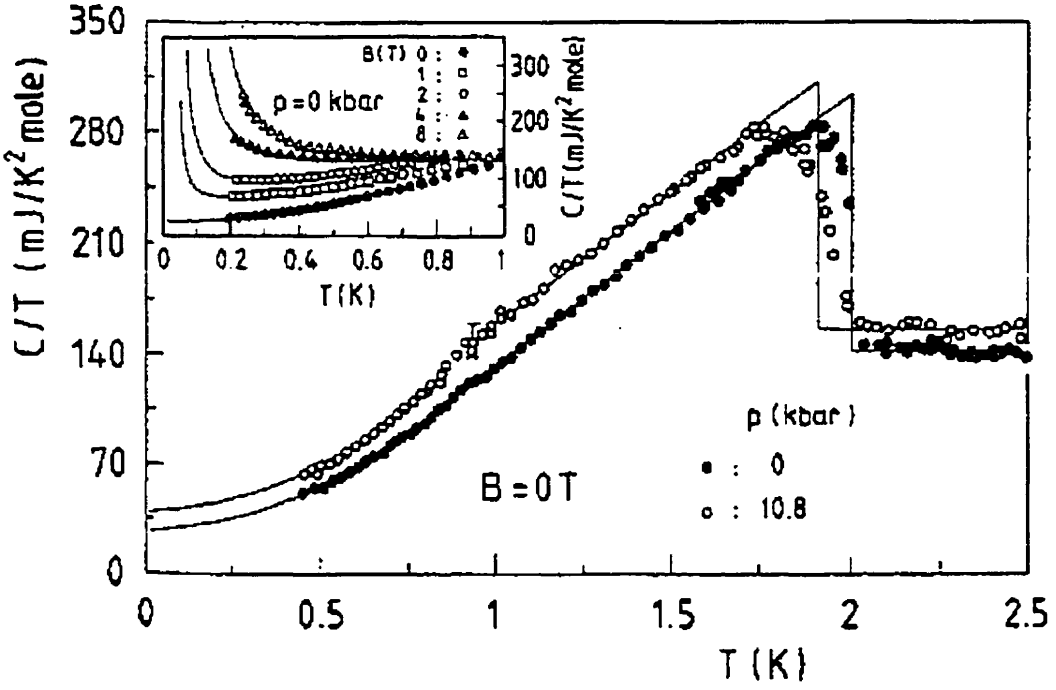


**Figure 3.5:** Specific heat of $UPd_2Al_3$ showing the jump at $T_c$, obtained by Caspary *et al.* (1993), at ambient pressure and also at 10.8 kbar. The inset shows the field dependence and the growing upturn at low temperature.

example e-ph coupling in Pb. By the application of a magnetic field strong enough to drive Pb normal but below $H_{c2}$ of $UPd_2Al_3$, $UPd_2Al_3$-$AlO_x$-Pb becomes an SIN tunnel junction. In a field of 0.3 T, the standard Dynes fit yields a zero temperature gap $\Delta_0 = 235$ $\mu$eV. Beyond the gap energy, a modulation in the conductivity at $V \approx 1.22$ meV can be observed in Fig. 3.6. In this case, the energy scale is low compared to a $\Theta_D$ of roughly 150 K (13 meV), so Jourdan and co-workers have ruled out conventional e-ph coupling [3]. However, we point out that long wavelength acoustic phonons are ungapped, though the proximity of the modulation to the spin wave gap of 1.5 meV (17 K) (Metoki *et al.* 1998) does suggest that the order parameter may be coupling to this particular magnon mode. Assuming e-mag coupling is responsible for *d*-wave superconductivity, there is a critical energy $\omega_c$ below which spin fluctuations are pair-breaking (Millis, Sachdev and Varma 1988). Note that this is in contrast to e-ph coupling, where it is only *below* some energy $\omega_0$ that pair *attraction* takes place. So above $\omega_c$, e-e attraction causes an increase in the tunneling conductivity

[3] In Pb, $\Delta_0 = 15$ K and $\Theta_D = 88$ K, compared to 2.7 K and 150 K, respectively, in $UPd_2Al_3$. Tunneling spectra of Pb show modulations at $\Theta_D/2$ and $\Theta_D$, in support of e-ph coupling.

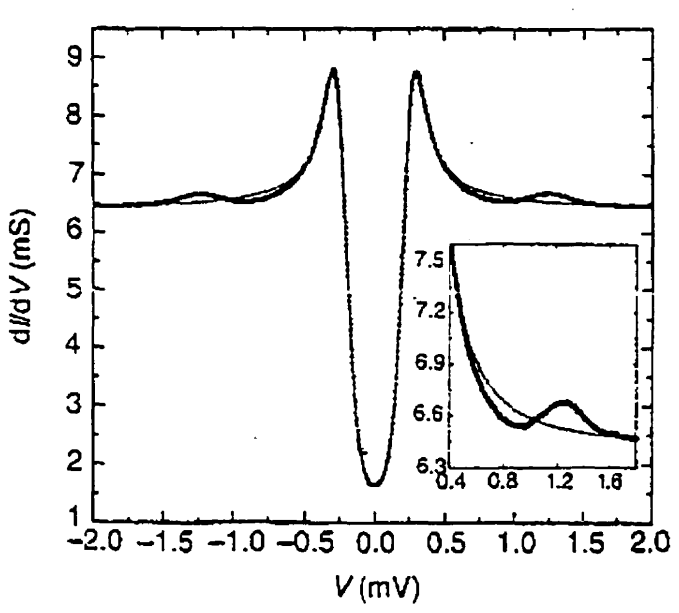


**Figure 3.6:** Differential conducitivity of a $UPd_2Al_3$-$AlO_x$-Pb tunnel junction, with the grey trace the fit to the Dynes formula (after Jourdan, Huth and Adrian (1999)). Inset, modulations attributed to strong-coupling to spin fluctuations.

with respect to the Dynes fit (see inset of Fig. 3.6), while below, pair-breaking causes a decrease. Thus, spin-fluctuation mediated superconductivity can explain the tunneling data, from which an $A_{1g}$ ($Y_{20}$ spherical harmonic $k_x^2 + k_y^2 - 2k_z^2$ with 2 lines of nodes about the $c$ axis) order parameter emerges. Of course, this measurement cannot rule out other mechanisms.

In brief, we have shown that a common belief in heavy fermion systems is that the superconductivity is mediated by antiferromagnetic spin fluctuations. Quantum oscillation observations confirm the heaviness of the itinerant $f$ electrons and give us a measure of the scattering time in the superconducting state. From the NMR relaxation rate, lines of nodes on the Fermi surface are inferred, supported by SIN tunneling spectra, which in addition claim the absence of nodes on the $c$ axis. However, $c(T)$ suggests point nodes with a linear $k$-dependence. Furthermore the specific heat jump at $T_c$ and the temperature dependence of the penetration depth indicate conventional weak-coupling BCS superconductivity. We need another probe of the low energy excitations about the gap zeroes, and thermal conductivity is one such way to elucidate the gap structure.

# 4 The High-$T_c$ Superconductor $YBa_2Cu_3O_{7-\delta}$

Now that more than ten years have passed since the discovery of $YBa_2Cu_3O_{7-\delta}$ (Wu *et al.* 1987), most researchers agree on its singlet $d$-wave pairing state (an example of triplet pairing is $^3$He), but this only comes as a result of an intense rivalry between the $s$-wave and $d$-wave camps. In fact, when $YBa_2Cu_3O_{7-\delta}$ was celebrating its third year in the limelight, many believed that "the data as a whole... suggest[ed] that 's-wave' pairing [was] the most likely scenario" (Annett *et al.* 1990), though they did emphasize that it was still rather premature to draw any conclusions based on the existing data, then lacking reproducibility and accuracy.

Before becoming entangled in the details of the nature of the pairing state, we must first convince ourselves that electron or hole pairing, rather than some new and exotic mechanism, is indeed what causes superconductivity in the cuprates. Fortunately, there has been evidence for pairing ever since practically the beginning of the $YBa_2Cu_3O_{7-\delta}$ story.

By disturbing the trapped flux in a superconducting ring, it is possible to measure the change in magnetic flux of a system. In the case of a sintered $YBa_2Cu_3O_{7-\delta}$ ring, application of electromagnetic noise caused the flux to change in quantized steps of $\Phi = (0.97 \pm 0.04)hc/2e$, indicating a unit charge of $2e$ (Gough *et al.* 1987, Koch *et al.* 1987). Further evidence comes from point contact measurements. When an electron is injected at a point contact into a normal metal, upon reaching a metal-superconductor interface, it combines with an electron from the normal metal and forms a Cooper pair in the superconductor. This process of Andreev reflection leaves in the normal metal a hole of the opposite momentum and spin to that of the incident electron. Detection is in principle quite simple. Since the hole is of the opposite momentum, it returns to the point contact and contributes to the current, thereby reducing the contact resistance. If the incident energy is less than the superconducting gap energy $\Delta$, every incident electron leaves behind a hole, resulting in a factor of 2 reduction in the contact resistance; otherwise, i.e. if the incident energy exceeds $\Delta$, the electrons enter the superconductor as quasiparticles and no change occurs

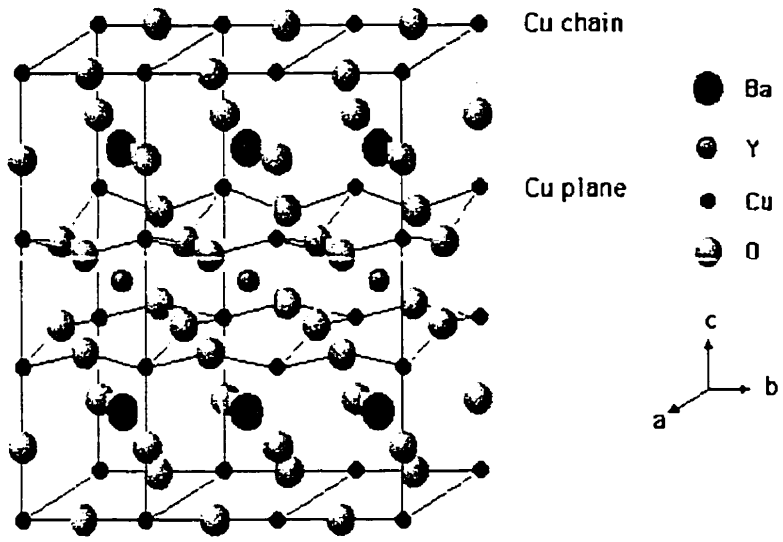


**Figure 4.1:** Structure of $YBa_2Cu_3O_{7-\delta}$ depicting three unit cells along the *b*-axis.

in the resistance. Thus this technique can measure $\Delta$, and moreover, the angular dependence of $\Delta(k)$ can be resolved by placing the contacts on different crystalline faces.

So very early on, it was established that Cooper pairs do indeed exist in *d*-wave superconductors, although the exact pairing mechanism is not known. For this reason, the BCS theory is applicable to the cuprates, since the same ingredients, namely electron/hole pairing and the presence of an energy gap, are responsible for superconducting state properties.

## 4.1 Crystal Structure

$YBa_2Cu_3O_{7-\delta}$ has a layered perovskite-like crystal structure (see Fig. 4.1) with lattice parameters $a = 3.8198(1)$ Å, $b = 3.8849(1)$ Å and $c = 11.6762(3)$ Å, giving a unit cell volume $V = 173.27$ Å$^3$. These give a molar volume $V_m = VN_A = 104.3$ cm$^3$/mol. There are two roughly tetragonal $CuO_2$ planes, spaced 8.3 Å apart, per unit cell (Akoh *et al.* 1990). In addition, there are one-dimensional CuO chains running along the *b*-axis, making conduction in the basal plane anisotropic. The presence of these chains complicate band structure calculations, and it is only because high quality, relatively large crystals can be grown that $YBa_2Cu_3O_{7-\delta}$ has become the high-$T_c$ representative.

The carriers are holes, and are believed to reside primarily in the $CuO_2$ planes, with the CuO chains acting as charge reservoirs to regulate the doping levels in the planes. Currently, the chains are under investigation as to whether they are superconducting intrinsically or due to their proximity to the superconducting $CuO_2$ planes. Positron annihilation experiments indicate that the effective mass in the chain band is much less than that in the plane band (Pankaluoto *et al.* 1994). This suggests that the electrons in the chains are not strongly correlated, and therefore not superconducting on their own.

What we mean by the electrons in these materials being strongly correlated is that the average interaction energy exceeds the average kinetic energy of the Cu d states. Electrons move through these orbitals by hopping to weakly correlated orbitals on neighbouring ions, such as the p orbital on oxygen ions. The 3d shell $Cu^{2+}$ contains one vacancy, which affects what happens when a cuprate is hole- or electron- doped.

To sum up, the $CuO_2$ planes are not exactly tetragonal, but orthorhombic due to the presence of the CuO chains along $b$. We therefore expect anisotropy in transport measurements due to this extra channel of conduction.

## 4.2 Phase Diagram

The strong correlations in these systems tend to drive them towards localized (insulating) electronic states. For instance, in $La_2CuO_4$, the $Cu^{2+}$ Coulomb repulsion leads to an insulating ground state, and superconductivity can only be achieved when the oxygen p bands are (hole) doped with $Sr^{2+}$ or $La^{3+}$.

In Fig. 4.2, we show the phase diagram of $YBa_2Cu_3O_{6+x}$ as a function of oxygen doping $x$. Between the antiferromagnetic and superconducting phases is a smeared out region often referred to as a spin glass. As it is difficult to prepare samples with $x \sim 0.4$, this area of the phase diagram has not been extensively studied. Above this fuzzy boundary, the appearance of chains along $b$ induces an orthorhombic crystal structure. The plateau around $x \sim 0.6$ is due to ordering in the chains.

One key feature in Fig. 4.2 is the proximity of the superconducting and antiferromagnetic states. This observation led to the SO(5) theory of superconductivity of Zhang (1997) which has a 5-component order parameter—3 for antiferromagnetism and 2 for superconductivity. Could high-$T_c$ superconductivity be mediated by antiferromagnetic spin fluctuations, as is assumed in the heavy fermions?

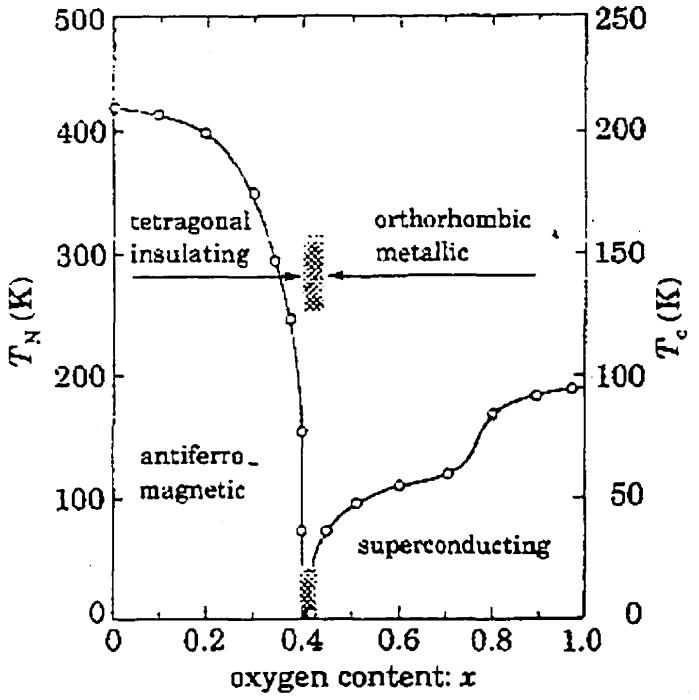


**Figure 4.2:** Doping phase diagram of $YBa_2Cu_3O_{6+x}$ showing Néel temperature $T_N$ or $T_c$ (after Rossat-Mignod *et al.* (1988)).

## 4.3 Normal State

Strongly correlated electrons lead to many interesting phenomena in the normal state. For instance, ions with localized orbitals can have magnetic moments large enough to lead to antiferromagnetic order. In the heavy fermions, antiferromagnetism can co-exist with superconductivity ($UPd_2Al_3$ and $UNi_2Al_3$), but this has never been found in any cuprate material.

In the normal state of $YBa_2Cu_3O_{7-\delta}$, there are several anomalous, non-Fermi liquid properties. First of all, the question of whether a Fermi surface even exists remains an open one. Secondly, the resistivity along $a$ is perfectly linear; along $b$, there is a slight upward curvature, as shown in Fig. 4.3. Recall that in Fermi liquids, $\rho \sim T^2$, so even in the normal state, $YBa_2Cu_3O_{7-\delta}$ violates our basic understanding of metals.

In the absence of a well-defined metallic ground state, the challenge is to understand the normal state, which is practically as complicated as the superconducting state. One approach is to vary the level of oxygen doping to study the evolution

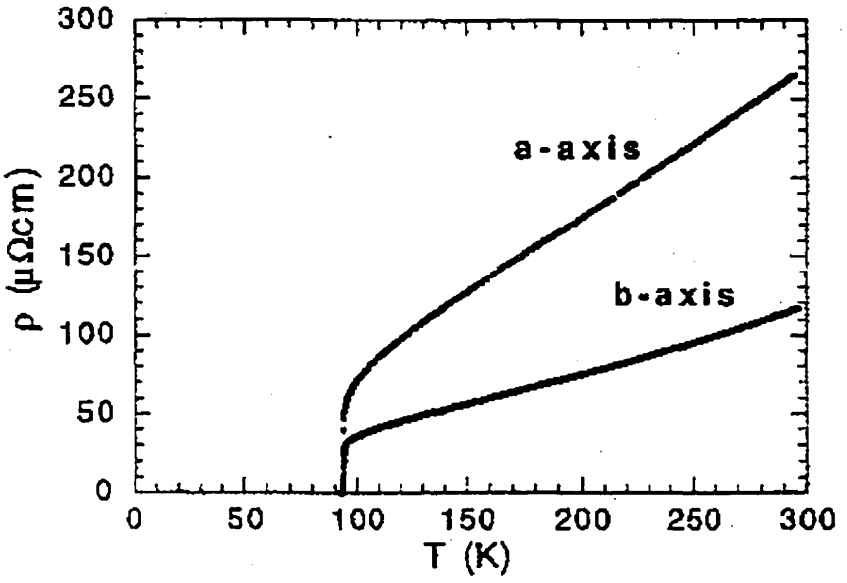


**Figure 4.3:** Resistivity as a function of temperature in $YBa_2Cu_3O_{7-\delta}$ for $a$ and $b$ axis samples.

of the metallic state from the insulating state. This has led to the discovery of a pseudogap above $T_c$.

### 4.3.1 Pseudogap

In the normal state of underdoped cuprates, several physical probes have detected a partial gap, called the pseudogap, at some temperature $T^*$ well above $T_c$. NMR measurements of the Knight shift in an underdoped superconductor first detected a decrease below a temperature $T^*$, which normally (in an optimally doped material) does not occur until $T_c$. This led Warren *et al.* (1989) to conclude that spin pairing was taking place in the normal state, thus producing a "spin gap". Many other measurements have since seen the pseudogap, such as the NMR relaxation rate $1/T_1$ (Takigawa *et al.* 1991), specific heat (Loram *et al.* 1993), $c$-axis conductivity (Homes *et al.* 1993), photoemission (Ding *et al.* 1996) and $ab$-plane resistivity (Bucher *et al.* 1993). In the latter, this suggests that the linear resistivity is due to spin fluctuation scattering of carriers, since below $T^*$ in underdoped materials this linearity is lost.

While the pseudogap does not exist in optimally doped or overdoped $YBa_2Cu_3O_{7-\delta}$, the fact that $T^*$ and $T_c$ meet at optimal doping $x$ on the phase diagram is intriguing, and the nature of their relationship could be very important

in understanding the mechanism for superconductivity in high-$T_c$ superconductors.

## 4.4 Superconducting State

Conventional superconductors (e.g. Al, Hg) have $s$-wave pairing states which have the full symmetry of the crystalline point group; unconventional pairing states used to describe $^3$He and $UPt_3$, for example, have a lower symmetry. Furthermore, the phase of the order parameter can serve as another distinguishing factor: for instance, the order parameter for the extended $s$-wave state does not change sign, whereas the $d$-wave does. Accordingly, there are many experiments which can help determine the symmetry of the order parameter and we now review the principal methods.

An extremely powerful phase-sensitive technique uses the double Josephson junction dc SQUID ring. A Josephson junction refers to the interface between two superconductors through which pairs can tunnel, even when there is *zero* voltage difference (Josephson 1962). Due to a phase difference $\Delta\phi$ between the superconductors, a zero voltage supercurrent $I_s = I_c \sin\Delta\phi$, where $I_c$ is the maximum critical current supported by the junction, can flow from one superconductor to another through an insulating barrier. Josephson also predicted that in the presence of a potential difference $V$ across the barrier, the phase difference would change as $d(\Delta\phi)/dt = 2eV/\hbar$. This means that we would have an ac current with frequency $\nu = 2eV/h$. In the following discussion, we use dc junctions and we refer to Fig. 4.4.

We start with a simple $d_{x^2-y^2}$ gap of $\cos(2\phi)$, where $\phi$ is the angle from the $x$-axis. If two Josephson contacts to the YBCO are rotated by $\frac{\pi}{2}$ in the $ab$-plane, the $\cos(2\phi)$ factor for the two junctions will differ by $\cos(\pi)$ = -1. From the relation $\Delta\phi = \frac{2\pi\Phi}{\Phi_0} (\mathrm{mod} 2\pi)$ (from Tinkham (1996, p.215)), we see that a $\pi$ phase shift changes the enclosed flux $\Phi$ by $\Phi_0/2$. Thus the lowest energy state of the ring now corresponds to one containing $\Phi_0/2$ of trapped flux, instead of zero flux. Consequently, in an external magnetic field, allowed states will correspond to those with half-integer fluxoid quantum numbers. Recent scanning SQUID microscope studies which have observed half-integral flux quantization (Tsuei *et al.* 1994, Mathai *et al.* 1995). Mathai and co-workers used a junction similar to that described in Fig. 4.4 and found half quanta of trapped flux. In the work of Tsuei and co-workers on three-junction and two-junction rings on $YBa_2Cu_3O_{7-\delta}$ film (where twin boundaries give the $\pi$ phase shift), they found half integer quanta of trapped flux in the first case and

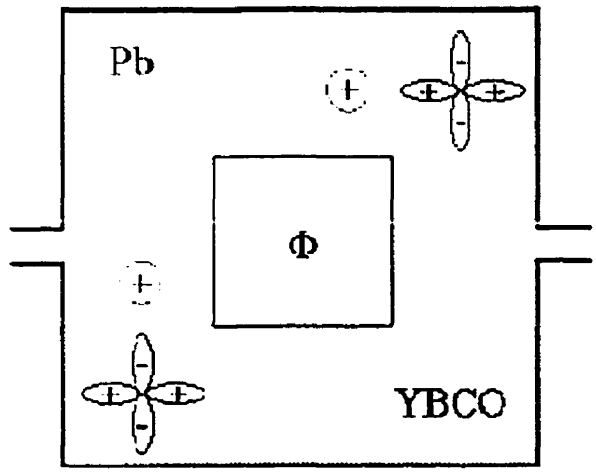


**Figure 4.4:** Superconducting SQUID ring composed of Pb and $YBa_2Cu_3O_{7-\delta}$ films. The two Josephson junctions are located at the interfaces of the two materials, and are phase shifted by $\pi$. Thus the ring traps half-integral quanta of flux.

integer quanta in the second. Such experiments undoubtedly provide the strongest evidence to date for the *d*-wave picture.

Another indication of unconventional superconductivity came from nuclear magnetic resonance (NMR) studies of the nuclear relaxation rate $1/T_1$. Experimental $1/T_1$ results in $YBa_2Cu_3O_{7-\delta}$ differ markedly from those in BCS superconductors, namely in the low temperature power law behaviour (consistent with *d*-wave) and in the absence of the Hebel-Slichter peak just below $T_c$. The latter is very well understood within BCS theory to be due to the singular peak in the DOS just above the gap and the BCS coherence factors. This suggests that radical changes to the coherence factors would have to be made in order to use the framework of BCS to explain the simple drop in $1/T_1$ below $T_c$. Moreover, in conventional superconductors, the Knight shift (which measures uniform spin susceptibility) is temperature independent in the normal state, and drops below $T_c$ when the spins pair into singlet Cooper pairs. In the cuprates, this drop also occurs, but much slower than the exponential behaviour seen in BCS superconductors; rather, the drop follows a power law, consistent with *d*-wave pairing.

Several other experiments have also fortified the *d*-wave picture, such as tunneling conductance, angular resolved photo-emission and muon spin resonance. For a review,

see that of Maple (1998). We believe there is little doubt that the order parameter for $YBa_2Cu_3O_{7-\delta}$ is $d$-wave. Below we examine in detail the experiments which have a direct bearing on thermal conductivity, and with which we will compare our results to see if a consistent *quantitative* description of the superconducting state properties of $YBa_2Cu_3O_{7-\delta}$ emerges.

### 4.4.1 Specific heat

The specific heat $c(T)$ in the $T \to 0$ limit provides a direct probe of the quasiparticle DOS near the Fermi level $\varepsilon_F$. Unfortunately, it also probes all other excitations. Phonons and ferromagnetic magnons may contribute $T$, $T^2$ and $T^3$ terms, while antiferromagnetic magnons may contribute $T^{1/2}$, $T$ and $T^{3/2}$ terms. Schottky anomalies usually give a $T^{-2}$ dependence, as does the nuclear moment. Amidst all these excitations, one must isolate the electronic part of $c/T$, which is proportional to $N(\varepsilon)$ averaged over an interval $\sim k_BT$ around $\varepsilon_F$. To further complicate matters, there exists an additional linear term which is sample dependent, perhaps attributable to $BaCuO_2$ (flux) (Alain Junod (1990), and references therein). This term decreases when twins are removed or when oxygen is added (Moler *et al.* 1997).

In $s$-wave superconductors where the excitation spectrum is fully gapped, the electronic specific heat is vanishingly small. For $d$-wave symmetry, the gap vanishes linearly at the nodes on the Fermi surface, so the $k$-space average of the DOS goes as $N(\varepsilon) \propto |\varepsilon|$: hence for electrons, $c/T = \alpha T$ for gaps which vanish linearly at the Fermi surface, which also occurs for $s$+$d$ mixing. The coefficient of the $T^2$ term is (Kopnin and Volovik 1996, Kübert and Hirschfeld 1998a)

$$\alpha = \frac{18\zeta(3)}{\pi}\frac{k_B^3}{\hbar^2}\frac{1}{v_F v_2} \tag{4.1}$$

where $v_F$ and $v_2$ describe the quasiparticle excitations as described in Section 2.1.3, and $\zeta(n)$ is the Riemann sum, with $\zeta(3) = 1 + 2^{-3} + 3^{-3} + \ldots \simeq 1.3$. In zero field, one thus obtains the product $v_F v_2$.

Several measurements of $c(T)$ claim to see the $T^2$ term, so that fits are usually of the form

$$c(T) = A_2/T^2 + \gamma(0)T + \alpha T^2 + \beta T^3, \tag{4.2}$$

even when the data look linear. The data of Moler *et al.* (1997) are consistent with both a small or zero value of $\alpha$. Plotted vs $T^2$, the upturn would tend to cancel out the $T^2$ term, so it was concluded that the latter was not resolvable. More recently, samples with a reduced number of paramagnetic centres (and hence less of an upturn) were measured to try to bring out the $T^2$ term (Wright *et al.* 1999). Now a slope is apparent in a plot of $c/T$ vs $T$, and the fitted $\alpha$ is 0.064 mJ $K^{-3}$ $mol^{-1}$. By further increasing sample quality, the Geneva group has obtained specific heat data which requires no fitting at all (Alain Junod 1999). Thus their measurement of $\alpha = 0.19$ $K^{-3}$ $mol^{-1}$ we consider the most reliable, though their crystal is fully oxygenated in order to achieve such a low level of defects so we cannot make a direct comparison. Specific heat is also a good diagnostic tool in the presence of a magnetic field, which will be discussed in Section 4.5.2.

### 4.4.2 Microwave conductivity and the London penetration depth

This section describes the microwave experiments used to probe thermally excited quasiparticles. In particular, the temperature dependence of the penetration depth $\lambda(T)$ and charge conductivity $\sigma(\omega, T)$ have both helped to establish the $d$-wave state as being the appropriate state for $YBa_2Cu_3O_{7-\delta}$. As we shall see, these two quantities give direct measures of the quasiparticle parameters $v_F$ and $v_2$, so any theory describing $\lambda$ and $\sigma$ had better apply to $\kappa$ as well.

In a surface impedance measurement at microwave frequencies, a planar sample is placed in an axial field, say along $b$, so that a current develops along $a$ (and even along $c$, though for thin crystals this effect is negligible). The study of the complex surface impedance has illuminated a number of electromagnetic properties of $YBa_2Cu_3O_{7-\delta}$. Early measurements of a linear temperature dependence in the penetration depth $\lambda(T)$ by Hardy *et al.* (1993), obtained from the imaginary part of the surface impedance, were among the first evidence for nodes in the gap function. From the real part of the surface impedance, $R_s$, one obtains the real part of the charge conductivity by thermally excited quasiparticles.

In weak coupling BCS theory, charge conductivity is activated at low temperature due to the presence of an energy gap, as is the temperature dependence of the London penetration depth, which provides information on the superfluid density responsible for the screening of electromagnetic fields. Should the gap exhibit line nodes on the Fermi surface, it is expected that the temperature dependence of the

penetration depth is that of a power law, rather than exponential (Annett *et al.* 1991). Thus conventional and unconventional pairing states lead to qualitatively different $T$-dependences which experiments can easily differentiate.

For short coherence length superconductors like $YBa_2Cu_3O_{7-\delta}$, which guarantees the local electrodynamic limit $\xi_0 \ll \lambda$, the low frequency ($\omega\tau \ll 1$) complex conductivity is given by (Bonn and Hardy 1996)

$$\sigma(\omega, T) = \sigma_1(\omega, T) - \frac{i}{\mu_0 \omega \lambda^2(T)}. \tag{4.3}$$

At low temperature, a Drude-like peak in $\sigma_1(\omega)$, centred at $\omega = 0$, will have a width which can be interpreted as the quasiparticle lifetime.

In the local limit, the conductivity is related to the surface impedance $Z_s = R_s + iX_s$, where $R_s$ is the surface resistance and $X_s$ is the surface reactance, by

$$X_s(\omega, T) = \mu_0 \omega \lambda(T) \tag{4.4}$$

$$R_s(\omega, T) = \frac{\mu_0^2}{2} \omega^2 \lambda^3(T) \sigma_1(\omega, T). \tag{4.5}$$

Thus $X_s$ gives a measure of the superfluid density $\frac{\rho_s(T)}{\rho_s(0)} = \frac{\lambda^2(0)}{\lambda^2(T)}$ responsible for screening the microwave fields and $R_s$, governed by the absorption by the normal fluid within $\lambda$ of the surface, gives a measure of the normal fluid density. The surface resistance is a bit complicated, but at low temperature, $R_s$ can be described as the absorption of microwaves by quasiparticles ($\sigma_1(\omega, T)$) within a shallow depth ($\omega^2\lambda^3$).

Unfortunately, the absolute value of $\lambda(T)$ cannot be determined by the microwave technique since precision measurements require that only shifts in the frequency can be detected. By comparing with the penetration depth at some reference temperature, one can measure the temperature dependence of $\delta\lambda(T) = \lambda(T) - \lambda(1.2\ K)$. Then by taking $\lambda(1.2\ K)$ from another measurement, usually far infrared reflectivity, one obtains the desired superfluid fraction in the previous paragraph. Ideally, $\lambda(1.2\ K)$ should be determined in similar conditions as $\delta\lambda(T)$.

We can relate $v_F/v_2$ to the temperature dependence of the London penetration depth. Within a formulation based on well-defined quasiparticles (well-defined in the sense that they are formed by the constructive interference of particle- and hole- like excitations) in the superconducting state, Xu *et al.* (1995), Lee and Wen (1997) and Millis *et al.* (1998) have found a simple expression for the temperature dependence

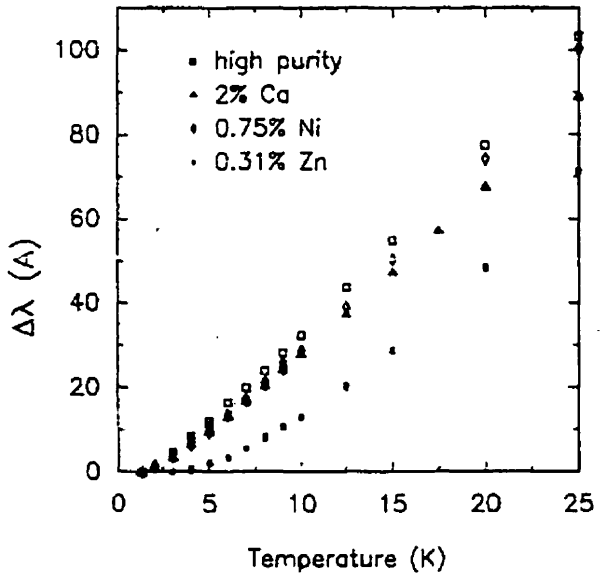


**Figure 4.5:** The temperature dependence of the penetration depth of $YBa_2Cu_3O_{7-\delta}$, pure and doped, after Bonn *et al.* (1995). Notice the linear behaviour in the pure sample (squares) evolves with Ca and Ni doping and reaches $T^2$ behaviour with Zn.

of the superfluid density $\rho_s$:

$$\frac{\rho_s(T)}{m^*} = \frac{\rho_s(0)}{m} - \frac{2\ln 2}{\pi\hbar^2} n(\frac{v_F}{v_2}) k_B T \tag{4.6}$$

where $m$ is the mass of the carriers, $n$ is the number of $CuO_2$ planes per unit cell and $\lambda(T) = \lambda(0) + \delta\lambda(T)$, where $\lambda(0)$ is the zero temperature value. Now since

$$\frac{\rho_s(T)}{m} = \frac{c^2}{4\pi e^2} \frac{1}{\lambda^2(T)}. \tag{4.7}$$

we can relate the derivative of $\rho_s(T)$ at $T = 0$ to $\delta\lambda(T)$, which is the more direct measurement:

$$\frac{1}{\lambda^3(0)} \frac{\delta\lambda(T)}{T} = 4\ln 2 \frac{k_B e^2}{\hbar^2 c^2} n(\frac{v_F}{v_2}). \tag{4.8}$$

Thus we have another way of measuring the ratio $v_F/v_2$.

In high purity samples of $YBa_2Cu_3O_{6.95}$, $\delta\lambda(T)$ is indeed linear (Hardy *et al.* 1993), evident in Fig. 4.5. This is in contrast to previous measurements on thin films and lower quality crystals which yielded $T^2$. Hardy and co-workers also measured a

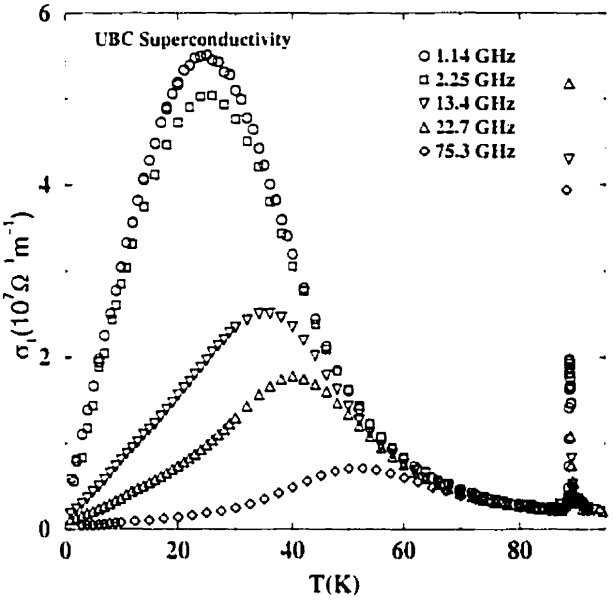


**Figure 4.6:** The real part of the charge conductivity $\sigma_1(\omega, T)$ at five different frequencies (after Hosseini *et al.* (1998b)). Note that the peak below $T_c$ is reminiscent of that in $\kappa(T)$ (Fig. 7.2).

sample of $Pb_{0.95}Sn_{0.05}$ and found a very weak temperature dependence below about $0.4T_c$, which is consistent with the $s$-wave scenario.

Another important property is the charge conductivity $\sigma_{00}$. Moreover, the Wiedemann-Franz law connects $\kappa_{00}/T$ and $\sigma_{00}$, which was already shown in Section 2.1.3. Surface resistance measurements of undoped $YBa_2Cu_3O_{7-\delta}$ show a linear $T$ dependence at low temperature (Zhang *et al.* 1994). The $T = 0$ extrapolations yield $\sigma_{1a} = (0.45 \pm 0.15) \times 10^6\ \Omega^{-1}m^{-1}$ along $a$ and $\sigma_{1b} = (0.7 \pm 0.2) \times 10^6\ \Omega^{-1}m^{-1}$ along $b$, at 34.8 GHz. For $YBa_2(Zn_xCu_{1-x})_3O_{7-\delta}$ with 0.15% Zn, the real part of the conductivity as $T \to 0$ is $\sigma_{1a} = (0.64 \pm 0.20) \times 10^6\ \Omega^{-1}m^{-1}$ and $\sigma_{1b} = (1.8 \pm 0.5) \times 10^6\ \Omega^{-1}m^{-1}$ at 22.9 GHz (Hosseini *et al.* 1998a). The errors are due to the $\lambda_0^3$ appearing in $\sigma_1$ and also due to the fact that the numbers are nearing the resolution limit. Within the generous error bars, the $a$-axis values do agree, suggesting universal transport, though not convincingly. The true power of this technique comes to light at higher temperature, where different scattering mechanisms may be studied.

Below $T_c$, $\sigma_1$ has a peak (just as $\kappa$) attributed to the competing effects of the collapsing quasiparticle DOS and inelastic scattering rate, where the latter "wins". At the peak, however, the scattering time reaches a limit set by (elastic) impurities, so that down to zero temperature the decreasing DOS gives us the overall decrease,

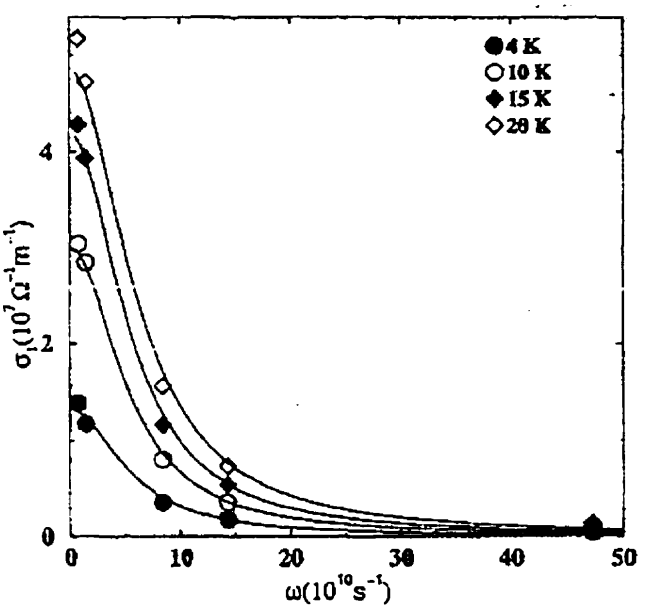


**Figure 4.7:** The real part of the charge conductivity $\sigma_1$ vs microwave frequency $\omega$ for fixed temperatures between 4-20 K (after Hosseini *et al.* (1998b)). While at low frequency the lineshape is not exactly Drude-like, the fit is close enough that it is possible to extract a scattering time $\tau$ from the linewidth. Notice that $\sigma_1$ is linear at low temperature.

though not to zero but a finite value. It is actually possible to determine the elastic scattering time in a spectroscopic study. By performing surface resistance measurements at several frequencies, Hosseini, Bonn and co-workers have found that $\sigma_1(\omega)$ at low temperature does have a Drude-like lineshape. Below 20 K, the width has a nearly temperature independent value of 8 GHz (as seen in Fig. 4.7), which means a very long quasiparticle scattering lifetime of $2\times10^{-11}$ s, evident in Fig. 4.8. For $v_F = 1 \times 10^7$ cm/s (Lee and Wen 1997), this means a quasiparticle mean free path of 2 $\mu$m!

One main advantage charge conductivity has over thermal conductivity is that the signal is purely electronic, so we can actually see the temperature dependence of the quasiparticles. Measurements show that the surface resistance (or $\sigma_1$) below 30 K is linear (Fig. 4.6). This indicates one serious flaw in the theory, for a $T^2$ dependence is the predicted behaviour for a pure crystal (Hirschfeld and Putikka 1996). In a Zn-doped crystal, a $T^2$-dependence does emerge, while Ni-doping induces an upward curvature which is not quite $T^2$. At low frequencies, the temperature dependence actually becomes sub-linear for a pure crystal. For these reasons, Hosseini and co-workers have chosen to compare results obtained in high purity (better than 99.99%)

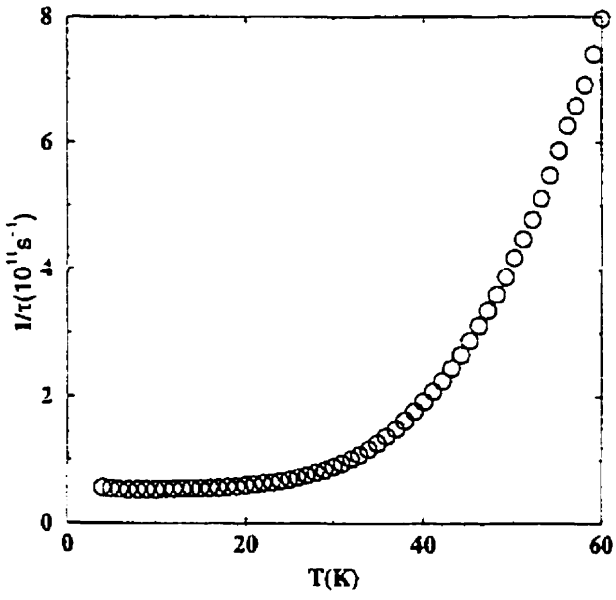


**Figure 4.8:** $1/\tau$ vs $T$ extracted from the $\sigma_1(\omega)$ data of Hosseini *et al.* (1998b) by interpreting the linewidth as the lifetime of the quasiparticles. Notice that the elastic scattering rate is roughly constant below about 20 K.

with calculations in the weak scattering or Born limit.[4] Qualitatively, Born scattering causes $\sigma_1(T)$ to rise rapidly from its universal value $\sigma_{00}$ to some large value and to remain roughly independent of temperature until inelastic scattering effects become important. As for the frequency dependence, $\sigma_1(T)$ in the Born limit does predict a sub-linear to super-linear behaviour with increasing $\omega$. We do point out that while this appears consistent with the measurements, there could be non-local effects at high frequencies when $\lambda$ develops a frequency dependence, which would then produce some effective $\tau$ which is not impurity dominated (Waldram *et al.* 1997).

We have shown in this section that the linear temperature dependence of the penetration depth is a consequence of $N(E) \sim E$, so that $\delta\lambda(T)$ is also described by $v_F$ and $v_2$. While the linear penetration depth supports $d$-wave theory, there remains a problem with the predicted $\sigma_1 \sim T^2$, casting some doubt as to whether the assumption of unitarity scattering is correct. The frequency dependence of $\sigma_1$ indicates that below 20 K, elastic scattering has hit the impurity limit, with a mean free path of 2 $\mu$m, or a scattering time of $2\times10^{-11}$ s (scattering rate $\Gamma = 1/(2\tau) =$

[4]These are indeed the "second generation" crystals grown in $BaZrO_3$ (Liang, Bonn and Hardy 1998). To avoid clustering of oxygen vacancies, the crystals were oxygenated to $7 - \delta = 6.993$ and thus almost free of defects.

$0.002T_c$). From the anisotropy $\sigma_{1b}/\sigma_{1a} = 1.5 - 2.8$, we expect a similar anisotropy in $\kappa_b/\kappa_a$.

### 4.4.3 Infrared reflectivity

Optical properties of superconductors can provide a wealth of information, particularly concerning energy gaps and scattering rates. Roughly speaking, the $ab$-plane optical properties of high-$T_c$ superconductors follow those of a metal in which charge carriers move coherently through the lattice. It is this coherent motion which accounts for the zero frequency Drude peak in the conductivity. The width of the peak has been interpreted as the inverse lifetime of the carriers.

Using infrared reflectivity, one can directly measure the reflectance $R(\omega)$, absorption $(1 - R(\omega))$, surface impedance $Z(\omega)$ and transmission $T(\omega)$. These provide information on microscopic properties such as the conductivity $\sigma(\omega) = \sigma'(\omega) + i\sigma''(\omega)$ and the dielectric function $\epsilon(\omega) = \epsilon'(\omega) + i\epsilon''(\omega)$, where $\epsilon'' = 4\pi\sigma'/\omega$. However, extracting useful quantities from $R(\omega)$ can be quite involved, and one often relies on Kramers-Kronig analysis—when one quantity is known over a large frequency range, the other can be obtained via an integration over all frequencies. [5] Alternatively, it is possible to fit $R(\omega)$ to $(\frac{\sqrt{\epsilon}-1}{\sqrt{\epsilon}+1})^2$ and use the assumption that

$$\epsilon(\omega) = \epsilon_D + \epsilon_e + \epsilon_\infty \tag{4.9}$$

where $\epsilon_D$ is from the Drude model, $\epsilon_\infty$ is some known constant background term and $\epsilon_e$ is given by

$$\epsilon_e = \frac{\omega_p^2}{\omega I(\omega) - \omega^2 - i\omega\Gamma(\omega)} = \epsilon_e' + i\epsilon_e'' \tag{4.10}$$

which can be arranged to give

$$\Gamma(\omega) = \frac{\omega_p^2}{\omega}\frac{\epsilon_e''}{(\epsilon_e'^{\,2} + \epsilon_e''^{\,2})} = \frac{\omega_p^2}{\omega} Im(1/\epsilon_e). \tag{4.11}$$

Without getting into too many details, we show a "recipe" for extracting the frequency dependent scattering rate $\Gamma(\omega)$, courtesy of Timusk (1995).

[5] For example: $r = \sqrt{R}e^{i\theta}$, $\theta(\omega) = \frac{\omega}{\pi}\int_0^\infty d\omega' \frac{lnR(\omega') - lnR(\omega')}{(\omega^2 - \omega'^2)}$. Then $\epsilon' = f_1(R,\theta)$ and $\epsilon'' = f_2(R,\theta)$.

1. Obtain $\epsilon(\omega)$ from $R(\omega)$

2. Subtract $\epsilon_D$ and $\epsilon_\infty$

3. Get $\epsilon_e'' = 4\pi\sigma/\omega$

4. Kramers-Kronig transform $\epsilon_e''$ to get $\epsilon_e'$ and therefore $\epsilon_e$

5. Calculate $\Gamma(\omega)$ from Eq.(4.11)

Experimental $1/\tau(\omega)$ measurements of optimally doped $YBa_2Cu_3O_{7-\delta}$ with $T_c$=93.5 K at 95 K show a linear temperature dependence at high frequency (Puchkov, Basov and Timusk 1996). By fitting the range 900-3000 $cm^{-1}$, the zero frequency extrapolation is $\Gamma_0 = 1280$ K or over $10T_c$, which is enormous compared to other estimates. This large discrepancy can be explained given that $\Gamma = \Gamma(\omega)$ as soon as the energy departs from zero. Moreover, FIR experiments usually start at 30-50 $cm^{-1}$, or about 43-72 K. This is a significant proportion of $\Delta_0$ (about 200 K)! Recall that for strong scattering in the unitarity limit the scattering rate is predicted to be temperature dependent (Gross *et al.* 1986, Prohammer and Carbotte 1991, Hirschfeld, Putikka and Scalapino 1994) (Fig. 2.7). So for $\omega/\Delta_0 \simeq 0.3$, $1/\tau$ is 10 times smaller than at zero energy. In this respect, we really should be comparing with other measurements in the gapless regime, well below 10 K.

## 4.5 Vortex State

In the vortex state, there are two natural regions of interest: within the cores and between the cores. In type-II BCS superconductors, Caroli, de Gennes and Matricon (1964) showed that bound states within the cores have an energy level spacing $\Delta\varepsilon \approx \Delta^2/\varepsilon_F$, comparable to the energy level spacing of a particle in a box of size $\xi_0$. Now in $YBa_2Cu_3O_{7-\delta}$ where $\xi_0$ is of order 10 Å, $\Delta\varepsilon$ can be comparable to $\Delta$, so that there may be only one bound state or so. However, in conventional superconductors, $\Delta\varepsilon$ can be as small as $10^{-4}\Delta$ so that the excited states are essentially gapless (Tinkham 1996). Far from the cores, Volovik (1993) has shown that the extended states become populated. We now look closer at what experiments can tell us about bound vs extended states in $YBa_2Cu_3O_{7-\delta}$.

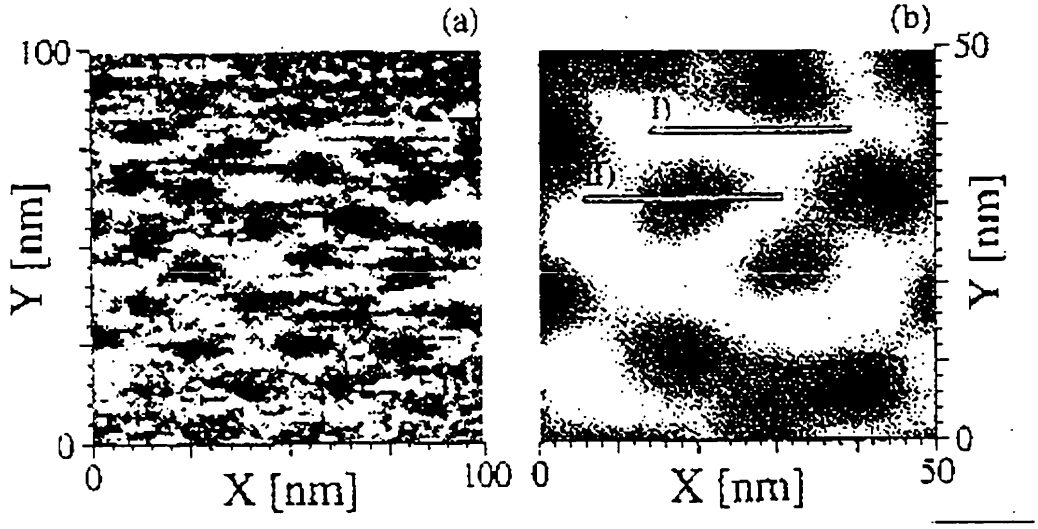


**Figure 4.9:** STM image of the vortex lattice of $YBa_2Cu_3O_{7-\delta}$ taken at $T$=4.2 K and $H$=6 T by Maggio-Aprile *et al.* (1995). (a) 100×100 nm$^2$ scan-area, raw data. (b) 50×50 nm$^2$ scan-area, filtered data.

### 4.5.1 Scanning tunneling spectroscopy (STS)

We introduce vortex state experiments with an STM image of the vortex lattice in Fig. 4.9, produced at 4.2 K in 6 T applied along $c$ (Maggio-Aprile *et al.* 1995). Although the vortex lattice had been previously seen using the Bitter decoration technique (Dolan *et al.*, Vinnikov *et al.* 1989), it took another 8 years before the first STM image appeared. Part of the reason it took so long is related to the dead insulating layer which tends to form on the surface of $YBa_2Cu_3O_{7-\delta}$ crystals. In 1995, the so-called "second generation" $YBa_2Cu_3O_{7-\delta}$ crystals were born in $BaZrO_3$ crucibles (Erb, Walker and Flükiger 1995). $BaZrO_3$, a by-product of flux growth in yttria-stabilized zirconate crucibles, is inert to the highly reactive solvents used to grow $YBa_2Cu_3O_{7-\delta}$, so these new crystals are the purest to date, with improved surface quality.

This technique also has the advantage of probing the quasiparticle local density of states (LDOS) by tunneling. Outside the vortex cores, the tunneling spectra are essentially identical to those obtained in the Meissner state. As the tip approaches the centre of a vortex core, the 20 meV conductance peak (associated with the gap $\Delta$) decreases in magnitude before disappearing altogether in the middle of the core. What is remarkable in Fig. 4.10 is the appearance of low energy peaks in the core: bound states! These peaks are separated by 11 meV, in agreement with the

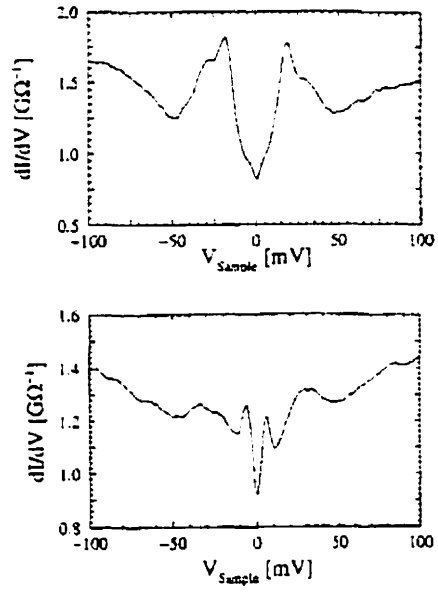


**Figure 4.10:** Tunneling spectra of $YBa_2Cu_3O_{7-\delta}$ at 4.2 K in zero field (top) and in 6 T (bottom) (after Maggio-Aprile *et al.* (1995)). For $H = 0$, we see the main peaks corresponding to $\Delta_0 = (20 \pm 0.02)$ meV. In field, there are two conductance peaks representing core states.

measured 9.5 meV from infrared absorption measurements, taken to be the lowest quasiparticle pair creation energy. Since the first excited state energy $\varepsilon_1 = \pm 5.5$ meV and $\varepsilon_2 = \pm 16.5$ meV, there can be at most 4 bound states considering $\Delta = 20$ meV (obtained by their spectra and in good agreement with the weak-coupling result $\Delta_0 = 2.14 k_B T_c = 17$ meV), although the $\varepsilon_2$ states were not seen.

### 4.5.2 Specific Heat

In Section 2.2.2, we showed the effect of an applied magnetic field on the density of states of a clean *d*-wave superconductor. This DOS enhancement can be probed by specific heat measurements. However, specific heat in a field contains contributions from many different excitations. Although phonons are not affected by the field, various other paramagnetic centres are, so that again there is the problem of multi-parameter fits as in zero field. Despite these complexities, measurements by Moler *et al.* (1997), Fisher *et al.* (1995) and Wright *et al.* (1996) all report the presence of this *d*-wave behaviour.

Before we get into the details of *d*-wave theory, we must point out that $\sqrt{H}$ behaviour has been seen in conventional *s*-wave superconductors. In Fig. 4.11, we

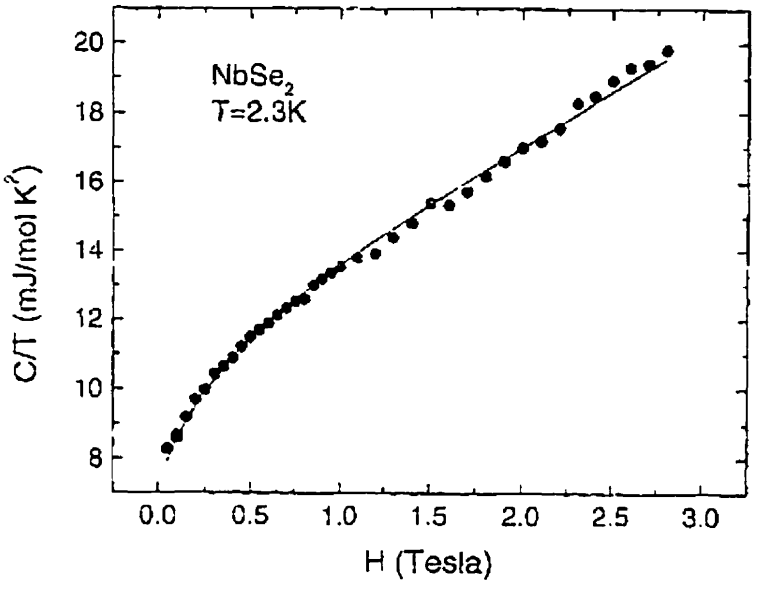


**Figure 4.11:** Field dependence of the specific heat of $NbSe_2$ obtained by Sonier *et al.* (1998). A fit to $\sqrt{H}$ appears to follow the data.

can see this sublinear $H$-dependence, which was at first puzzling, since bound core states are expected to give a linear $H$-dependence. Sonier *et al.* (1998) have explained this effect in terms of the changing core size with field.

Recall that in zero field, the clean limit quasiparticle specific heat is $\alpha T^2$. In field, a $\sqrt{H}$ dependence is predicted. From the DOS (Equation (2.33)), we can write down the field dependent specific heat as

$$\begin{aligned} \frac{c(T;H)}{T} = \gamma_\perp(H) &= \frac{\pi^2}{3} k_B^2 N(0;H) \\ &= \frac{8}{3}\frac{k_B^2}{\hbar}\frac{a}{v_2}\sqrt{\frac{H}{\Phi_0}}. \end{aligned} \tag{4.12}$$

Notice that a measurement of $c(T;H)$ will give $a/v_2$.

In Fig. 4.12, we see that an application of field does cause an increase in the specific heat of quasiparticles. Specific heat data are usually described by (Moler *et al.* 1997)

$$c(T,H) = [\gamma(0) + \gamma_\perp(H)]T + bT^3 + nc_{Schottky}(g\mu_B H/k_b T) \tag{4.13}$$

where the Landé $g$ factor is 2.0. The values of $\gamma(0)$ and $b$ are constrained by zero

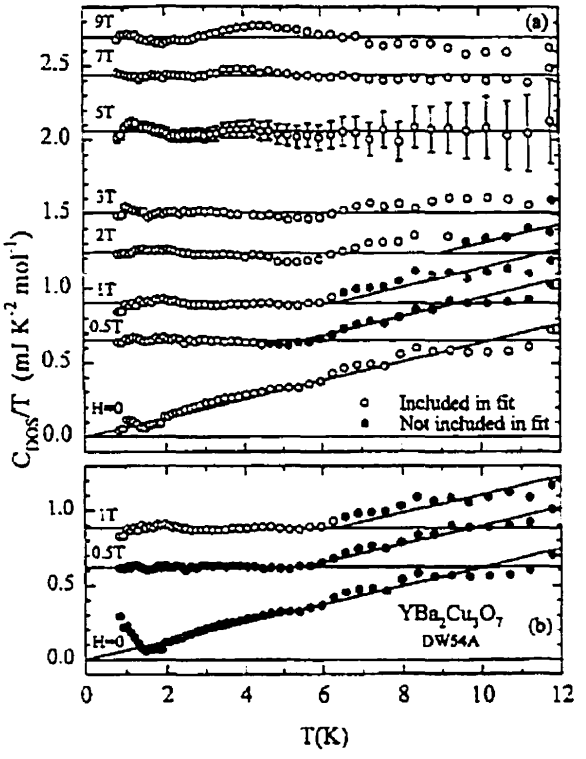


**Figure 4.12:** The quasiparticle specific heat measurement of Wright *et al.* (1999) showing a growing intercept with field. Furthermore, there is evidence of a crossover from $T$ to $T^2$ behaviour.

field fits. Here, the term of interest, which corresponds to the field enhancement of the quasiparticle DOS, is $\gamma_\perp(H)$. By allowing a different value of $\gamma_\perp(H)$ at each field, Moler *et al.* (1997) have obtained $\gamma_\perp(H) = \mathcal{J}\sqrt{H}$, with $\mathcal{J} = 0.9$ mJ/(mol K$^2$ T$^{1/2}$). Wright *et al.* (1999) have found essentially the same value, 0.91 mJ/(mol K$^2$ T$^{1/2}$). Using this value of $\mathcal{J}$ in Equation (4.12), we get $v_2 = 2.2a\times10^6$ cm/s. We show an example of this $\sqrt{H}$-dependence in Fig. 4.13.

If we examine the data of Wright *et al.* (1999), plotted as $c/T$ vs $T$ in Fig. 4.12, we see that for $H = 0$, there is the characteristic $d$-wave $T$-linear behaviour, i.e. $c = \alpha T^2$. With a magnetic field, $c/T$ is flat, but then crosses over to a linear behaviour, with the crossover temperature increasing with field. When $k_BT < E_H$, we have $c/T \sim \sqrt{H}$, which crosses over to $c/T \sim \sqrt{H}T$ when $k_BT > E_H$. Thus we should be able to read $E_H$ off Fig. 4.12. At $H = 1$ T, the crossover temperature is about 6.3 K. By setting $k_BT(6.3K) = E_H(1T)$, we get $av_F$ equals $4.7\times10^6$ cm/s. We could take $v_F/v_2$ from microwave measurements and determine $a$, but the error is large so we will put all the pieces together in Chapter 7 when we have another measure of $v_F/v_2$ (from zero

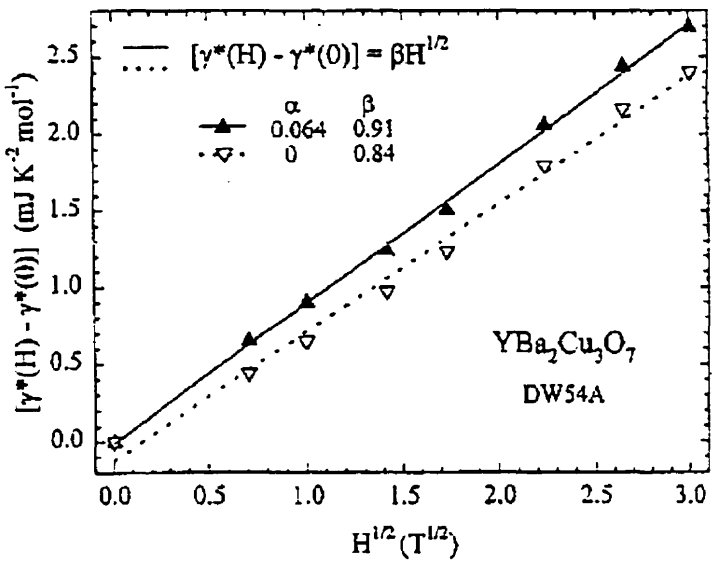


**Figure 4.13:** Field dependent $T$-linear coefficient plotted vs $\sqrt{H}$, after Wright *et al.* (1999).

field $\kappa_0/T$) and also $av_F$ (from in field $\kappa_0/T$).

Upon generalizing to finite temperature, Simon and Lee (1997) have predicted that thermodynamic and transport properties should obey scaling relations with respect to the variable $T/\sqrt{H}$. Recent work by Kübert and Hirschfeld (1998a) show a breakdown of scaling when the impurity band width $\gamma$ becomes comparable to the average quasiparticle energy shift $E_H$ due to a magnetic field. In the dirty limit, the specific heat is predicted to have an $H \ln H$ field dependence rather than a $\sqrt{H}$. The low temperature data (Moler *et al.* 1997, Fisher *et al.* 1995) seem compatible with both forms.

Already, we see how complementary specific heat measurements are to thermal conductivity. Both are governed by the same parameters, so we are in a position to make a direct comparison between theory and the two measurements. Moreover we shall see whether the assumptions built into the current theory, namely that inelastic and vortex scattering of quasiparticles are negligible, are indeed reasonable.

# 5 Experimental Details

In this chapter we describe details of the experiments in a dilution refrigerator which can be inserted into a homogeneous magnetic field. Together, they can produce an environment of 15 mK in 15 T, although typical operation limits are 50 mK and 8 T for the measurements we describe.

## 5.1 The Cryomagnetic System

To probe the residual quasiparticle behaviour, it is necessary to cool the samples below 100 mK, so we use an Oxford Instruments Kelvinox 300 $^3$He-$^4$He dilution refrigerator (fridge) whose base temperature is 7 mK unloaded. With all the wiring and interference from a nearby radiofrequency (RF) antenna, experiments tend to start at 50 mK or higher. In order to access the 20 mK range, we have recently enclosed the system in a 100 dB shielded copper room; work on lower temperature thermometry is currently underway.

Although the $^3$He-$^4$He mixture is in a closed system and therefore constantly recycled, we do use roughly 25 litres of $^4$He (LHe) per day, so in order to keep the consumption of LHe at a minimum, there are two layers of insulation between the main $^4$He bath and the outside world. The Dewar consists of an outer vacuum chamber, a liquid nitrogen ($LN_2$) filled jacket and then the main bath, which holds 38 litres of LHe.

The principle of $^3$He-$^4$He dilution refrigeration was first proposed by H. London (1951) but it was only in 1965 that a University of Leiden group first built one that reached 220 mK. These days, commercial units are available which can easily go down to 2 mK. To go any lower, most apparatus include dilution refrigerators as a preparatory stage of cooling.

By pumping on $^4$He whose boiling temperature is 4.2 K, it is possible to reach 1.2 K, whereas with $^3$He, it is possible to reach 0.3 K due to its higher vapour pressure. However, by creating a mixture of the two, the millikelvin range becomes accessible. Below 0.86 K, phase separation occurs, with the lighter pure $^3$He phase floating on top of the dilute phase, so-called because the 6.4% $^3$He is "diluted" in

an inert superfluid bath consisting of the 93.6% $^4$He. It is owing to this miscibility that the whole process is possible. Why should $^3$He want to be in the lower $^4$He rich phase? In this phase, the $^4$He are closer together than the $^3$He atoms are in the $^3$He rich phase, due to the higher zero point motion of the lighter $^3$He. So in other words, the $^4$He atoms are closer to each other. This means that for a $^3$He atom in the dilute phase, it is closer to its $^4$He neighbour and therefore its binding energy is larger—this is the energy required to remove an atom from the liquid phase into vacuum. Moreover, when $^3$He crosses the phase boundary into the dilute phase, the change in enthalpy is positive so that the temperature of the mixture *decreases*. By removing $^3$He from the dilute phase, more $^3$He will cross the boundary and further cooling results. This is accomplished by pumping on the still, in which the dilute phase is heated to roughly 0.7 K, at which temperature the vapour pressure of $^3$He is about 1000 times higher than that of $^4$He, so that $^3$He is distilled and circulated.

In practice, the dilution refrigerator is extremely efficient. Let us trace the circulation of $^3$He from the two storage dumps maintained at room temperature. When first cooling down, the gaseous mixture goes into two $LN_2$-cooled traps at 77 K to remove impurities like nitrogen and oxygen before being further purified by the main bath, which traps hydrogen and other light gases. From this point onward, a vacuum held by the inner vacuum chamber (in which the samples are located) isolates everything from the main bath. The gas now enters the condenser, which is in thermal contact with the 1 K pot, fed by the main bath through a needle valve and maintained at roughly 1 K, as the name suggests. The high impedance of the condenser causes the mixture to liquify before passing through a series of heat exchangers into the mixing chamber, in which phase separation occurs. At the same time, some of the dilute phase is going up into the still via the same heat exchangers, thereby cooling the incoming liquid. From the still, $^3$He is pumped away by a roots pump backed by a sealed rotary pump. Once the dynamical equilibrium is achieved, only the $^3$He is circulated and one gets continuous cooling of the mixing chamber.

The entire fridge can be inserted into a commercial 15 T superconducting magnet. At the temperature of the main bath of 4.2 K, the quench field of the magnet is 13 T. In order to obtain 15 T, it is necessary to further cool the magnet. Of course one could pump directly on the main bath, but in this case brute force is neither necessary nor particularly desired! Instead, one can use a lambda-point refrigerator ($\lambda$-fridge), which is a toroidal coil that can be fed by the main bath via a needle valve. By

pumping on this small volume of $^4$He. the surrounding bath cools and the cooler helium sinks to the bottom of the bath. This cooling process continues until the helium reaches 2.17 K. the lambda-point at which $^4$He becomes a superfluid. Further cooling pushes the superfluid boundary up to the top of the $\lambda$-fridge so that the bath around the magnet is cool enough to sustain a current of 100 A. supplied by a PS-120-10 power supply from Oxford Instruments.

For sensors or experiments which are sensitive to a magnetic field. there is a cancellation field which produces a zone of zero field about the mixing chamber. This is where we keep our main thermometer. a calibrated Ge resistor from Lakeshore.

Before commencing with an experiment. we must filter all the wires going into the fridge: otherwise. parasitic capacitance would heat up the sensors and give false readings. To this end. we have constructed filter boxes for the three connectors. These Al boxes hold capacitive-inductive filters from Spectrum Control with an attenuation of 20 dB (70 dB) at 3 MHz (1 GHz) which rid the higher frequency RF noise. The effect of the filters is most pronounced on the Ge sensor: for example. at 50 mK. removing the filter causes the Ge to immediately heat up to at least 100 mK. We also use a low-pass filter on the current going into the heater.

## 5.2 Thermal Conductivity: The Technique

In principle. the steady-state one heater. two thermometer technique employed to measure thermal conductivity is very simple (refer to schematic diagram in Fig. 5.1): however. complications arise from working at low temperature with samples of moderate thermal resistance.

A typical sample mount is 30 mm by 30 mm. on which we fit (a) a copper sample holder known as the "tongue". (b) a heater. (c) two thermometers and (d) 2×14 contact pads for wires:

(a) the sample holder is a thin plate of copper of sides 8 mm (plus protrusion on one side for the sample) and thickness 1 mm. with a 4 mm clear drilled in the centre so that an M4 brass screw can be used to establish good thermal contact with the mount. to which metallic samples are attached by solder and others by silver epoxy:

(b) the heater is simply a resin-embedded strain gauge from Micro-Measurements–prized for its lack of temperature and field dependence–which we heat resis-

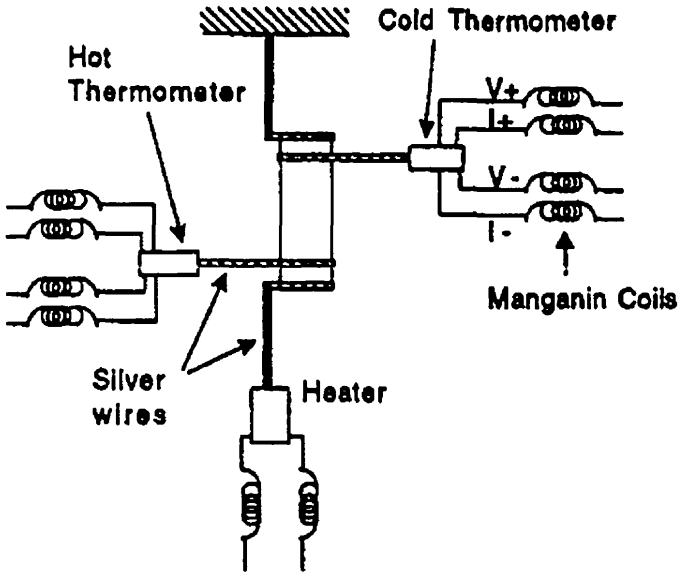


**Figure 5.1:** A schematic diagram of a thermal conductivity mount, adapted from Lambert (1998). The coils on the heater are made of Nb-Ti superconducting wire.

tively (order 0.3 nW power at 100 mK) by passing a current from a current source:

(c) each thermometer is a 1 kΩ $RuO_2$ resistor available in bulk from Dale, which we calibrate *in situ* against a calibrated Ge sensor *for each measurement*:

(d) the thermal conductivity measurement takes ten wires: two for the heater and four for each thermometer: the remaining four wires are for the resistivity measurement using the same contacts.

Before getting any further we must first construct miniature mounts for the heater and thermometers. The heater, or strain gauge, is glued with GE varnish to a 2×3 $mm^2$ piece of Cu foil: underneath the foil, there is a non-superconducting contact to which a 100 $\mu$m Ag wire from the sample is soldered. Mounting the thermometers is a bit more involved since we have to heat-sink the wires to make sure we are not heating the sample by measuring it. This is accomplished by constructing a 2×3×1.5 $mm^3$ rectangular base with a cylindrical extension 1.5 mm in diameter and 2.5 mm long around which to wrap wires: we apply a layer of Ecobond 286 epoxy and tissue paper between the rectangular face and the $RuO_2$ chip, having first sanded the wraparound contacts from the sides and bottom. Then one 40-gauge Cu wire from

a twisted pair is soldered to each of the two contacts on the $RuO_2$ chip, wrapped around the cylindrical part and soldered to two contact pads on the side of the rectangular base; the twisted pairs are brought into thermal contact with the Cu by GE 7031 varnish. Additionally, there is a 100 $\mu$m Ag wire soldered to the bottom of the rectangular base using non-superconducting solder to bring the thermometer and mount in thermal equilibrium with the sample. Finally, there is a thin Vespel post (made by DuPont, chosen for its poor heat conductivity) to hold the thermometer at sample height. Note that the wires were carefully selected to have high thermal resistances compared to the sample so that all the heat will go through the sample.

Now that we have the components, we can assemble a sample mount. The thermometer mounts are held in place by GE varnish on the sample mount and are christened T+ and T- depending on proximity to the heater. To each of the two contact pads on the thermometer mount are soldered two coiled 50 $\mu$m Manganin wires, one for current and one for voltage, making four wires in total going to each thermometer. Next we plant the heater mount in much the same fashion, only the current to and from the heater is carried by two 50 $\mu$m superconducting NbTi wires 3 cm in length. There remains only to attach the Ag wires from the heater and thermometers to the silver wires on the sample for the thermal conductivity part of the measurement. As regards the resistivity, we attach a Ag wire to the wire between sample and heater as I+; similarly, one to the wire from sample and thermometer T+ as V+ and one to the wire from sample to thermometer T- as V-. In this case, I- is Earth.

Once the sample mount is ready, it can be attached to the "tail" of the fridge using three M3 brass screws. The tail is machined from one solid rod of Cu, with an M6 screw on one end which screws into the bottom of the mixing chamber of the fridge and a flat sample stage large enough to accommodate three thermal conductivity mounts at the other end. The cylindrical part of the tail has two cross-sectional slices along the length to reduce eddy current heating, which goes as (diameter)$^4$. For samples requiring zero magnetic field when the main magnet is on, there is a separate sample stage which can be mounted on the bottom of the mixing chamber, in the compensated zone.

To measure the thermal conductivity of a sample, we use a Stanford Research Instruments SR-850 lock-in amplifier to measure each thermometer and a Keithley 224 current source for the heater. Temperature control is accomplished by a TS-530

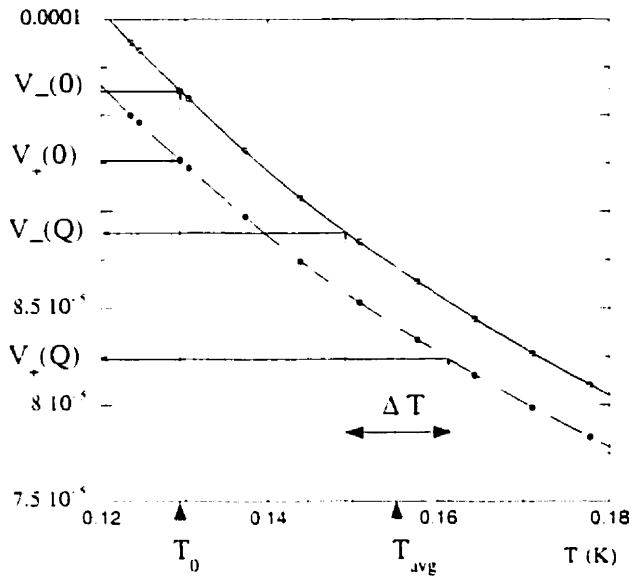


**Figure 5.2:** An example of $RuO_2$ calibration against the Ge (see text).

from RV-electronikka temperature controller and a Linear Research LR-700 resistance bridge monitoring a calibrated Ge sensor from Lakeshore Cryogenics. At a given temperature, we wait until the thermometers give a stable reading, which usually means that thermal fluctuations and electrical noise are less than 50 nV out of a typical signal of 60 $\mu$V: often the noise is less than 10 nV. Once deemed stable, we measure the thermometers with zero heat applied to the sample. This will eventually make up a calibration curve of each $RuO_2$. Next we apply a current to the heater to set up a temperature gradient ($\Delta T/T = 5\%$, typically) across the sample. After further waiting, we measure the thermometers again and then go to the next temperature.

Data analysis consists of fitting the thermometers. First we plot voltage vs temperature of one thermometer with no temperature gradient. Then from a polynomial fit of the temperature, we can determine the temperature corresponding to the signal with the heat on (see Fig. 5.2). The gradient is the difference between the two

thermometers, $\Delta T$, and the thermal conductivity $\kappa$ is simply [6]

$$\kappa = \frac{I^2 R}{\alpha \Delta T} \tag{5.1}$$

where $I$ is the current supplied to the heater of resistance $R$ ($\dot{Q} = I^2 R$) and $\alpha = (cross-sectional\ area)/(length\ between\ contacts) = A/L$ is the geometric factor of the sample.

With heat transport, one always worries about heat losses. Below 1 K, radiative effects are irrelevant, but not so current "leaks" via wiring on the mounts. To ensure that all the heat from the heater goes through the sample, that heat path must have the lowest thermal resistance of all possible paths. In the thesis of Lussier (1997), it was shown that losses for these mounts are less than 1% below 1 K for samples with a thermal resistance of roughly $W = 10^3$ W/mK, which corresponds to our least conducting sample.

As a test of the set-up, we measured the thermal conducitivity of a piece of dirty Au wire of thermal resistance $W = 1040$ W/mK. Since Au is a normal metal, both $\kappa$ and $\rho$ are constant at low temperature, giving a Lorenz number of $2.57\times10^{-8}$ $W\Omega K^{-2}$, which is 5% larger than $L_0$ (see Fig. 5.3). Thus heat loss is at most 5% for samples of comparable thermal resistance; in fact, it is much less considering the 5% error includes that from fitting the thermometers.

In a magnetic field, there are additional factors to consider. First of all, our $RuO_2$ thermometers have a measurable magnetoresistance. Since we calibrate the thermometers for each run against a known Ge resistor mounted in zero field, we always measure the true temperature. We have, however, made one modification to the sample mounts due to the long equilibration constants associated with the specific heat upturn due to the nuclear moment in Cu. By replacing the Cu thermometer mounts by Ag ones, we have reduced the waiting times by 75%; the remaining limitation comes from the Cu within the $YBa_2Cu_3O_{7-\delta}$ samples themselves.

For our study of the magnetic field effect on $\kappa_0/T$ of $YBa_2Cu_3O_{7-\delta}$, we normally measure the samples in zero field before applying a field. We were concerned about

[6] For low temperature, $\dot{Q} = \frac{A}{L}\int_0^L dx\, \dot{q} = \frac{A}{L}\int_{T_1}^{T_2} dT \kappa(T)$ where $A$ is the cross-sectional area and $L$ is the length between contacts. In the case of electrons, $\kappa_e = \kappa_0 T$ where $\kappa_0$ is a constant. This means that $\dot{Q} = \frac{A}{L}\frac{\kappa_0}{2}(T_2^2 - T_1^2) = \frac{A}{L}\frac{\kappa_0}{2}(T_2 - T_1)(T_2 + T_1) = \frac{A}{L}\kappa_0 T \Delta T = \frac{A}{L}\kappa_e(T)\Delta T$ if the gradient is small. This result is general, and works the same for phonons when $\kappa_{ph}$ is assumed to be proportional to $T^3$.

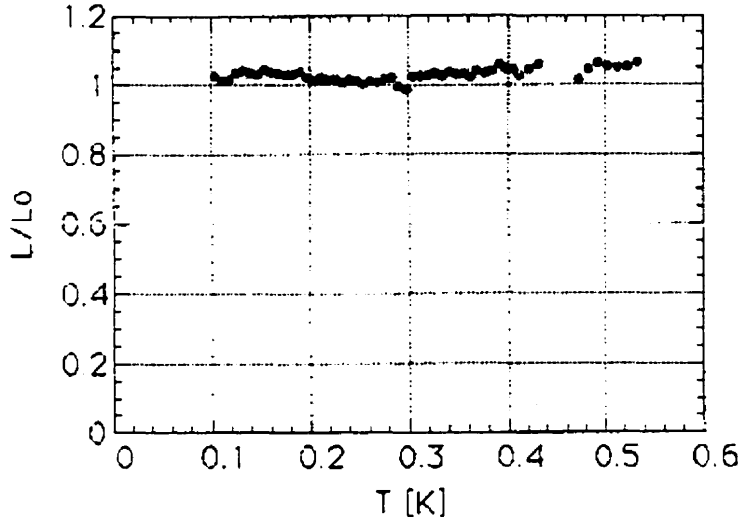


**Figure 5.3:** Lorenz number $L = \kappa_0\rho_0/T$ divided by $L_0 = 2.45\times10^{-8}$ W$\Omega$/K$^2$ vs temperature for a piece of Au wire.

the homogeneity of the vortex lattice because pinning is known to be strong in these materials, so we field-cooled a sample. This involved pre-cooling the magnet to 4 K while the samples within the IVC remained at room temperature. Then by slowly lowering the insert into the He bath (and using a lot of He!) and introducing some exchange gas into the IVC, we cooled the sample below the superconducting transition in a field of 8 T. Upon measuring the thermal conductivity, we got the same results as when the sample was cooled in zero field, so there is no need to field cool our samples.

# 6 The Thermal Conductivity of $UPd_2Al_3$

A finite limiting value for $\kappa_e/T$ is one of the major predictions of current theories of transport in unconventional superconducting states ((Norman and Hirschfeld 1996a, Graf *et al.* 1996) and references therein). A missing U-atom acts as a Kondo impurity in a compensated lattice, causing multiple scattering and large phase shifts $\delta_0 = \pi/2$. Within such a resonant impurity scattering model, a line of nodes in the gap can give a finite intercept in $\kappa/T$ vs $T$.

Here we present our experimental data on $UPd_2Al_3$, along with a review of similar work performed by others. We also include the thermal conductivity of $UPt_3$ since we will use the theory developed for $UPt_3$ to try to explain the situation in $UPd_2Al_3$.

## 6.1 Review

To the best of our knowledge, there have been two measurements of the thermal conductivity of $UPd_2Al_3$. The first one by Geibel *et al.* (1992), on a polycrystal of similar quality to ours (based on $T_c$), goes down to roughly 100 mK. We see in Fig. 6.1 that a smooth extrapolation of the low temperature zero field $\kappa/T$ has an intercept at $T = 0$. In an applied field, $\kappa/T$ increases, though there is no chance of seeing the Volovik effect (Doppler shifted quasiparticle states described in Section 2.2.2) since the lowest applied field is already $H_{c2}/2$, where there is significant pair-breaking.

In the first measurement of a single $b$ axis crystal, Hiroi *et al.* (1997) used a $^3$He fridge presumably, since the lowest temperature is about 300 mK (see Fig. 6.2). Below 1 K, they obtain $\kappa/T \sim T$, so we can extrapolate to $T = 0$. There is also a finite $\kappa_0/T$, though to determine the actual value it would be better to go below 100 mK. Indeed, our data go to lower temperature, and by measuring a $c$ axis crystal as well, we can determine whether there are nodes along $c$ (not seen by tunneling) and get a measure of the anisotropy.

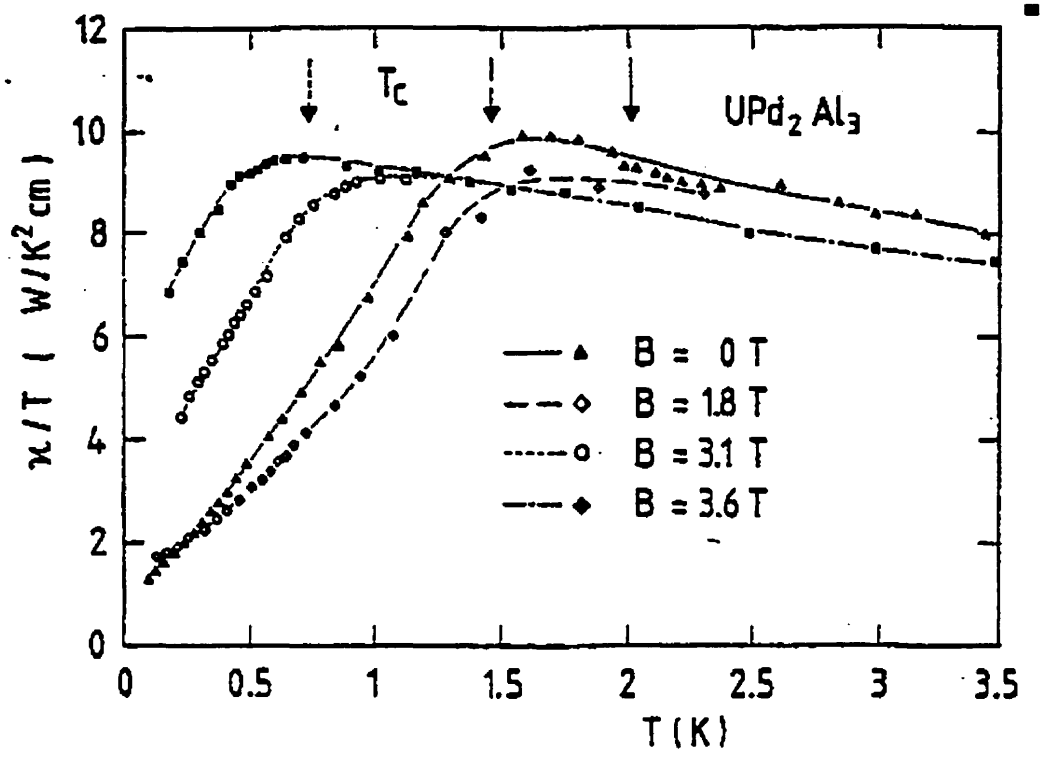


**Figure 6.1:** Temperature dependence of the thermal conductivity divided by temperature $\kappa/T$ in $UPd_2Al_3$ obtained by Geibel *et al.* (1992). A growth in $\kappa/T$ appears with applied field. The curves do not appear to be corrected for magnetoresistance, which is positive and therefore brings $\kappa$ down.

## 6.2 Sample Properties

A total of three crystals were measured—one polycrystal and two single crystals. The polycrystalline sample was grown and annealed using RF induction heating in ultrahigh vacuum. This sample has a $T_c$ of 1.86 K and a room temperature resistance ratio (RRR, $\rho(300\ K)/\rho_0$) of 36 ($\rho_0 = 3.8\ \mu\Omega$cm). The two unannealed single crystals, cut from the same ingot, were grown by N. Sato *et al.* (1992) at Tohoku University, Sendai, Japan, using the Czochralski pulling method in argon. From the resistivity measurements in Fig. 6.3, the single crystals have lower $T_c$'s, being 1.55 K for the *b*-axis crystal (RRR = 21) and 1.25 K for *c* (RRR = 7).

## 6.3 Experimental Results

We begin with the normal state (Fig. 6.4) attained in a field of 4.5 T, since it is metallic and easier to understand. Magnetoresistance is positive and roughly 20% in 4.5 T. In the polycrystalline sample, the Lorentz number $L = \kappa\rho/\mathrm{T}$ at 100 mK

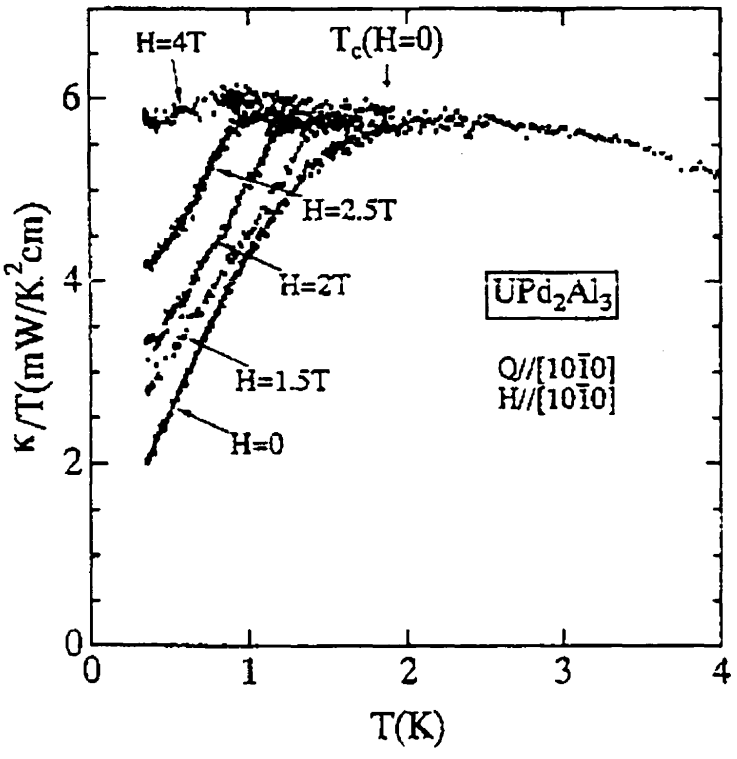


**Figure 6.2:** Temperature dependence of thermal conductivity divided by temperature $\kappa/T$ in a $b$ axis $UPd_2Al_3$ crystal obtained by (Hiroi *et al.* 1997). As in Fig. 6.1. $\kappa/T$ increases with field.

is $2.32\times10^{-8}$ $W\Omega K^{-2}$, which is $0.95L_0$ ($L_0 = 2.45\times10^{-8}$ $W\Omega K^{-2}$), in agreement with the Wiedemann-Franz law. For the single crystals, $\kappa_N/T$ is extremely flat, and $L = 0.96L_0$ along $b$ and $L = 1.1L_0$ along $c$. In all three cases, the agreement with the Sommerfeld value $L_0$ tells us that the linear term is purely electronic. As a result, we take the electronic part of $\kappa_N$/T to be $L_0/\rho_0$ from 0 to 1 K. Regarding the temperature dependent part, the roughly linear increase in $\kappa_N$/T seen in Fig. 6.4 must be due to phonons, since magnons have a gap of about 17 K, determined from high resolution inelastic scattering (Metoki *et al.* 1998).

Next, using $\kappa_{ph} = c_{ph}v_{ph}\Lambda_{ph}/3$, where the specific heat $c_{ph} = 8.0\times T^3$ $Jm^{-3}K^{-4}$ (Caspary *et al.* 1993) and the average sound velocity $v_{ph} = 5.73\times10^3$ $ms^{-1}$ (from elastic constants of Modler *et al.* (1993)), we estimate the phonon mean free path $\Lambda_{ph}$ to be 50 $\mu$m at 0.6 K. By 175 mK it has increased to 160 $\mu$m, roughly 1/4 the sample size. These are surprisingly long phonon mean free paths for a metal.

Let us now turn to the superconducting state data, shown in Fig. 6.5. We observe the existence of a substantial intercept in $\kappa/T$ in all three samples. A smooth

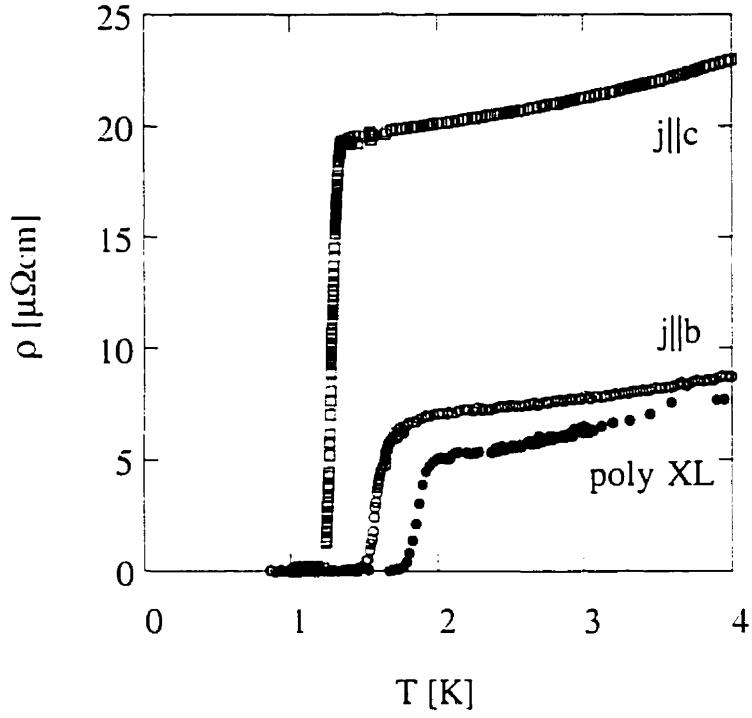


**Figure 6.3:** Resistivity $\rho$ vs temperature $T$ for the three samples of $UPd_2Al_3$. The polycrystal has the highest $T_c$ and sharpest transition, showing that it is of a higher purity than the single crystals.

extrapolation of the data for the polycrystal to $T = 0$ gives a limiting $\kappa/T = 0.6$-$0.8$ mW K$^{-2}$ cm$^{-1}$, about 15% of the normal state value $L_0/\rho_0$, most likely due to residual quasiparticle excitations. For the single crystals, we find $\kappa/T$ to be linear for $T < 0.5$ K, from which fit $\kappa_0/T$ is (0.92±0.06) mW K$^{-2}$ cm$^{-1}$ (0.29±0.02) along $b$ ($c$). Here, the residual quasiparticles comprise about 25% of the normal state value. We can compare all three quantitatively.

Since $UPd_2Al_3$ is hexagonal, we can average $\kappa$ for the single crystals to see if they agree with the polycrystal, by taking $\frac{2}{3}\kappa_b + \frac{1}{3}\kappa_c$. Indeed, when we compare this average value with the polycrystal, we find agreement at low temperature, shown in Fig. 6.6. At higher temperature, the phonons come into play, which are highly sample dependent, so the agreement breaks down.

With respect to the previous low temperature measurement in a polycrystal, Geibel *et al.* (1992) find a residual linear term of roughly 0.8 mW K$^{-2}$ cm$^{-1}$, which agrees very well with our value. In the $b$ axis measurement of Hiroi *et al.* (1997), at 300 mK (their lowest temperature), $\kappa/T$ is about 2 mW K$^{-2}$ cm$^{-1}$, which is what

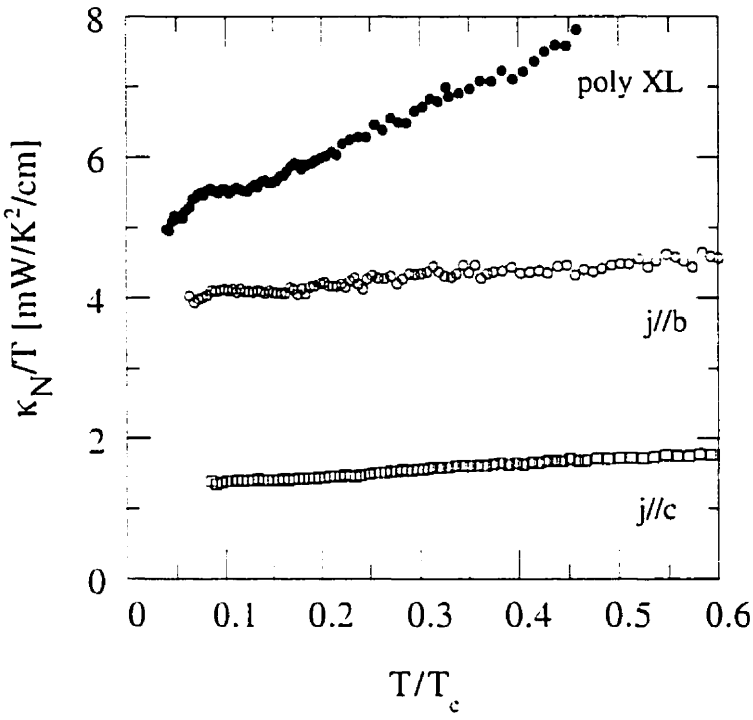


**Figure 6.4:** Normal state thermal conductivity divided by temperature $\kappa_N/T$ in $UPd_2Al_3$ for the polycrystal (solid circles), $b$ axis crystal (open circles) and $c$ axis crystal (open squares).

we obtain. All experimentally determined values of $\kappa/T$ that we know about agree extremely well.

At this point, we see that the normal state behaves as a metal, obeying the WFL at $T = 0$. A slope develops at finite temperature, which we attribute to phonons, since the magnons are gapped. In the superconducting state, the main result is the observation of a linear term in $\kappa$, indicating the existence of a residual normal fluid. We point out that in comparing different samples, $\kappa_0/T$ does not appear to be much affected by the impurity concentration.

## 6.4 Comparison with Theory

Assuming the dominant scattering of phonons to come from grain boundaries and electrons, we can estimate the boundary scattering rate $B$ and the e-ph coupling

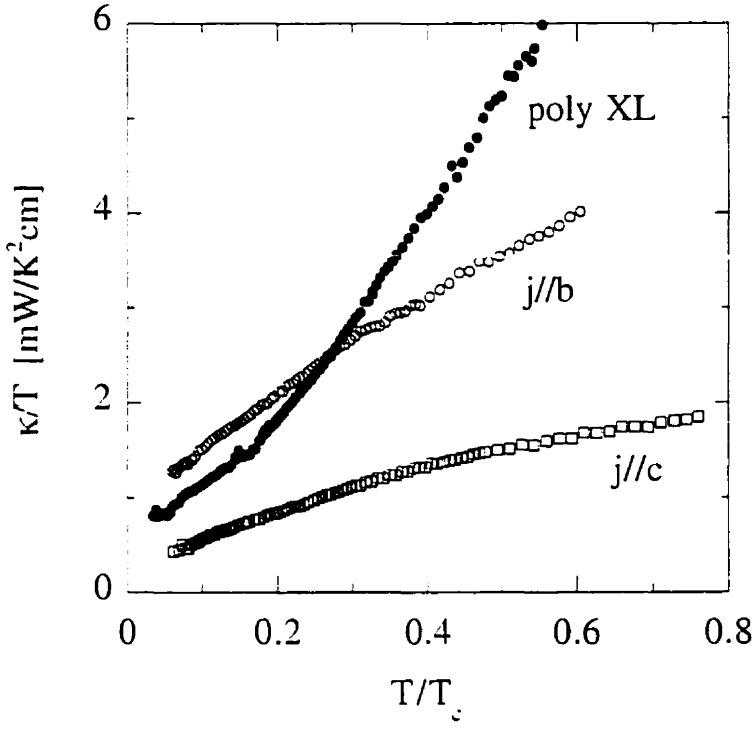


**Figure 6.5:** The thermal conductivity of $UPd_2Al_3$, divided by temperature, for the polycrystal (solid circles), *b*-axis crystal (open circles) and *c*-axis crystal (open squares).

strength $E$ from Debye theory:

$$\kappa_{ph} = \frac{k_B^4 T^3}{2\pi^2 \hbar^3 v_{ph}} \int_0^\infty dx \frac{x^4 e^x (e^x - 1)^{-2}}{B + ExT} \tag{6.1}$$

A fit to $\kappa_N(T)$-$\kappa_N(0)$ using Eq.(6.1) yields $B = 1.5\times10^6$ s$^{-1}$ and $E = 5.9\times10^6$ K$^{-1}$s$^{-1}$, which means that electron scattering dominates at all but the lowest temperatures. This value of $E$ is somewhat less than in $URu_2Si_2$ ($1.5 \times 10^7$) (Behnia *et al.* 1992), and much less than in Nb ($2\times10^9$) (Kes *et al.* 1974) and V($3\times10^9$). This anomalously weak e-ph coupling is the most unusual feature of the normal state $\kappa$ in $UPd_2Al_3$.

Now, as seen in BCS superconductors such as Nb (Kes *et al.* 1974), the large reduction in the number of quasiparticles available for scattering phonons at low temperature should cause a major increase in $\Lambda_{ph}$. We focus our attention on the polycrystal since it is the purest sample: the other two may exhibit extrinsic effects. If the rise in $\kappa_N/T$ is due to phonons scattering off electrons, one would expect the slope of $\kappa$/T in the superconducting state to increase dramatically. It does not. In

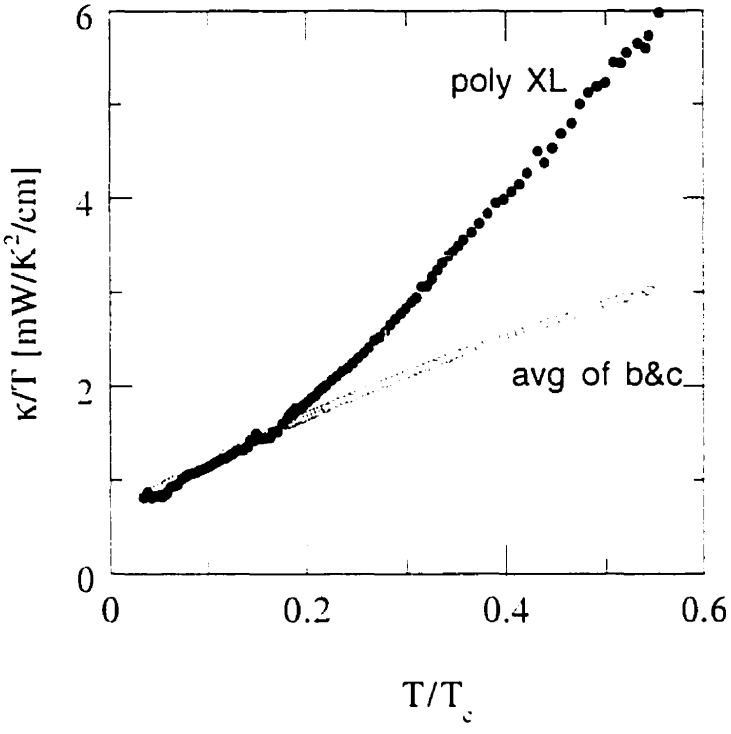


**Figure 6.6:** Thermal conductivity divided by temperature $\kappa/T$ vs $T$ for average of $b$ and $c$ compared with the polycrystal.

fact, it seems that the non-electronic contribution to $\kappa_N/T$ is unaffected by superconductivity, evidenced by the similarity of slopes seen in Fig. 6.7 for the polycrystal. (It would have been informative to measure $\kappa$ through $T_c$, except this was not possible in a dilution refrigerator.) Whether other scattering mechanisms play a role requires further study. At this stage, we adopt the following simple-minded procedure: the electronic thermal conductivity $\kappa_e/T$ in the superconducting state is obtained by subtracting from the $H = 0$ data in Fig. 6.5 the slope of $\kappa_N/T$. The result is shown in Fig. 6.8, normalized by $L_0/\rho_0$.

Calculations such as those performed for $UPt_3$ using a spherical Fermi surface [7] give the curves shown in Fig. 6.8 (Norman 1996b). The unitary limit is assumed, inelastic scattering neglected and the impurity scattering rate taken to be $\Gamma_0 \equiv$

[7] For a spherical Fermi surface we use spherical harmonics to represent the gaps: $Y_{10} \sim cos\phi$ corresponds to the polar gap. $Y_{11} \sim sin\phi$ the axial gap. $Y_{20} \sim 3cos^2\phi - 1$ the "tropical" gap, $Y_{21} \sim sin\phi cos\phi$ the hybrid-I gap and $Y_{32} \sim sin^2\phi cos\phi$ the hybrid-II gap. Calculations were not done for the axial and tropical gaps since the axial gap contradicts our measurements and the tropical gap was only later considered.

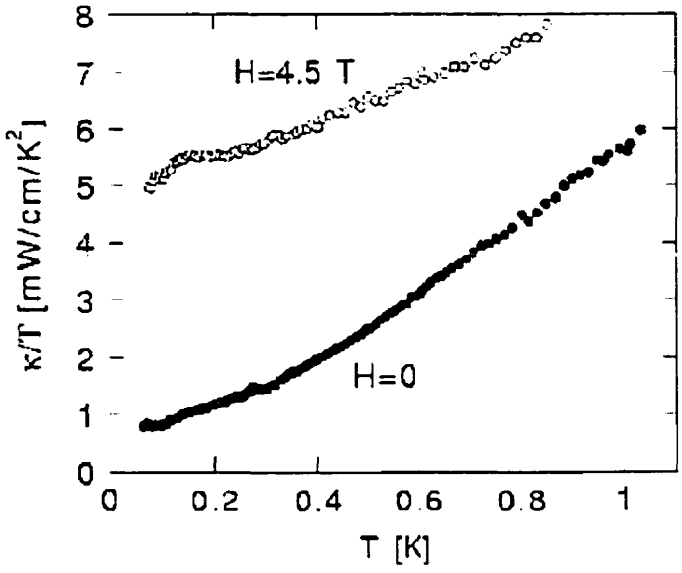


**Figure 6.7:** Thermal conductivity divided by temperature vs temperature in polycrystalline $UPd_2Al_3$, showing similar low temperature $T$-dependence in superconducting and normal states.

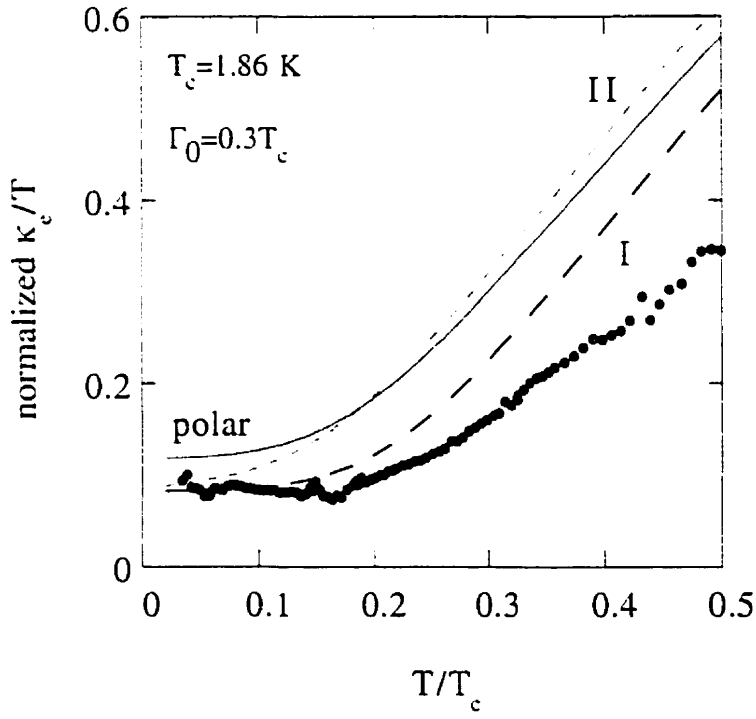


**Figure 6.8:** Normalized electronic thermal conductivity (see text). The data (points) are compared with resonant impurity scattering calculations using spherical harmonics for 3 gaps with a line node: polar (solid line), hybrid I (dashed line) and hybrid II (dotted line). By magnitude alone, it is not possible to discriminate between the hybrid gaps.

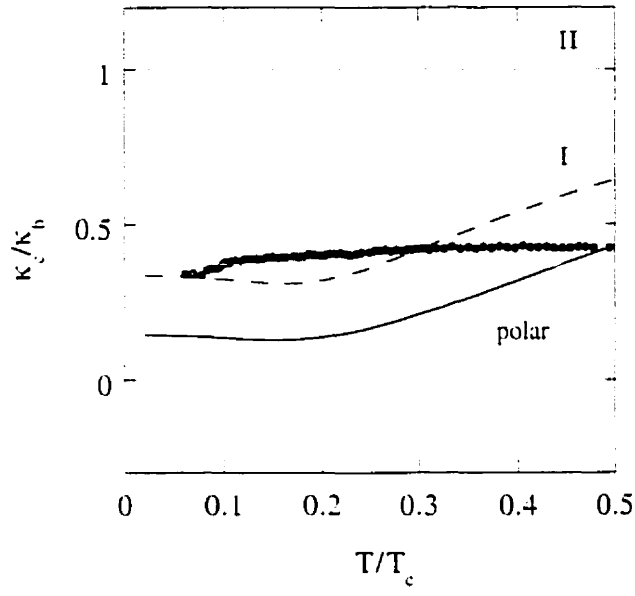


**Figure 6.9:** The ratio $\kappa_c/\kappa_b$ in $UPd_2Al_3$, which is finite down to $T = 0$. The theoretical curves correspond to the polar gap (solid line), the hybrid-I gap (dashed line) and hybrid-II gap (dotted line).

$\frac{1}{2\tau} = 0.3T_c$ (Norman 1996b), in agreement with the value determined from de Haas-van Alphen measurements (Inada *et al.* 1994). The comparison in Fig. 6.8 shows that the theory predicts the right magnitude for the residual linear term, which is independent of the way we treat the phonons. This is not true for the $T$-dependence, thus the discrepancy seen in Fig. 6.8 must be taken with caution. We emphasize that this treatment only makes any sense at $T = 0$.

Now as for the anisotropy, we see in Fig. 6.9 that the ratio $\kappa_c/\kappa_b$ remains finite at $T = 0$. Right away we can discard the polar gap, which has no node along $c$, and hence a ratio of identically zero. We can also rule out the axial gap which has only nodes at the poles. Since the "tropical" $A_{1g}$ gap has *two* line nodes shifted off the equator, there can be a quasiparticle momentum component along $c$ even though there are no nodes in the $c$ direction: in fact, at $T = 0$, the ratio is expected to be $\kappa_c/\kappa_b = 1$. With only spherical Fermi surfaces in the calculations, it is difficult to judge between the two hybrid gaps. Until further calculations are performed, we will have to be content with having eliminated the polar and axial gaps.

It is interesting to compare with measurements in other heavy fermion superconductors. In high purity $UPt_3$ single crystals, the anisotropy $\kappa_c/\kappa_b$ drops as one enters phase B below $T_c^-$ (see Fig. 3.1). This immediately strikes out the axial gap. Of the

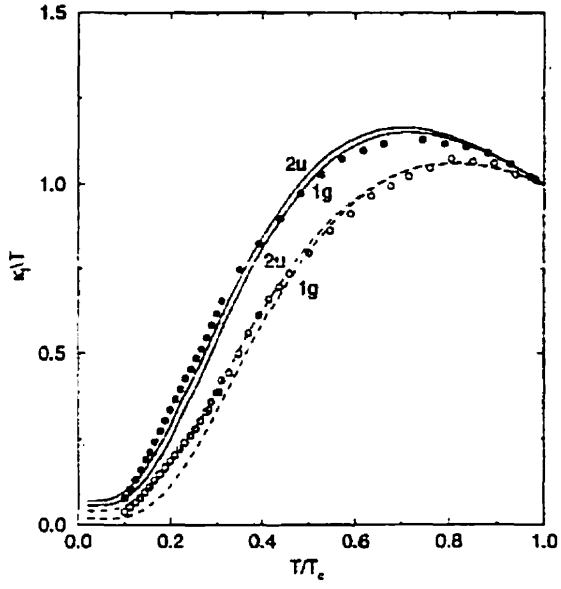


**Figure 6.10:** Thermal conductivity of $UPt_3$ of Lussier *et al.* (1996) along $c$ (open circles) and $b$ (solid circles). The curve marked $1g$ is for the $E_{1g}$ (or hybrid-I) gap, and $2u$ for $E_{2u}$ (or hybrid-II), with the solid (dashed) line corresponding to **J** along $b$ ($c$).

simple gaps which we consider, the polar and hybrid gaps are consistent with this finding. As for the separate $\kappa_b/T$ and $\kappa_c/T$ data, there is no evidence for a finite intercept (Lussier *et al.* 1996), even in data taken down to 16 mK as Suderow *et al.* (1997) have done. This may be due to a lower impurity scattering rate, in accordance with the lower residual resistivities (0.23 and 0.61 $\mu\Omega$cm). However, estimates show that the scattering rates are not so different, with $\Gamma_0$=0.1-0.2$T_c$ (Lussier *et al.* 1996). From theoretical fits of $UPt_3$ shown in Fig. 6.10, from which we observe that the hybrid-II gap ($E_{2u}$) provides a better fit, $\Gamma_0$=0.05$T_c$ or less (Norman 1996b). Recent measurements of Suderow *et al.* (1999) do see a linear term in electron-bombarded samples of high purity $UPt_3$, up to 50% of the normal state value when $\rho_0$ is increased to 4 $\mu\Omega$cm. This contradicts the popular $E_{2u}$ gap, which predicts a universal linear term. Several "new" gaps have been proposed, but we refrain from describing them in detail as they may well be overthrown in light of more theoretical and experimental work.

As for $URu_2Si_2$, a large residual $\kappa/T$—approximately 30% of the normal state value—was observed for a crystal with $\rho_0$=9.5 $\mu\Omega$cm (Behnia *et al.* 1992). Roughly speaking, this makes sense within the theory since $\rho_0$ is 3 times greater than in our $UPd_2Al_3$ sample. Finally, we point out that in $URu_2Si_2$, the phonon contribution

is more easily explained. The slope in $\kappa/T$ in the superconducting state at low temperature is roughly 4 times steeper than in the normal state, consistent with the idea that phonons conduct better due to the loss of electrons, their main scatterers. Again, it is puzzling that in $UPd_2Al_3$, with a comparable e-ph coupling, the loss of electrons appears to have no affect on the phonons.

We have seen that all existing thermal conductivity data of $UPd_2Al_3$ in the superconducting state show a $T = 0$ linear term of comparable size. However, without knowing the details of the samples measured by others, and with such a limited scope so far, it is difficult to claim any universal behaviour. Compared with $URu_2Si_2$, the e-ph coupling term in $UPd_2Al_3$ seems anomalously low. With respect to the observed linear terms, $UPd_2Al_3$, (dirty) $UPt_3$ and $URu_2Si_2$ all have order parameter zeroes. While both the axial and polar gaps have been ruled out in $UPd_2Al_3$, there still remain several possibilities of varying degrees of exoticism to be examined more closely.

## 6.5 Conclusion

Various probes show the existence of nodes in the gap of $UPd_2Al_3$. The power law temperature dependences of the NMR $1/T_1$ and specific heat in $UPd_2Al_3$ were among the first indications. From $\mu$SR and the specific heat jump, it appears that the behaviour follows that found within weak-coupling BCS theory, only with an unconventional gap. However, tunneling conductance data seem to favour strong-coupling of the order parameter to spin wave fluctuations. While this is the prevalent opinion, there has not yet been any unambigous evidence supporting spin-wave mediated superconductivity.

By using thermal conductivity, we have observed a finite $\kappa_0/T$ in $UPd_2Al_3$, of comparable magnitude to measurements made by others. From this, we also conclude there must be a line node along the $b$ direction. Our observation of a finite residual anisotropy $\kappa_c/\kappa_b$ indicates that either there are nodes along the $c$-axis or there are line nodes about $c$ which are not in the equatorial plane. The latter would support tunneling results favouring an $A_{1g}$ gap with two line nodes about $c$ but no nodes along it. The structure of the superconducting gap remains unclear, with several possibilities–either a combination of polar point nodes and one or more line nodes–remaining open. More work, both experimental and theoretical, are necessary.

In a sense, this work on $UPd_2Al_3$ serves as an introduction to the possibilities of a directional probe such as thermal conductivity. We will see, in the next chapter, the strength of this technique in revealing the character of residual quasiparticles when the order parameter is better known.

# 7 The Thermal Conductivity of $YBa_2Cu_3O_{7-\delta}$

## 7.1 High temperature review

Considering the results reported in this thesis have been mainly performed in a dilution refrigerator, anything above 1 K is deemed "high temperature"! Of course, $^3$He people would call our temperature range "high". So we hereby *define* "high temperature" as being above 5 K within the confines of this thesis. In this section we review $\kappa$ above 5 K, where we can already learn a lot about the dominant scattering mechanisms in the cuprates, as well as the contribution to $\kappa$ from both electrons and phonons.

The main feature of $\kappa(T)$ in $YBa_2Cu_3O_{7-\delta}$ at high temperature is the peak below $T_c$, displayed later in our discussion of Zn doping (Fig. 7.2). Whether this peak is due to electrons or phonons was unclear for some time. In charge conductivity (Section 4.4.2), which only involves the electrons, the peak arises as a result of the falling inelastic scattering rate beating out the decreasing number of electrons. The same argument can be applied to $\kappa$, but we have also phonons to consider: given that the electrons are condensing into the superconducting state, phononic heat conduction will certainly increase when their main scatterers "disappear" from sight. Can we somehow separate the charged from the neural carriers? Fortunately, there is a way: thermal Hall conductivity, an energy analogue of the Hall effect.

The main advantage of thermal Hall conductivity $\kappa_{xy}$, also known as the Righi-Leduc effect, is that it is possible to measure quasiparticle heat transport at all temperatures. In principle, in a field applied transverse to the current, the quasiparticle scattering amplitude to the right is different from that to the left. This asymmetric scattering produces a transverse current which changes sign with the applied magnetic field. By contrast, phonons are scattered symmetrically, and as long as the vortices remain pinned, $\kappa_{ph}$ can be subtracted. Moreover, it is possible to extract the quasiparticle mean free path as a function of temperature, as in the inset of Fig. 7.1.

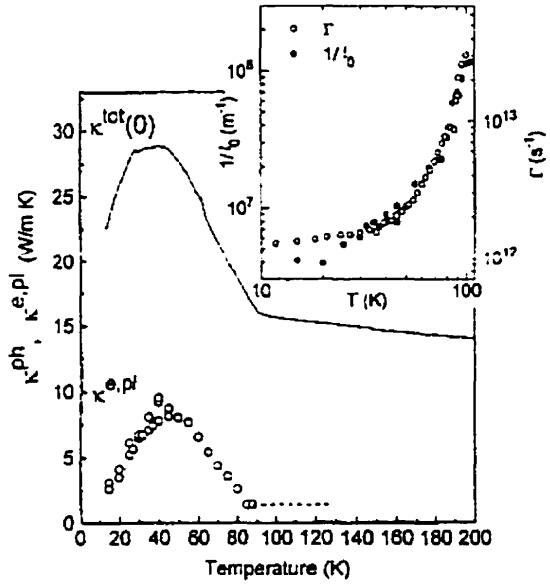


**Figure 7.1:** The total in-plane thermal conductivity (solid curve) and the electronic portion $\kappa^{e,pl}$ (open circles) measured by Krishana *et al.* (1995). Inset: the extracted mean free path $\ell_0$ (solid circles) in $YBa_2Cu_3O_{7-\delta}$ from $\kappa_{xy}$ compared to that determined from charge conductivity data of Bonn *et al.* (1994) (open circles).

Due to the application of a magnetic field, however, the quasiparticle mean free path determined from $\kappa_{xy}$ will be different from that in $\kappa$ in zero field if vortex scattering is important.

In $YBa_2Cu_3O_{7-\delta}$, the measurement by Krishana *et al.* (1995) of $\kappa_{xy}$ has been instrumental in identifying the electronic contribution to the peak below $T_c$. The electron peak coincides with the total peak, rising from a small normal state value to a peak of comparable size to the total peak (Fig. 7.1). Thus roughly half of the peak is electronic in origin, with the other half coming from phonons. Below the peak, the saturation in the inelastic scattering rate means that the decreasing number of electrons dominates and so $\kappa$ drops rapidly as $T \to 0$; phonons naturally drop out with decreasing temperature. This leaves mainly elastic impurity scattering below about 20 K, in agreement with Hosseini *et al.* (1998b). By comparing the extracted scattering rate $\Gamma$ of order $0.08T_c$ with the mean free paths determined from microwave conductivity (Bonn *et al.* 1994), one gets $v_F = 2\times10^7$ cm/s.

Now the effect of impurities can be profound. With Zn doping, the peak is dramatically reduced, as seen in Fig. 7.2, while the position of the peak shifts nonmonotonically. Initially, the electronic peak dominates and moves to higher temperature with

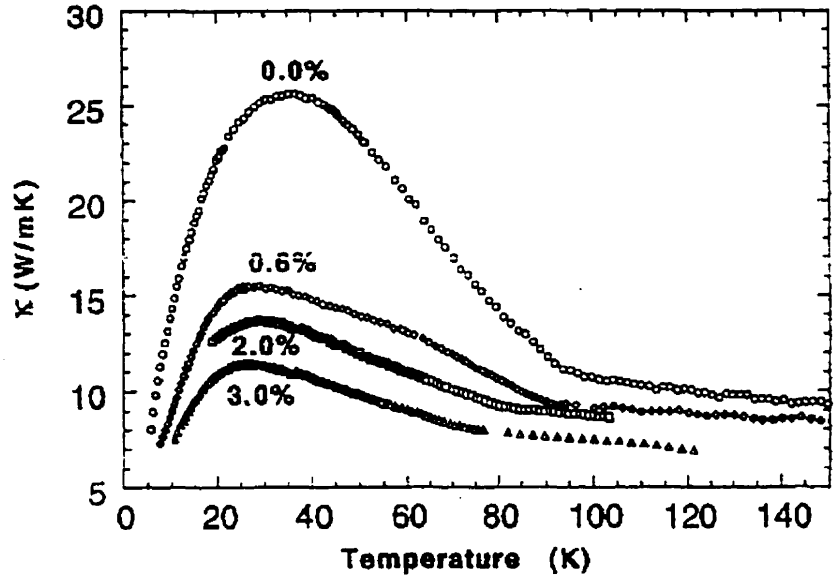


**Figure 7.2:** Thermal conductivity $\kappa$ of $YBa_2(Zn_xCu_{1-x})_3O_{7-\delta}$ as a function of temperature, with $x = 0.0\%$, 0.6%, 2% and 3% (Pu 1997).

disorder. At some point, however, the phonon peak (at 20-25 K) gains importance as the electronic conductivity is further suppressed by impurity scattering. Eventually, the peak should stop moving when $\kappa_{el}$ disappears, leaving only the phonon peak.

Thus from high temperature $\kappa$ in $YBa_2Cu_3O_{7-\delta}$, we have learned that inelastic scattering gives rise to a peak, after which it saturates and leaves only elastic scattering below 20 K or so. Also, this peak comes from both phonons and electrons, so we see there are indeed a lot of phonons in these systems. Furthermore, the peak height is very sensitive to impurities such as Zn. It remains to be seen if this impurity dependence carries over to low temperature.

## 7.2 Low temperature review

While $T_c$ for $YBa_2Cu_3O_{7-\delta}$ is 93 K, it is necessary to study thermal excitations down to $T_c/1000$ for meaningful interpretations of electronic properties: in fact, for all temperatures, phonons make a significant contribution to $\kappa$, as mentioned above. In order to see the clear electronic signature (linear temperature dependence), it is necessary to go low enough in temperature so that phonons and quasiparticles can be distinguished from one another. This occurs when the phonons have reached their boundary-limited mean free path where the thermal conductivity has a well-known

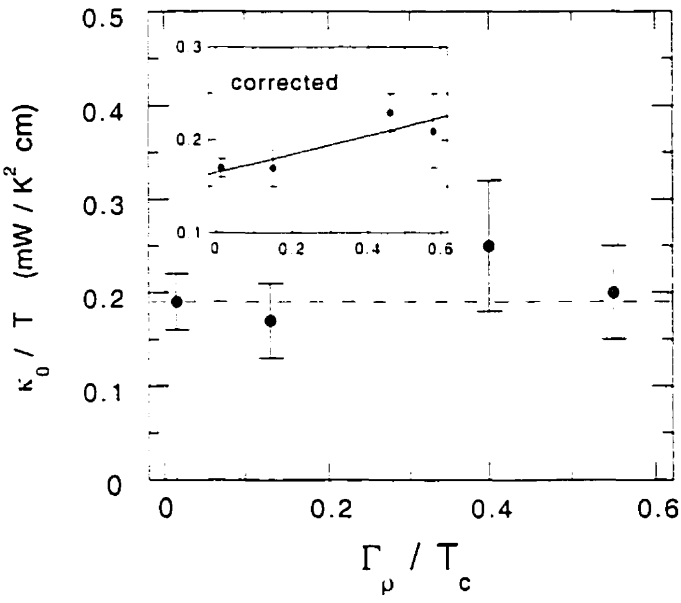


**Figure 7.3:** Residual linear term $\kappa_0/T$ as a function of scattering rate $\Gamma$ (in units of $T_c$) for $YBa_2(Zn_xCu_{1-x})_3O_{7-\delta}$, measured by Taillefer *et al.* (1997). Note that an increase in $\Gamma$ by a factor of 40 hardly changes the residual linear term. The inset shows the same data when the geometric factors are adjusted according to Section 7.3.

$T^3$ dependence. Only in this limit can a reliable zero temperature extrapolation be made.

There exist several measurements of the low temperature thermal conductivity of $YBa_2Cu_3O_{7-\delta}$. Since single crystals have become widely available, we will concentrate on reviewing measurements on single crystalline $YBa_2Cu_3O_{7-\delta}$, and we refer interested readers to earlier reviews (Burns 1992, Cyrot and Pavuna 1992) for results on powders and films. We will see that even with single crystals there can be inconsistencies between different measurements.

### 7.2.1 Universal Heat Conduction

Four years after universal conductivity in $d$-wave superconductors was first predicted by Lee (1993), it was observed in heat transport in $YBa_2Cu_3O_{7-\delta}$ (Taillefer *et al.* 1997). By varying the Zn concentration in $YBa_2(Zn_xCu_{1-x})_3O_{7-\delta}$ from 0.00 to 0.03 in four $a$-axis single crystals, it is possible to effectively increase the scattering rate by a factor of 40, determined from the change in $\rho_0$. It was found that the finite linear term $\kappa_0/T$ as $T \to 0$ is virtually independent of the scattering rate $\Gamma$, as seen in Fig. 7.3.

In addition, Taillefer and co-workers found that the magnitude of the residual linear term bears quantitative agreement with theory based on the $d_{x^2-y^2}$ pairing state. If we take the simplest $d$-wave gap $\Delta(\phi) = \Delta_0 cos(2\phi)$, with slope $S = d\Delta/d\phi = 2\Delta_0$, where we take the weak-coupling $\Delta_0 = 2.14 k_B T_C$ together with the experimental value of $\hbar\omega_p$ equal to 1.3 eV (Basov *et al.* 1995) and put these into Equation (2.25), we get

$$\kappa_{00}/T = 0.11 \text{ mW K}^{-2} \text{ cm}^{-1} \tag{7.1}$$

which is within a factor of two of the measured value of 0.19±0.03 mW $K^{-2}$ $cm^{-1}$.

This confirmation of universal transport provides a strong validation of $d$-wave transport theory. Having thus established the basic theory, there remain tests of the various predictions of in-plane anisotropy and magnetic field effects.

### 7.2.2 Anisotropy

The crystal structure of $YBa_2Cu_3O_{7-\delta}$ supports two channels of electronic conduction in the basal plane: the roughly tetragonal $CuO_2$ planes, stacked in pairs along the $c$-axis, and the one-dimensional CuO chains running along the $b$ direction, positioned half-way between the $CuO_2$ bilayers. Charge conduction along the $b$-axis is therefore higher than along the $a$-axis, by a factor which depends on the degree of oxygenation, being maximum for $\delta = 0$, and on the level of defects in the chains. In optimally-oxygenated crystals of high purity ($\delta \simeq 0.1$), the anisotropy in the electrical resistivity at 300 K can be as high as $\rho_a/\rho_b = 2.3$ (Gagnon *et al.* 1994). This factor drops significantly (down to 1.2 or less) in the presence of impurities such as gold, which tends to go preferentially into the chains. A satisfactory treatment of the $ab$ anisotropy in the electronic conduction of $YBa_2Cu_3O_{7-\delta}$ has not yet been reached.

At the gross level, it would appear that one can account for the anisotropy in both the plasma frequency $\omega_p$ in the superconducting state (as measured by far infrared reflectance) and the DC conductivity $\sigma$ in the normal state simply in terms of an anisotropy of 2.2±0.2 in $n/m^*$, the ratio of carrier density to effective mass (Basov *et al.* 1995). However, upon closer investigation, there are several indications that this simple picture fails. First, the scattering rate is clearly not the same for electrons in the chains as in the planes, i.e. it is not isotropic as the simple picture would imply. From Fig. 7.4, the temperature dependence of the resistivity is linear along

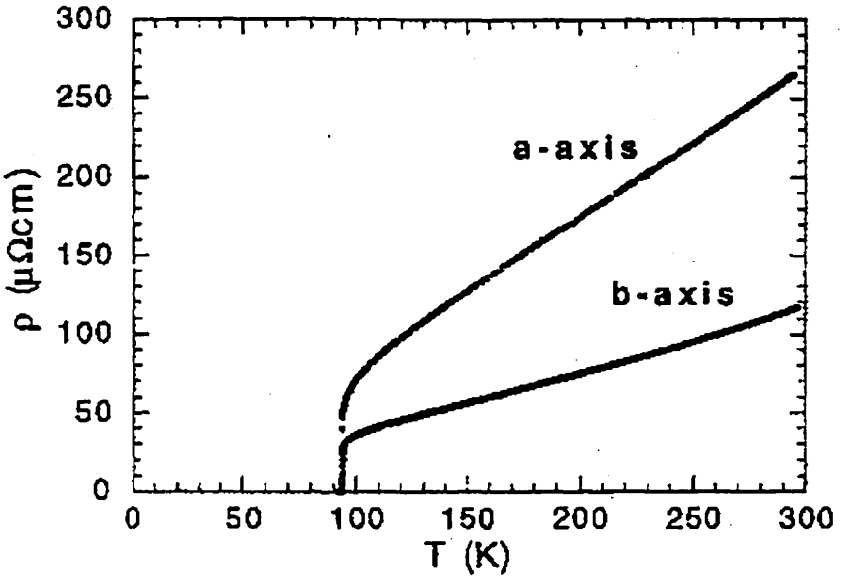


**Figure 7.4:** The electrical resistivity of $YBa_2Cu_3O_{7-\delta}$ for current along $a$ and $b$ obtained by Gagnon *et al.* (1997). Along $a$, $\rho$ is linear in $T$, whereas along $b$, there is noticeable curvature.

the $a$-axis but not along the $b$-axis, revealing that inelastic scattering is different in the chains (Gagnon *et al.* 1994). The elastic scattering from defects will also in general be different, either because of preferential impurity distributions (e.g. Au in the chains, Zn in the planes) or because of the large density of oxygen vacancies found in the chains of most crystals (e.g. 10% in $YBa_2Cu_3O_{6.9}$). A second indication comes from the anisotropy in the thermal conductivity above 5 K (see Fig. 7.5), which strongly suggests that the contributions of chains and planes are qualitatively different (Gagnon *et al.* 1997). Note that the other extreme of a model which treats the chains and the planes as being entirely uncoupled is equally simplistic, though a straight subtraction ($\kappa_b - \kappa_a$) may give a somewhat qualitative measure of chain conductivity. One finds that this difference shows no feature at $T_c$, and develops a peak below about 55 K. Indeed, the reasonably good conduction along the $c$-axis indicates a fair coupling between the two channels (for recent example see work of Hosseini *et al.* (1998b)).

Previous attempts to measure the anisotropy of transport in the superconducting state of $YBa_2Cu_3O_{7-\delta}$ have been somewhat inconclusive. The real part of the charge conductivity, $\sigma_1$, estimated from microwave measurements of the surface impedance and of the London penetration depth combined with infrared measurements of the

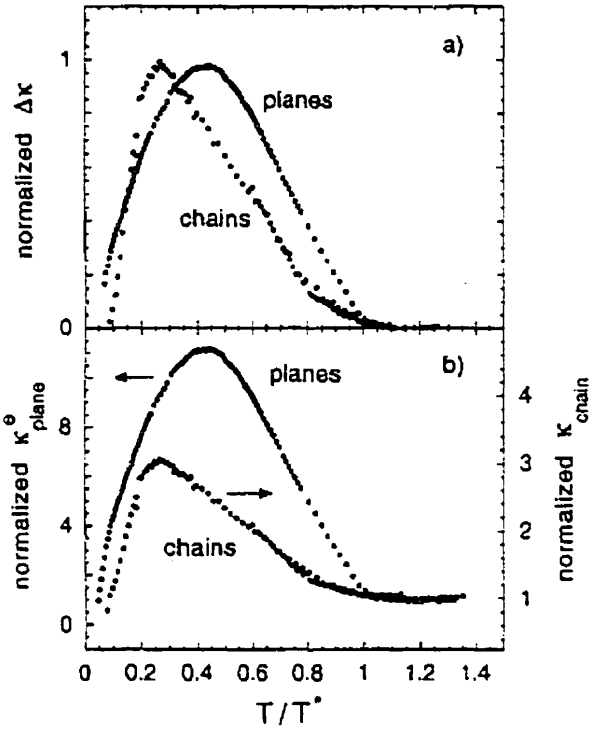


**Figure 7.5:** Plane and chain thermal conductivity, after Gagnon *et al.* (1997), where $T^*$ is $T_c$ for the planes and about 55 K for the chains. (a) Comparison of plane ($\kappa_a$) and chain ($\kappa_b - \kappa_a$) heat conduction with normal state value subtracted. (b) Extracted electronic contribution of $\kappa_{plane}$ and $\kappa_{chain}$.

plasma frequency, exhibits an anisotropy of 2.4 in the normal state which decreases to approximately 1.6 as $T \to 0$ (Zhang *et al.* 1994) in a pure crystal and roughly stays the same ($\sim 2.8$) in 0.15% Zn-doped crystals (Hosseini *et al.* 1998b). However, the experiments are difficult and the uncertainty is at least 30-40%.

Several attempts to measure the anisotropy in $\kappa$ do not go low enough in temperature. Without entering the regime in which the phonons have reached the limit of boundary scattering, it is impossible to extract the quasiparticle linear term. Furthermore, little information can be extracted at finite temperature because the phonon contribution is sample dependent.

An early measurement of $\kappa(T)$ in single crystals makes no distinction between $a$ and $b$ (Bredl *et al.* 1992). They appear to assume $\kappa_a$ and $\kappa_b$ to be equal at low temperature and do not specify along which crystalline axis the heat is propagating; in fact, they only distinguish between J $\parallel$ $c$ and J $\perp$ $c$. By extrapolating one set of data (J $\perp$ $c$) from 200 mK down to $T$=0, they obtain a linear term of 0.17 mW $K^{-2}$ $cm^{-1}$,

which is slightly larger than a previously measured 0.13 mW $K^{-2}$ $cm^{-1}$ (Sparn *et al.* 1989).

Two years later, another publication appeared, with $\kappa_a$ measured down to 200 mK and $\kappa_b$ to 100 mK (Gold *et al.* 1994). Where they overlap, i.e. above 200 mK, $\kappa$ appears to be isotropic in the basal plane. A similar conclusion was drawn by Behnia *et al.* (1995). Oddly enough, another group trying to measure the anisotropy also had difficulty obtaining $\kappa_a$ below 200 mK though for $\kappa_b$ there is data down to 100 mK (Wand *et al.* 1996). Again, the two sets of data only overlapped above 200 mK. Thus, their conclusion was to regard the question of anisotropy below 200 mK as remaining open.

### 7.2.3 Field Dependence

Existing measurements of $\kappa/T$ with $\mathbf{H} \perp c$ both support and contradict the theory. Wand and co-workers report that a field of 6 T produces no effect on the electronic linear term $\kappa/T$ for both J || a and J || b, while earlier observations by Bredl and co-workers indicate an increase, attributed to pair breaking, for the same conditions (Wand *et al.* 1996, Bredl *et al.* 1992).

Not only do impurities suppress the peak in high temperature thermal conductivity, so does an applied field, as in Fig. 7.6. By applying 10 T, Palstra *et al.* (1990) have shown the peak to be strongly suppressed. This indicates the importance of vortex scattering at high temperature.

At high temperature (above 5 K), the thermal conductivity is always seen to decrease with field. In both $Bi_2Sr_2CaCu_2O_8$ (BSCCO) (Krishana *et al.* 1997), and in underdoped YBCO Krishana *et al.* (1998), the decrease flattens to a plateau, indicating that beyond a field $H^*$, there is something happening (which is much more pronounced in BSCCO). Based on their observation, shown in Fig. 7.7, of an abrupt kink followed by a plateau in the field dependence of the thermal conductivity of BSCCO, Krishana *et al.* (1997) have proposed a phase transition to a gapped state for fields higher than some temperature dependent $H^*$. Quasiparticles in such a state would have an exponentially small density of states and so contribute nothing to the thermal conductivity beyond $H^*$. Of course the phonon conductivity would also have to be independent of field in the plateau region. We now concentrate on the quasiparticles and investigate how a phase transition to a new state can occur.

As previously stated, Krishana *et al.* have suggested that the order parameter

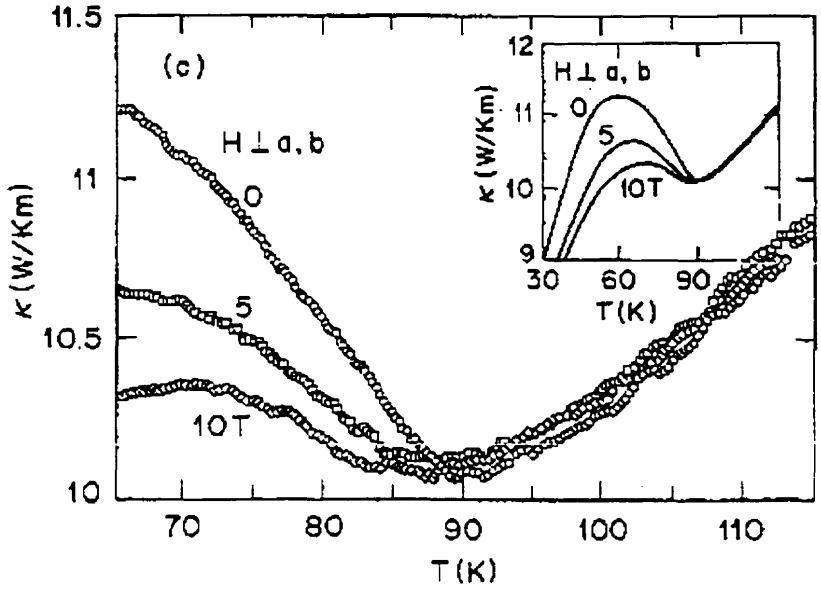


**Figure 7.6:** High temperature thermal conductivity of $YBa_2Cu_3O_{7-\delta}$ in an applied field, after Palstra *et al.* (1990). Inset: expansion of temperature scale.

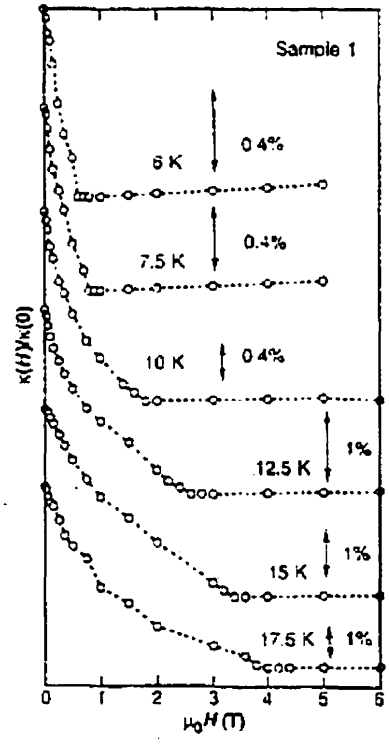


**Figure 7.7:** The stunning discovery of Krishana *et al.* (1997) in $Bi_2Sr_2CaCu_2O_8$. With increasing field, the thermal conductivity $\kappa(H)$ drops rapidly and then crosses over abruptly at a field $H^*$ to a plateau region, which is shown to be temperature dependent.

changes abruptly from a simple $d$-wave to a complex order parameter with an admixture of $d$ or $s$: in effect, the addition of a small, out of phase (by $\pi/2$) order parameter creates a finite gap everywhere since the nodes do not coincide. A field-induced phase transition to a $d_{x^2-y^2} + id_{xy}$ $(d + id')$ symmetry state was first proposed by Laughlin (1997). Mao and Balatsky (1999) have calculated the density of states for this state, repeating the treatment of Volovik (1993) for the pure $d_{x^2-y^2}$. The only difference is in the gap function in the quasiparticle spectrum, namely $\Delta(k) = \Delta_0(k) + i\Delta_1(k)$, where $\Delta_0(k)$ is the standard $d_{x^2-y^2}$ gap and $\Delta_1(k)$ the $d_{xy}$. It turns out that the Doppler shift due to the superfluid flow can be sufficient to boost the quasiparticles above the finite gap $|\Delta_1|$, so that the DOS remains gapless: in other words, for *both* $d_{x^2-y^2}$ and $d_{x^2-y^2} + id_{xy}$, $N(0; H) \propto \sqrt{H}$. Considering this same field dependence, the relative size of the coefficients become extremely important in distinguishing the two.

So there is a lot of interest in the field dependence of quasiparticles. Considering the claim of a phase transition based on high temperature data, it may be possible to set an upper bound on the size of a sub-dominant order parameter, if it should exist, by inducing low energy excitations. For either pure $d$-wave or $d + id'$, the Volovik effect is expected at low temperature. The question is whether the dependence is $\sqrt{H}$, as predicted in the clean limit, or something more slowly varying, as predicted in the dirty limit by Kübert and Hirschfeld (1998b).

## 7.3 Sample Characteristics

A typical sample is less than 2 mm in length, so we try to maximize the distance between the voltage contacts, which are 50 $\mu$m in size, in correspondance to the size of the silver wires. In general, the largest source of error on the absolute value of $\kappa$ stems from the geometric factor $\alpha$. There are two ways to find $\alpha$, either by the physical geometry of the sample (cross-sectional area divided by the distance between the contacts) or by comparing the sample resistance to a known resistivity at a given temperature ($\alpha_\rho = \rho_{ref}(300K)/R_{sample}(300K)$).

For the geometrically determined $\alpha_{geo}$, we use scanning electron microscopy (SEM), with a typical error of order 10%. However, the *relative* uncertainty in comparing $a$-axis samples together or $b$-axis samples together, can be made negligible by using geometric factors obtained from the resistivity measured using the same

| Crystal | $T_c$ [K] | length [$\mu$m] | width [$\mu$m] | thickness [$\mu$m] | $\alpha_{geo}$ [$\times 10^{-3}$ cm] | $\alpha_\rho$ [$\times 10^{-3}$ cm] |
|---|---|---|---|---|---|---|
| A1 | 93.6 | 1310 | 740 | 86 | 4.9±0.2 | 4.9 |
| A2 | 93.5 | 1360 | 500 | 61 | 2.24±0.09 | 1.89 |
| A3 | 93.3 | 1410 | 880 | 103 | 6.4±0.3 | 5.4 |
| B1 | 93.3 | 960 | 610 | 67 | 4.3±0.2 | 3.8 |
| B2 | 93.5 | 540 | 443 | 108 | 8.9±0.4 | 7.5 |
| 0.6% | 89.2 | 1200 | 630 | 93 | 4.9±0.3 | 4.6 |
| 3% | 74.6 | 1300 | 540 | 69 | 4.3±0.1 | 3.8 |

**Table 7.1:** Sample characteristics of the five crystals used in the anisotropy study along with the two additional Zn-doped ones used in the field dependence study. Note that $A_2$, $B_1$ and $B_2$ were sanded.

contacts as for the measurement of $\kappa$. This is done by forcing the resistivity curves of all $a$-axis samples (or $b$-axis samples) to be parallel, under the reasonable assumption that the only difference between samples is in the elastic, temperature-independent term. In other words, we fit the $a$-axis resistivity curves (shown in Fig. 7.4) to $\rho_0 + AT$ and set all the values of $A$ to be the same for the $a$-axis crystals. Then by setting the room temperature value of $\rho_a/\rho_b$ to 2.3 (Gagnon *et al.* 1994), a number whose uncertainty is at most 10%, we can determine geometric factors for the $b$-axis samples, given a fixed value for one reference $a$-axis sample A1, defined in Table 7.1 [8]. In the data presented, we have used the resistive geometric factors.

For determining the anisotropy in the thermal conductivity $\kappa(T)$ of $YBa_2Cu_3O_{6.9}$, we measured five high-purity untwinned single crystals: three with the current along the $a$-axis (A1, A2 and A3) and two along the $b$-axis ($B1$ and $B2$). For the field dependence study, we used A3 as our pure sample and two Zn-doped $a$-axis samples, called 0.6% and 3%. The sample characteristics are summarized in Table 7.1.

[8] Certain samples lack straight edges or are missing a corner, so an optically determined geometric factor would be more prone to error than would a resistive geometric factor. Furthermore, some sample surfaces were sanded in order to ensure diffuse rather than specular reflection of phonons; in this case, only the resistive geometric factor is relevant since the sanded surface area creates an uncertainty in the actual path length of the phonons.

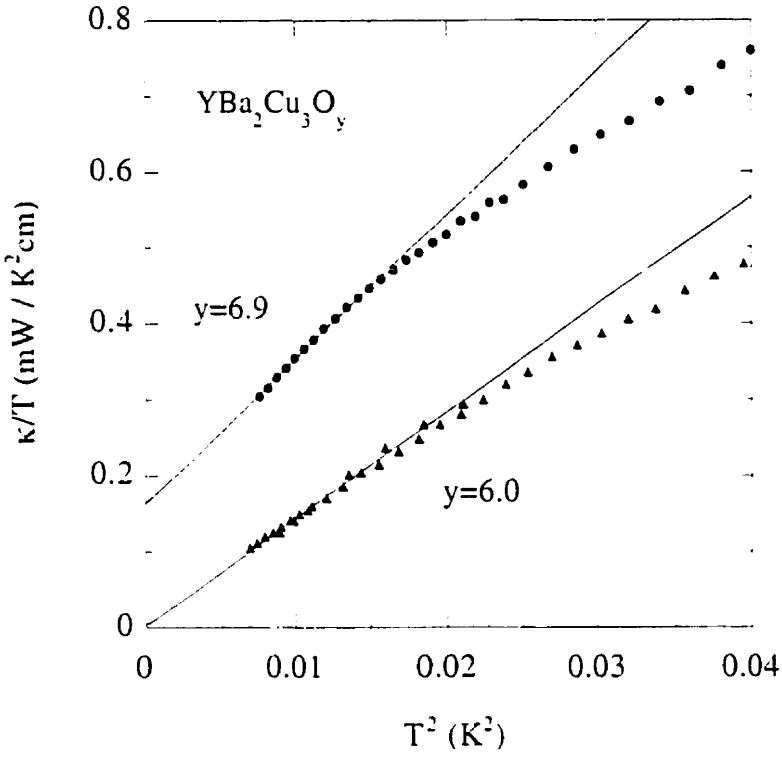


**Figure 7.8:** Thermal conductivity divided by temperature $\kappa/T$ vs $T^2$ of $YBa_2Cu_3O_{6.9}$ and $YBa_2Cu_3O_{6.0}$. For $YBa_2Cu_3O_{6.0}$ (triangles) we see that the intercept of $\kappa/T$ is zero, consistent with the absence of electronic carriers. However, for the optimally doped sample where $\delta$ is 0.1 (circles), a finite intercept appears.

## 7.4 Results on In-plane Anisotropy

Before presenting data on the anisotropy of heat conduction, we must convince ourselves that we are indeed probing the residual quasiparticles. By comparing a pure sample of $YBa_2Cu_3O_{7-\delta}$ of optimal oxygen doping ($\delta = 0.1$) with a deoxygenated sample $YBa_2Cu_3O_{6.0}$ (measured by Lussier (1997)), one sees that the linear term disappears in the latter case, i.e. only the $T^3$ phonon term remains, as seen in Fig. 7.8. Thus one can systematically "turn on" the quasiparticles and study their evolution with increasing doping concentration.

The data below 170 mK for the five crystals are shown in Fig. 7.9, plotted as $\kappa/T$ vs $T^2$ in order to separate the quasiparticles from the phonons. The solid lines are linear fits to the data below 130 mK (same fitting range for all samples). The first point to stress is that the intercept of those lines, i.e. the residual linear term in $\kappa(T)$, is entirely attributable to quasiparticles, since fully deoxygenated samples

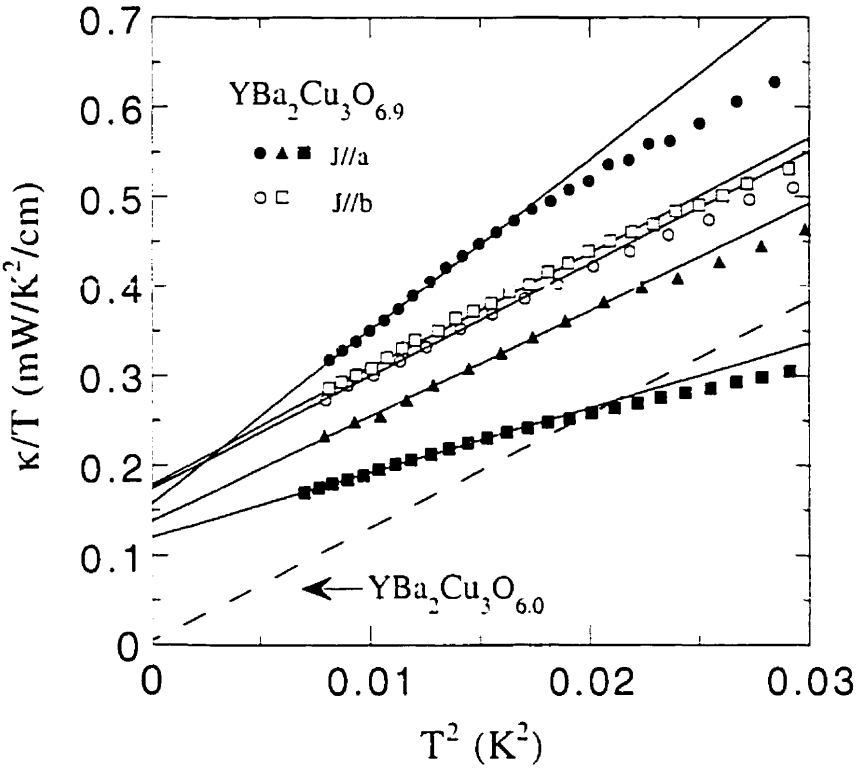


**Figure 7.9:** Low temperature thermal conductivity of $YBa_2Cu_3O_{6.9}$, divided by temperature vs $T^2$ for sample $A1$ (solid circles), $A2$ (solid triangles), $A3$ (solid squares), $B1$ (open squares) and $B2$ (open circles). The dashed line represents $\kappa/T$ for a deoxygenated, insulating sample $YBa_2Cu_3O_{6.0}$. It is clear that our measurements reach the asymptotic $T^3$ dependence of the phonons, with the oxygenated samples gaining a linear term due to the addition of electronic carriers.

show no linear term (see data reproduced as dashed line in Fig. 7.9) (Taillefer *et al.* 1997).

As for the increase in $\kappa(T)/T$ with $T$, it is mostly (perhaps entirely) due to phonons. This conclusion is supported by the fact that metallic and insulating crystals show a very comparable increase with temperature (see Fig. 7.8). We now calculate the phonon contribution to $\kappa$, starting with the phonon specific heat, since the two are related by $\kappa_{ph} = \frac{1}{3} c_{ph} v_{ph} \Lambda$, where $\Lambda$ is the phonon mean free path. Since we are assuming boundary scattering for the phonons, $\Lambda$ is related to the mean geometric width $\bar{w} \equiv \sqrt{w \times t}$ by $\Lambda = 2\bar{w}/\sqrt{\pi}$. We also need the mean sound velocity $v_{ph}$, which we now determine from experimental data.

Sound velocity measurements, usually a straightforward task, yield wildly varying results. Reported values of longitudinal $v_\ell$ fall in the range 4190-5165 m/s; transverse $v_t$, 2350-3061 m/s (Dominec 1993). Still, we need these values in order to estimate the

phonon specific heat. By averaging over 8 different measurements from Dominec's review, we find $\langle v_\ell \rangle = 4500 \pm 400$ m/s and $\langle v_t \rangle = 2700 \pm 200$ m/s. Then the average $\langle v_{ph} \rangle$ can be found by

$$\langle v_{ph} \rangle = v_\ell \frac{2s^2 + 1}{2s^3 + 1} \tag{7.2}$$

where $s = v_\ell / v_t = 1.7 \pm 0.2$. This gives $\langle v_{ph} \rangle = 2900 \pm 200$ m/s. Compared to just an in-plane average of roughly 4000 m/s (Lussier 1997), this is small, but since we are interested in calculating the maximum phonon specific heat, we will use the former value. Thus we calculate the specific heat to be

$$\begin{aligned} c_{ph} &= \frac{2\pi^2}{5} k_B \left(\frac{k_B}{\hbar \langle v_{ph} \rangle}\right)^3 \\ &= 5.0 \times 10^{-3} \text{ mJK}^{-4}\text{cm}^{-3}. \end{aligned} \tag{7.3}$$

At temperatures low enough that the mean free path of phonons reaches its maximum, temperature-independent value, governed by boundary scattering, and hence given by the dimensions of the crystal, the Debye theory gives a $T^3$ temperature dependence of the correct magnitude, as seen in Table 7.2. Only in the case of A3 do we find some discrepancy, which is not understood. It has the largest cross-sectional area so we expect the phonon term to be the largest; instead, it is the smallest, suggesting that the *effective* phonon mean free path is perhaps limited by some defect, like a sandwich for instance. We chose this particular sample for the field study since the $T^3$ regime exists over a larger temperature range.

Note that it is only by going well below 200 mK that one can reliably extract a meaningful residual linear term, $\kappa_0/T$, from a linear fit to $\kappa/T$ vs $T^2$. From Fig. 7.8, if we try to extrapolate $\kappa/T$ to zero temperature for $YBa_2Cu_3O_{6.0}$ from about 150-200 mK, we would have a linear term, even though there are no charge carriers in the system! In previous studies of the anisotropy in $\kappa$, measurements were limited to temperatures above 200 mK (Gold *et al.* 1994, Behnia *et al.* 1995, Wand *et al.* 1996) and the extrapolations were therefore overestimated.

The values of $\kappa_0/T$ obtained from the fits to the data in Fig. 7.9 are given in Table 7.2, and are summarized as follows:

$$\mathbf{J} \parallel \mathbf{a} \; : \kappa_{0,a}/T = 0.14 \pm 0.03 \text{ mW} \cdot \text{K}^{-2} \cdot \text{cm}^{-1}, \tag{7.4}$$

| Crystal | $\kappa_0/T$ [mWK$^{-2}$cm$^{-1}$] | $\kappa_{ph}/T^3$ [mWK$^{-4}$cm$^{-1}$] | $\kappa_{ph}/T^3$ (calc) [mWK$^{-4}$cm$^{-1}$] |
|---|---|---|---|
| A1 | 0.15±0.01 | 18±1 | 14 |
| A2 | 0.14±0.04 | 12±3 | 10 |
| A3 | 0.12±0.01 | 6±1 | 17 |
| B1 | 0.17±0.03 | 12±2 | 11 |
| B2 | 0.18±0.01 | 13±1 | 12 |

**Table 7.2:** Fitting parameters of $\kappa/T$ to $a + bT^2$ (for $T < 130$ mK) where $a$ is the quasiparticle linear term $\kappa_0/T$ and $b$ is the phonon term $\kappa_{ph}/T^3$. In calculating the (maximum) phonon term, we have used $\beta = 5.0$ mJ K$^{-4}$ cm$^{-3}$ and $\langle v_{ph} \rangle = 2900$ m/s, determined from Equation (7.3).

$$\mathbf{J} \parallel \mathbf{b} \; : \kappa_{0,b}/T = 0.18 \pm 0.03 \text{ mW} \cdot \text{K}^{-2} \cdot \text{cm}^{-1}: \tag{7.5}$$

$$\text{Anisotropy} \; : \kappa_{0,b}/\kappa_{0,a} = 1.3 \pm 0.3. \tag{7.6}$$

Along the $a$-axis, our value of 0.14±0.03 mW K$^{-2}$ cm$^{-1}$ is slightly lower than the previously reported value of 0.19±0.03 mW K$^{-2}$ cm$^{-1}$ (Taillefer *et al.* 1997), though still within the experimental uncertainty. We attribute this difference to a better fit at low temperature due to an increased point density at the lowest temperatures.

The quoted uncertainty of about 20% on both $\kappa_0/T$ and $\kappa_{0,b}/\kappa_{0,a}$ is a combination of the uncertainty on the geometric factors (roughly 10%) and the uncertainty on the $T$=0 extrapolation. The scatter in the values obtained for the various crystals within each set is consistent with the latter uncertainty. An additional 10% uncertainty comes from the scatter in the values obtained for the two sets of crystals. Of course, the value of 1.3 is directly dependent on our estimate of the resistivity ratio at room temperature, taken to be 2.3.

Our results are comparable to the existing data on charge conductivity of Zhang *et al.* (1994) (reviewed in Section 4.4.2): multipying their values for $\sigma_1(T \to 0)$ by the Sommerfeld value of the Lorenz number give $\kappa_{0,a}/T = (0.11 \pm 0.04)$ mW K$^{-2}$ cm$^{-1}$ and $\kappa_{0,b}/T = (0.17 \pm 0.05)$ mW K$^{-2}$ cm$^{-1}$. The $\sigma_1(T \to 0)$ data of (Hosseini *et al.* 1998a) for 0.15% Zn-doped samples correspond to $\kappa_{0,a}/T = (0.16 \pm 0.05)$ mW K$^{-2}$ cm$^{-1}$ and $\kappa_{0,b}/T = (0.44 \pm 0.13)$ mW K$^{-2}$ cm$^{-1}$. It appears that

the Wiedemann-Franz law is applicable along $a$, although we do note that the uncertainty for $\sigma_{1,0}$ is almost 50%. In order to fully test the Wiedemann-Franz law, it is necessary to await further $\sigma_1$ measurements. As for the anisotropy, in the case of pure $YBa_2Cu_3O_{7-\delta}$, the residual charge conductivity anisotropy is 1.5±0.7, but with 0.15% Zn-doping, 2.8±1.2 (the large uncertainty is not due to the surface resistance measurement alone, but rather to the $\lambda_0^3$ used to get the conductivity). Considering that Zn preferentially goes into the planes, and that within the planes, $a$-axis heat conduction is independent of impurities, it is surprising that such a low level of Zn doping should produce such a change. However, the more recent data were taken with improved accuracy, and so one wonders whether the problem has to with the earlier set of data. This would leave us questioning (1) the validity of the Wiedemann-Franz law and/or (2) the origin of the "disappearance" of chain thermal transport compared to charge transport.

### 7.4.1 Comparison with Theory

We are now in a position to make a quantitative comparison with the theory for a superconductor with $d_{x^2-y^2}$ symmetry. As this is meant to apply only to the $CuO_2$ planes, we focus at first on $a$-axis properties. As usual, the gap function is taken to be $\Delta_0\cos(2\phi)$. Apart from the gap maximum $\Delta_0$, the only other relevant energy scale is the impurity bandwidth $\gamma$ (Graf *et al.* 1996, Xu *et al.* 1995). For temperatures less than $\gamma$, $N(\omega)$ is roughly constant, so impurity scattering dominates.

For the bi-layer structure of YBCO, $n = 2/c$ where $c = 11.7$ Å is the $c$-axis lattice constant. Combining this with Equations (2.25) and (7.6) yields

$$\frac{v_F}{v_2} = 14 \pm 3. \tag{7.7}$$

Recall that the temperature dependence of the penetration depth is also related to the ratio $v_F/v_2$, by Eq. (4.8). However, when we set $v_F/v_2 = 14$ and $\lambda(0) = 1600$ Å Basov *et al.* (1995), $\delta\lambda/T$ comes out to be larger by a factor of 2 than the measured $a$-axis value of 4.7 Å/K Zhang *et al.* (1994). This factor of 2 discrepancy could be due to Fermi liquid corrections from quasiparticle interactions (Wen and Lee 1998, Millis *et al.* 1998, Xu *et al.* 1995). After all, there are quasiparticles, so it is fair to ask if they are interacting. In this case, Eq. (4.8) would have to be modified by the Fermi

liquid parameter $\alpha^2$:

$$\frac{1}{\lambda^3(0)}\frac{\delta\lambda(T)}{T} = 4\ln 2\frac{k_B e^2}{\hbar^2 c^2} n\alpha^2(\frac{v_F}{v_2}). \tag{7.8}$$

Now measurements of $\kappa/T$ and $\delta\lambda/T$ agree if $\alpha^2 = 0.56$, a sizeable correction to the charge current. This supports a recent ARPES study in BSCCO which finds a correction of the same magnitude (Mesot *et al.* 1999). Note that heat currents are expected to be unaffected by Fermi liquid corrections (Lee 1998).

Along $b$, our measurement of $\kappa_{0,b}/T = (0.18\pm0.03)$ mW K$^{-2}$ cm$^{-1}$ gives $v_F/v_2 = 18\pm3$. Again using Eq. (4.8), with $\lambda(0) = 1050$ Å Basov *et al.* (1995), one obtains $\delta\lambda_b(T)/T = 3.2 \pm 0.5$ Å/K. Experimentally, $\delta\lambda_b(T)/T = 3.6$ Å/K (Zhang *et al.* 1994). Although the values agree without invoking any Fermi liquid corrections, we note that along $b$ there are chains, which have not been folded into the theory. In other words, this direct comparison between $\kappa/T$ and $\delta\lambda(T)/T$ with theory may not be meaningful.

It is better to compare the measured anisotropy ratios, $\kappa_b/\kappa_a = 1.3\pm0.3$ and $\delta\lambda_a^2/\delta\lambda_b^2 = 1.7$ (no error bars provided). Though they seem to agree within error, we allow that the anisotropy in $\kappa/T$ may well be lower than that in $\delta\lambda/T$. We also note that the anisotropy in the plasma frequency $\omega_p = c/\lambda(0)$, $\omega_{p,b}^2/\omega_{p,a}^2 = 2.4$, is supported by a similar anisotropy ratio $\sigma_{1,b}/\sigma_{1,a} = 2.8\pm1.2$, although the samples have 0.15% Zn. Considering that our $\kappa$ data is consistent with zero anisotropy, we must try to understand how this can be.

So let us look at conduction in the one-dimensional chains. It has been shown that in a quasi-one-dimensional regime, dc conductivity is dependent on the scattering rate $\Gamma$ so that there is no universality expected in chain transport (Balatsky *et al.* 1994). Hence above some critical impurity concentration, it is possible that the chains cease to conduct because the scattering time is too short. Furthermore, it may be that within the chains, the nodes, if they exist, do not intersect the Fermi surface; hence the quasiparticle excitation spectrum would be gapped, resulting in the absence of zero-energy quasiparticles to conduct heat in the chains (O'Donovan and Carbotte 1997). Finally, there is the possibility of localization effects in the chains (Lee 1998, Senthil *et al.* 1998); it has been shown (Lee 1993) that disorder can lead to a mobility gap for low energy quasiparticles in the $d$-wave state. This last scenario is very likely because the chains are definitely more prone to disorder

than the planes, so that even a low concentration of impurities can lead to activated conduction along the chains, thereby reducing the anisotropy at low temperature. Incidentally, our $a$-axis data are compatible with the calculation of Senthil *et al.* (1998): putting $\frac{v_F}{v_2} = 14$ into (2.26), the predicted value of $\kappa_0/T$ is 0.14 mW K$^{-2}$ cm$^{-1}$, which agrees with the measured value. This shows that the quasiparticles in the planes are not localized.

Recently chain disorder has been specifically incorporated in band structure calculations within a proximity model (Atkinson 1999). In this treatment, oxygen vacancies in the chains serve to break them into finite segments of length $\ell_{ch}$. Thus an electron needs to tunnel into a neighbouring plane in order to contribute to conductivity. The characteristic time for tunneling depends on the plane-chain coupling strength. If that time is longer than $\ell_{ch}/v_F$, the electron will not have tunneled out of the chain by the time it has encountered an oxygen vacancy and will be back-scattered. However, if the tunneling time is shorter than $\ell_{ch}/v_F$, the electron may be forward-scattered since there is a probability that it is in the plane layer. Atkinson argues that because of band structure effects, the tunneling time is strongly $k$-dependent, and so some electrons are strongly coupled to both planes and chains while others are mostly chain-like. These latter quasi-one-dimensional ones are susceptible to localization. By including disorder, he was able to fit $a$ and $b$ axis penetration depth data which was not possible with previous proximity models, which tended to diverge at $T$=0. Moreover, he has also fit specific heat data. From the good agreement with existing data which are highly anisotropic, he concludes that localization must not be important. Although this model works well for $\lambda^2(0)/\lambda^2(T)$, it cannot explain the small anisotropy in $\kappa$.

We would also like to examine the case where one takes into account the anisotropy of the gap due to the presence of an $s$-wave component, in addition to an orthorhombic elliptical Fermi surface associated with the planes, i.e. the Fermi surface is distorted from tetragonality due to the presence of the chains (Wu, Branch and Carbotte 1998). Such a $d_{x^2-y^2}+s$-wave superconductor would have nodes shifted off the diagonals, which can perhaps account for the measured *ab* anisotropy without even considering conduction along the chains. In fact, by including both band and gap anisotropy, anisotropic universal features (in the impurity independent sense) have been found. Unfortunately, existing data on the penetration depth and the thermal conductivity are not mutually compatible with this theory, since to fit $\kappa$

requires a large and negative $s$ component which contradicts the $\lambda$ data.

Wu and Carbotte (1998) have since returned to the proverbial drawing board, and come up with another explanation for the weak anisotropy in thermal conductivity that is compatible with a larger penetration depth anisotropy. Transport measurements ($\sigma_1$, $\kappa$) are sensitive to the nodes on the Fermi surface, whereas $\lambda(T)$ is not. Thus if the gap nodes do not cross the chain Fermi surface, there would be a suppression in chain transport which would yield a weak $ab$-anisotropy. Based on this idea, Wu and Carbotte have introduced a cut-off angle $\phi_c$ to the $d$-wave gap $\Delta = \Delta_0 \cos 2\phi$. So $\phi_c > \pi/4$ (position of node) corresponds to the opening of a minimum gap on the chain Fermi surface.

## 7.5 Results on Magnetic Field Dependence

Application of an external magnetic field parallel to the $c$-axis is predicted to increase the linear term in $\kappa(T)$, corresponding to the increased availability of extended quasiparticle states. Thus there are two main issues to resolve: does an external field increase the density of states, and if so, can the theory account for the magnitude of the effect?

### 7.5.1 $YBa_2(Zn_xCu_{1-x})_3O_{7-\delta}$

Since we are looking at samples doped with Zn, we need to have an idea of the scattering rates. These we can determine from the change in resistivity, which amounts to a rigid off-set due to the increase in $\rho_0$. In other words, elastic scattering due to impurities increases with doping while inelastic scattering is unaffected. Now the impurity scattering rate $\Gamma = 1/(2\tau_0)$ is related to $\rho_0$ by $\rho_0 = m^*/(ne^2\tau_0)$ in Drude theory. So as a function of doping $x$, the scattering rate can be written as

$$\Gamma(x) = (\omega_p^2/8\pi)[\rho_0(x=0) + \Delta\rho_0(x)] \tag{7.9}$$

where $\Delta\rho_0$ is the shift in the $\rho$ vs $T$ intercept seen in Fig. 7.10, equal to 8.3 $\mu\Omega$cm for the 0.6% Zn-doped sample and 37.2 $\mu\Omega$cm for the 3%. From microwave conductivity, the mean free path has been shown to increase one hundredfold between 100 K to about 10 K (Bonn *et al.* 1994), so with $\rho(100\ K) \simeq 75\ \mu\Omega$cm, we estimate $\rho_0(x=0) < 1\ \mu\Omega$cm. By taking $\omega_p = 1.3$ eV (Basov *et al.* 1995), we get $\hbar\Gamma/k_BT_{c0} =$

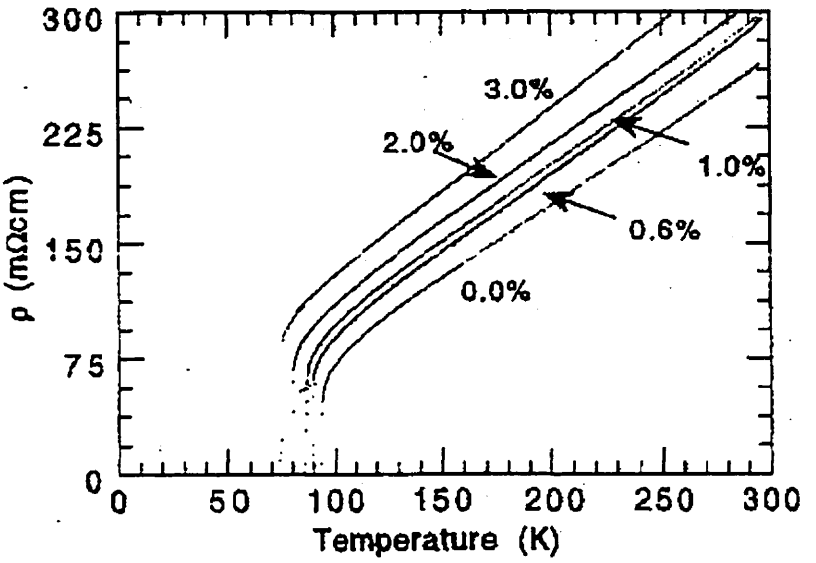


**Figure 7.10:** Electrical resistivity of $YBa_2(Zn_xCu_{1-x})_3O_{7-\delta}$ for $x = 0.0\%$, 0.6%, 1.0%, 2.0% and 3% measured by Pu (1997). The curves are all rigidly shifted by $\Delta\rho_0$ from the undoped sample.

0.014, 0.13, and 0.54 for $x = 0$, 0.006 and 0.03, respectively (Taillefer *et al.* 1997).

These values are not far from those predicted by the simplest theory for the suppression of $T_c$, from the value of $T_{c0}$ of 93.6 K in the pure sample, with impurity concentration (Sun and Maki 1995). By assuming a uniform reduction of $\Delta$ with the addition of impurities, Sun and Maki obtain $\hbar\Gamma/k_BT_{c0} = 0.06$ and 0.25, for $x = 0.006$ and 0.03. If spatial variations in the order parameter are included, a self-consistent calculation (within mean field theory) shows that the drop in $T_c$ with $\Gamma$ is less steep, giving values of $\Gamma$ roughly 3 times larger (Franz *et al.* 1997). This latter treatment gives a critical impurity concentration $n_c \approx 0.10$, which reflects the robustness of $T_c$ seen experimentally (Ishida *et al.* 1993). Our values determined above from a combination of resistivity, microwave conductivity and infrared reflectivity lie somewhere in between the two calculations, which is reasonable for such a simple Drude approach. Note also that the impurity bandwidth in the 3% Zn sample is a sizable fraction of the gap maximum, so that corrections to the universal limit are expected. Calculations by Sun and Maki (1995) give a 30% increase in $\kappa_0/T$ for 20% $T_c$ suppression (see Section 2.1.3), in good agreement with the observed slight increase (see Fig. 7.12 or Fig. 7.11).

Fig. 7.11 shows the total thermal conductivity divided by temperature $\kappa/T$ of

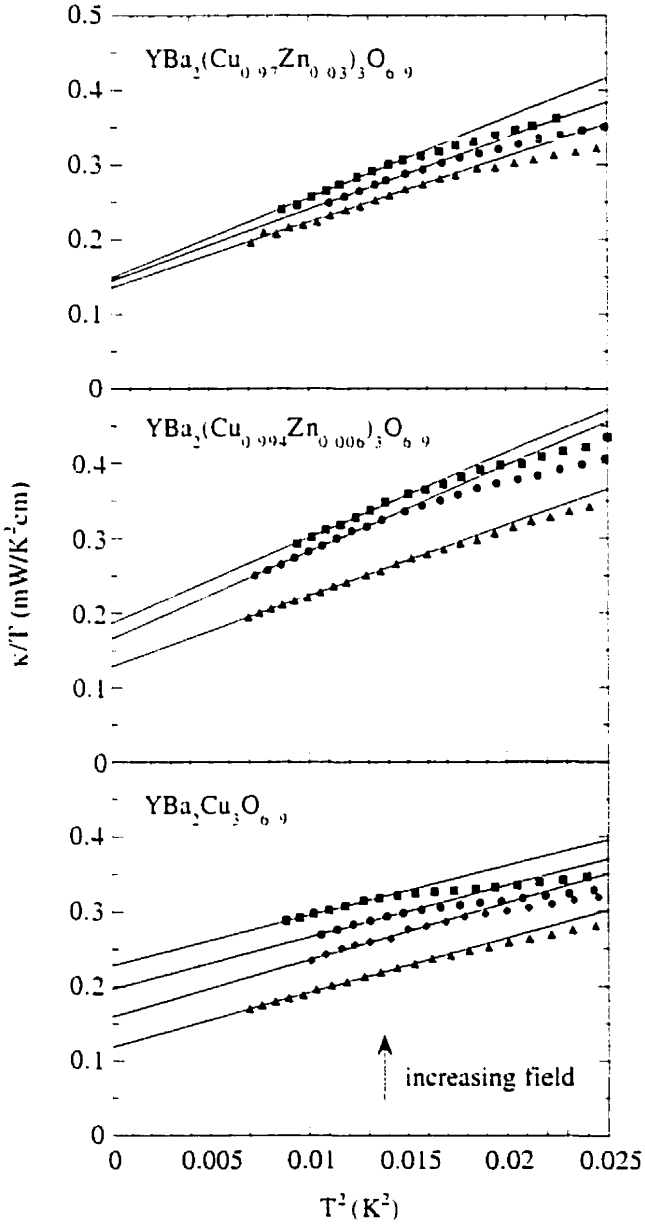


**Figure 7.11:** Thermal conductivity divided by temperature $\kappa/T$ vs $T^2$ of $YBa_2(Cu_{1-x}Zn_x)_3O_{6.9}$ in an applied field. The bottom panel corresponds to $x$=0: middle. $x$=0.006: top. $x$=0.03. Triangles correspond to zero field: diamonds. 2 T: circles. 4 T: squares. 8 T. Substitution of Zn at the planar Cu site suppresses the increase of $\kappa/T$ as T→0 with field.

$YBa_2(Zn_xCu_{1-x})_3O_{7-\delta}$ as a function of $T^2$ in fields up to 8 T. The bottom panel shows the data for the pure sample; the other two panels show data for Zn-doped samples, 0.6% in the middle panel and 3% in the top panel. First we observe a definite increase in $\kappa_0/T$ ($\kappa/T$ as $T \to 0$) as the field is increased, which indicates the population of the extended quasiparticle states. Secondly, we have effectively varied the scattering rate $\Gamma$ by at least a factor of 20, and clearly the field effects are suppressed rapidly with increasing $\Gamma$, as predicted by theory.

### 7.5.2 Comparison with Theory

We can now compare directly with the calculated magnetic field response of the residual normal fluid. In Fig. 7.12, we display the calculated $\kappa(0; H)/T$ by Kübert and Hirschfeld (1998b) (Equation (2.35)) as a function of field together with the data. From fitting $\rho$, we can then extract $\Gamma$ since $\rho = \sqrt{\frac{6}{\pi}}\frac{\gamma}{E_H}$ and $\gamma \simeq 0.61\sqrt{\Gamma\Delta_0}$. The first point to note is that the sub-linear dependence on field is well reproduced. Perhaps more important is the fact that the magnitude of the response in all three cases is very much as expected. Indeed, the fits yield the following values for $\rho$, evaluated at 8 T: 0.92, 1.63, and 4.32 for $x = 0$, 0.006, and 0.03, respectively. These correspond to a ratio $\gamma/E_H = 0.67$, 1.18 and 3.12, which shows that none of the crystals is in the clean limit over the field range investigated. Treating impurity scattering in the unitarity limit, the scattering rate becomes: $\hbar\Gamma/k_BT_{c0} = 0.02$, 0.07, and 0.5, respectively (taking $\Delta_0 = 2.14k_BT_{c0}$), given that $E_H \simeq 20$ K at 8 T (assuming $v_F = 1\times10^7$ cm/s and $a$=1/2). In Table 7.3, we compare these scattering rates to the independent estimates quoted above, as well as with those extracted from high temperature fits to the theory of Hirschfeld and Putikka (1996). We view our values of $a$ and $v_F$ as reasonable, at least to within a factor of 2.

We would like to point out that while we do use the $T = 0$ extrapolation to compare with the theory, our "raw" data works just as well. For instance, if we take the value of $\kappa/T$ at a fixed temperature, we can obtain the field-induced increase in the electronic thermal conductivity by subtracting $\kappa_0/T$. As long as this temperature is within the $T^3$ region, this quantity will be purely electronic. We show in Fig. 7.13 that at 100 mK, $\kappa_0(H)/T$ is very close to the extrapolated value, while at 200 mK, phonon "contamination" is present. Again, this emphasizes the importance of making measurements at temperatures low enough that we can separate the phonons from the quasiparticles. The agreement gives us confidence in our $T = 0$ extrapolation

| Method | pure | 0.06% | 0.3% |
|---|---|---|---|
| (1) | 0.014 | 0.13 | 0.54 |
| (2) | — | 0.06 | 0.25 |
| (3) | 0.02 | 0.07 | 0.5 |
| (4) | 0.007 | 0.09 | 0.4 |

**Table 7.3:** Values of independent estimates of $\Gamma/T_{c0}$, in units of $[\hbar/k_B]$: (1) obtained from a combination of $\rho_0$ and microwave estimates: (2) calculated from the decrease in $T_c$ with doping (Sun and Maki 1995): (3) fitted from theory of Kübert and Hirschfeld (1998b): (4) fitted from high temperature theory of Hirschfeld and Putikka (1996).

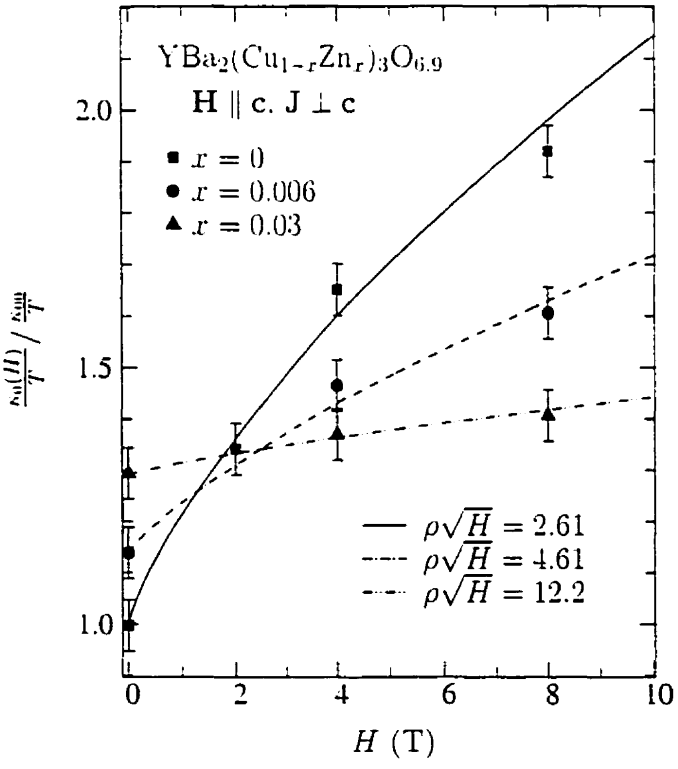


**Figure 7.12:** Normalized residual linear term $\kappa_0(H)/T$ as a function of applied field for pure (squares) 0.6% Zn-doped (triangles) and 3% Zn-doped (circles) samples. Fits to (2.35) for each crystal yields the values of $\rho$ shown.

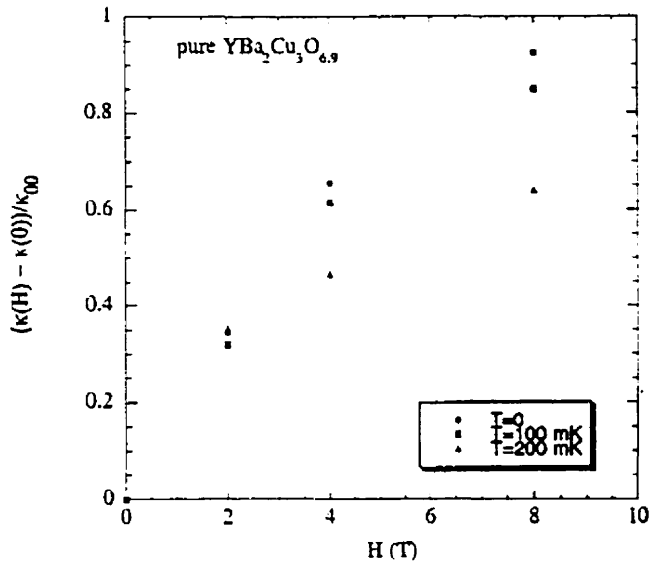


**Figure 7.13:** $\Delta\kappa(H)/\kappa_{00} = (\kappa(H) - \kappa(0))/\kappa_{00}$ in pure $YBa_2Cu_3O_{7-\delta}$ at $T = 0$ (circles), 100 mK (squares) and 200 mK (triangles).

and we will continue to use the latter approach in analysing our data.

From our measurements of the field dependence of the thermal conductivity in $YBa_2Cu_3O_{7-\delta}$, we have strong evidence for the Volovik effect, i.e. of the quasiparticle state Doppler shift being responsible for the occupation of the extended states. Moreover, the size of the magnitude of the increase as a function of impurity concentration follows the theory using a scattering phase shift of $\delta_0 = \pi/2$, showing unambiguously that these Zn-doped samples must be treated in the limit of strong unitarity scattering. This had always been assumed but not confirmed, until now.

### 7.5.3 Discussion

The same theoretical treatment applies to the specific heat as well. A numerical evaluation of Equation (4.12) using $A = 0.9$ mJ $K^{-2}$ $T^{-1/2}$ $mol^{-1}$ (Moler *et al.* 1997, Wright *et al.* 1999) gives $v_2 = 2.2a\times10^6$ cm/s. From the previous section, $\kappa(0; H)/T$ gave us $av_F = 5.0\times10^6$ cm/s. Moreover, the zero field $\kappa_0/T$ value gave the ratio $v_F/v_2$ to be 14. The first two expressions together yield $v_F/v_2 = 2.27/a^2$. If we set this ratio to be 14, we find $a = 0.40$. Thus $v_F = 1.2\times10^7$ cm/s and $v_2 = 0.9\times10^6$ cm/s. Furthermore, with $a = 0.4$ and $v_F = 1.2\times10^7$ cm/s, $E_H(1\ T) = 6.4$ K, which is what Wright *et al.* (1996) observe in Fig. 4.12. We see that we are indeed

getting a very consistent picture between experiments and *d*-wave theory.

Before further discussing other measurements, we would like to take a closer look at the thermal conductivity data *away from* $T=0$. There is something very interesting about the field dependence in the pure sample. In the lower panel of Fig. 7.11, the increase in $\kappa/T$ is slightly less pronounced at high temperature than at low temperature. It is very tempting to say that we are seeing the intrinisic finite temperature effects predicted by theory (Graf *et al.* 1996), i.e. that the scattering time (hence $\kappa$) decreases rapidly with temperature (or energy). However, according to the theory, for this to be the case, the temperature must be comparable to the impurity bandwidth, since the correction goes as $(\frac{k_B T}{\gamma})^2$. Given that our above estimates of $\gamma$ exceed 10 K in the purest sample, no temperature dependence should be seen below 1 K. Moreover, high temperature fits of $\kappa$ and $\sigma_1$ would have $\Gamma$ an order of magnitude smaller. We must therefore ask ourselves if we have overestimated $\Gamma$, i.e. if the theory is correct.

First of all, the fitting parameter is really $\rho$ and not $\Gamma$, so with $a$ and $v_F$ buried in $\rho$ as well, $\Gamma$ can easily be off by a factor of 2. We really do not think that we should speculate on the consistency of the theory based on a sample-dependent phonon slope which obscures any electronic contribution; rather, we believe in the zero temperature analysis. However, we suggest a few reasons why the field dependence of the pure sample may differ from that of a sample with a larger scattering rate.

1. The theory does not take into account e-e inelastic scattering. This effect should be more pronounced in a high purity sample due to the longer mean free path, so it is conceivable that there may be some inelastic scattering affecting the pure crystal.

2. While vortex scattering of phonons at higher temperature appears to be unimportant due to the plateau, there may be an effect at low temperature.

3. Finally we mention the phase shift. Our results show that there is no doubt that Zn is a unitary scatterer. However, Hosseini, Hardy, Bonn and co-workers seem to think Born scattering is more appropriate in pure crystals (Hosseini *et al.* 1998b), given that they observe a lower power than $T^2$ in $\sigma_1(T)$ at low temperature. Granted, their new crystals grown in barium zirconate crucibles are roughly ten times purer than our crystals grown in yttria-stabilised zirconia, so our nominally pure crystal could be somewhere between Born and resonant

scattering, although it would have to be close to the resonant limit since the $\delta_0 = \pi/2$ seems to describe the data extremely well.

For the moment, we resist making comments about finite temperature corrections until the effect can actually be seen in a careful study of samples of high purity. In any case, this does not affect our analysis at $T$=0.

Let us now compare our results with other $\kappa$ measurements. Recall that previous low temperature measurements in $YBa_2Cu_3O_{7-\delta}$ were done with the field in the basal plane where the Volovik effect is expected to be much smaller, since the quasiparticles travel parallel to the vortex tubes. Furthermore, the two studies were in disagreement, with a 50% increase in 8 T reported by Bredl *et al.* (1992), but no change detected in 6 T by Wand *et al.* (1996). At higher temperatures, the fact that $\kappa$ decreases with field (Krishana *et al.* 1998) could come from various scattering effects. Perhaps the most natural is vortex scattering of quasiparticles, as invoked in the case of Nb (Lowell and Sousa 1970). While this can apply to both quasiparticles and phonons, the fact that the largely electronic peak below $T_c$ is almost completely suppressed in 10 T (Palstra *et al.* 1990) suggests that the former suffer most of the impact.

Franz (1999) has shown that a disordered vortex lattice in a *d*-wave superconductor can result in quasiparticles scattering off the superflow. For high fields, the density of vortices means that the quasiparticle mean free path $\ell^{-1} = \ell_0^{-1} + \ell_H^{-1}$ is dominated by $\ell_H$, i.e. $\ell_0 = v_F\tau \simeq 0.25$ $\mu$m in the pure sample (0.070 $\mu$m with 0.6% Zn and 0.012 $\mu$m with 3%) and the upper bound of $\ell_H \simeq 2R \simeq \sqrt{\Phi_0/H} \simeq 0.02$ $\mu$m at 8 T. The actual $\ell_H$, governed by the amount of disorder in the vortex lattice, would be smaller than the intervortex distance. Since this mean free path goes as $1/\sqrt{H}$, it cancels the $\sqrt{H}$ in $N(0;H)$, producing a field-independent *universal* $\kappa/T$ at fields large enough that vortices are the dominant scattering process. The theory can account qualitatively for the observed field dependence of $\kappa$, at temperatures above 5 K. At low temperature, however, we find no indication of significant vortex scattering, a conclusion based on the good agreement between calculations, which neglect vortex scattering, and our data on crystals for which the relative strength of impurity and vortex scattering must differ markedly from one crystal to the next. Moreover, STM images of the vortex lattice at 6 T show a reasonably ordered vortex lattice (see Fig. 4.9). To reconcile the two temperature regimes, Franz has suggested that at low energies, the vortex scattering cross-section becomes sufficiently small that vortices are rendered "transparent" to quasiparticle motion Franz (1999).

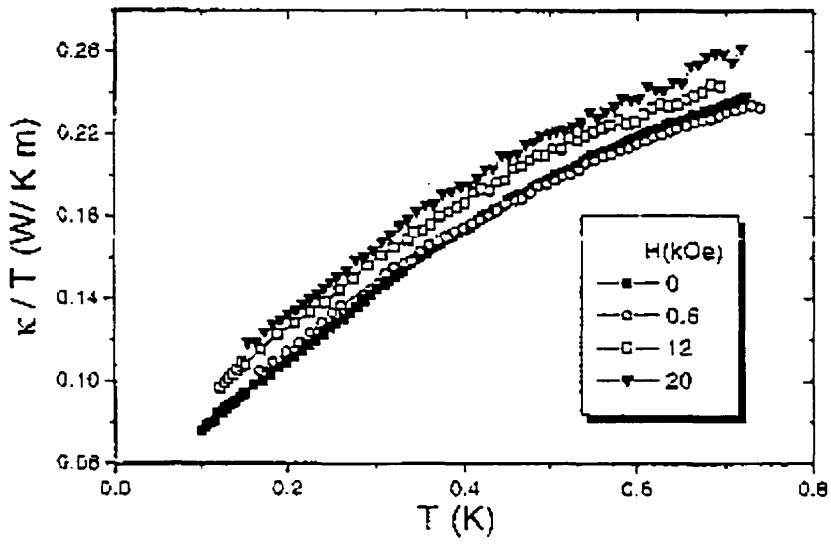


**Figure 7.14:** Thermal conductivity divided by temperature $\kappa/T$ in BSCCO, obtained by Aubin *et al.* (1999). Although there is no $T^3$ region, the rigid shift of the curves is evidence for an increase in linear electronic contribution.

It is interesting to compare our results on YBCO with the corresponding results on BSCCO, obtained recently by Aubin, Behnia and co-workers (1999) and displayed in Fig. 7.14. At temperatures below 0.7 K, an increase in $\kappa/T$ with field is also found, again with a sublinear (roughly $\sqrt{H}$) dependence. What is striking is the *magnitude* of the response in Fig. 7.15. The application of only 2 T increases $\kappa/T$ by about 0.20 mW $K^{-2}$ $cm^{-1}$. Now from our own measurements on pure, optimally-doped single crystals of BSCCO, the (presumably universal) residual linear term is $\kappa_0/T$ = 0.15±0.03 mW $K^{-2}$ $cm^{-1}$ (Lambert 1998). This means that in BSCCO a field of 2 T causes the quasiparticle conduction to *double*, whereas it produces only a 35% increase in our pure YBCO crystal. So a similar fit as for YBCO shows $\gamma/E_H$ to be 2.6 times smaller in BSCCO, or $\Gamma$ to be 7 times smaller. In reality, the field dependence in BSCCO is much more than 3 times stronger, since the impurity scattering rate in the crystal used by Aubin and co-workers is probably about 100 times larger. Indeed, its residual resistivity is 130 $\mu\Omega$ cm (Behnia 1998), compared with approximately 1 $\mu\Omega$ cm in our pure YBCO crystals. These considerations compel us to conclude that the nature of defect (or possibly vortex) scattering in these two (otherwise quite similar) materials is strongly different. Either the kind of defect found in nominally pure crystals is different, or the impact that a given scattering centre (e.g. impurity

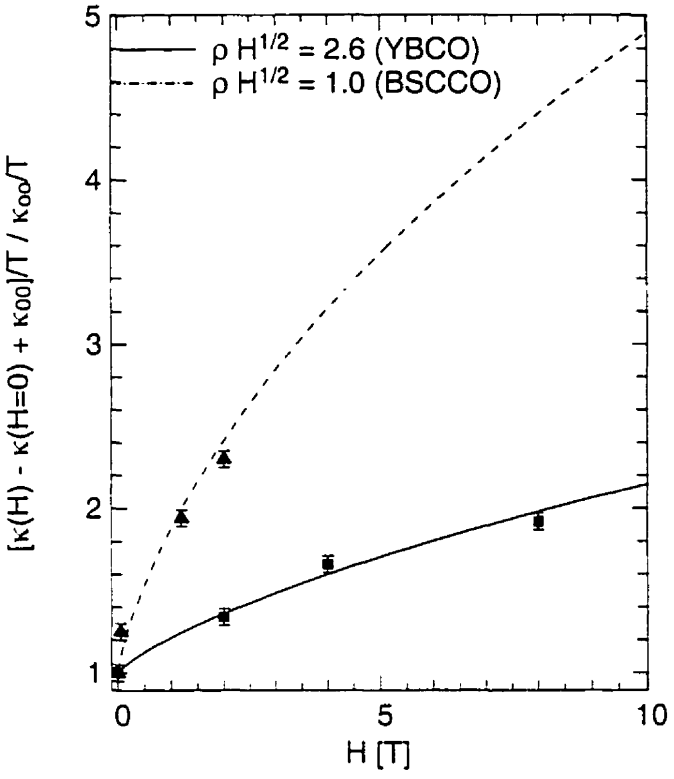


**Figure 7.15:** A comparison of the increase in $\kappa/T$ with applied field between BSCCO and pure YBCO. For BSCCO, the data were taken from Fig. 7.14 at 200 mK and normalized by $\kappa_{00}$ = 0.20 mW K$^{-2}$ cm$^{-1}$.

or vortex) has on the surrounding electron fluid is different.

## 7.6 Conclusion

In conclusion, low temperature thermal conductivity measurements along the $a$ axis of $YBa_2Cu_3O_{7-\delta}$ have yielded a Fermi velocity ratio $v_F/v_2 = 14 \pm 3$. When compared with penetration depth data, which also measures this ratio, one finds a sizeable Fermi liquid correction to the charge current as would arise from quasiparticle interactions.

By measuring $b$ axis crystals as well, we have found a weak anisotropy of 1.3±0.3 in the in-plane heat conduction of $YBa_2Cu_3O_{6.9}$ as $T \to 0$. This is consistent with the low temperature anisotropy observed in the real part of the microwave conductivity $\sigma_1$ in a pure sample, though not in a Zn-doped sample, and is much weaker than the oft-quoted anisotropy of 2.2 for transport in the normal state. We believe that the weak anisotropy reflects the lack of conduction along the Cu-O chains along the

$b$-axis, possibly due to a gapped excitation spectrum or quasiparticle localization in the chains.

We have also measured the low temperature thermal conductivity of $YBa_2Cu_3O_{7-\delta}$ with three different levels of impurities as a function of magnetic field applied along the $c$-axis. In all cases, the residual linear term $\kappa_0/T$ increases with field strength, reflecting the population of extended quasiparticle states. In addition, the growth of $\kappa_0/T$ follows very well the predicted $d$-wave behaviour: increased scattering rates strongly suppress the ability of the residual normal fluid to carry heat when there is an external field. The good agreement with calculations by Kübert and Hirschfeld for a $d$-wave superconductor allows us to draw the following conclusions: 1) the "Volovik effect" is fully verified, and it is the dominant mechanism behind the field dependence of transport in YBCO as $T \to 0$, for $\mathbf{H} \parallel \mathbf{c}$; 2) vortex scattering, invoked to explain the behaviour at intermediate temperatures, is weak at low temperature (except perhaps in the pure sample); 3) the widespread assumption that impurities (or defects) can be treated as unitary scatterers in correlated electron systems is verified in YBCO, not only in the special case of Zn-doped crystals, but also more generally in nominally pure samples; 4) the nature of impurity scattering appears to differ between BSCCO and YBCO.

# 8 Conclusion

From a materials point of view, heavy fermion superconductors and high-$T_c$ cuprates are extremely different. In the normal state, we have metals on the one hand, and poor conductors on the other. In the superconducting state, with critical temperatures differing by roughly 2 orders of magnitude, it is not obvious that there should be any similarities. This is where the physics comes in. By virtue of the existence of zeroes in the superconducting order parameter, all low temperature properties are dominated by the nodal regions. In particular, impurity scattering leads to a finite density of states near the nodes, and there exists a novel, residual normal fluid of quasiparticles even at zero temperature. This normal fluid deep in the superconducting state behaves just like that in a normal metal, with quasiparticle heat conductivity $\kappa$ varying as $T$. Using thermal conductivity, we can probe these zero energy quasiparticle states along high symmetry directions. Gap anisotropy can be directly revealed with this technique.

Our observation of a finite value of $\kappa/T$ in $UPd_2Al_3$ further supports the evidence for a residual normal fluid from other experiments such as specific heat, NMR relaxation rate and differential tunneling conductivity. In addition, our directional sensitivity showed a residual $\kappa/T$ of roughly 10% of the normal state value both within the basal plane and along $c$. This elimates those gap candidates with only polar or equatorial nodes (assuming a spherical Fermi surface), though the tropical gap has two line nodes displaced from the equator and at least two "popular" hybrid gaps have both a line of nodes in the basal plane and point nodes at the poles. To determine which of these gaps (or perhaps a different gap altogether) describe $UPd_2Al_3$ will require further work in both theory and experiment, as will the whole question surrounding the pairing mechanism, whether it is indeed strong coupling to spin fluctuations or not.

Fortunately for $YBa_2Cu_3O_{7-\delta}$, there exists a vast amount of evidence for the $d_{x^2-y^2}$ pairing state. Moreover, the residual normal fluid is well established, and its universal heat conduction already observed. We have also shown that along the $a$ axis, a comparison of $\kappa/T$ and the temperature dependence of the penetration depth

$\delta\lambda$ reveals that the latter may be affected by quasiparticle interactions leading to a Fermi liquid correction in the charge current.

Our study continued with the anisotropy of thermal conductivity by the residual quasiparticles, in an effort to understand the role of the CuO chains running along the $b$ axis. We found an anisotropy $\kappa_b/\kappa_a$ of 1.3±0.3 at $T = 0$, down from about 2.2 in the normal state. Compared with the anisotropy in the real part of the charge conductivity $\sigma_1$ (1.5-2.8), our ratio agrees is rather on the low side. Thus there are two issues: (1) why do we see a weaker anisotropy than other experiments and (2) where has the high temperature anisotropy gone? The answers are not clear, though we suspect that there is either localization of chain quasiparticles due to impurities causing short relaxation times or due to the opening of gap on the chain Fermi surface at low temperature.

Our main investigation has been the magnetic field dependence of low energy quasiparticles. According to theory, quasiparticle states are Doppler shifted due to the superflow around the vortices, leading to the population of extended states. We have found that $\kappa/T$ does indeed increase with applied magnetic field, reflecting the field-enhanced density of states. Furthermore, the growth in $\kappa/T$ can be suppressed by the addition of impurities, in quantitative agreement with the $d$-wave theory assuming resonant impurity scattering to dominate vortex scattering. Thus we conclude that the Doppler shift description of quasiparticles in field is correct, the oft-quoted assumption of impurity scattering in the unitarity limit has been verified by our measurements and that vortex scattering at low temperature does not appear to be important. From our analysis, combined with specific heat data (both in a magnetic field), we have reasonable values for the parameters $v_F = 1.2\times10^7$ cm/s and $v_2 = 0.90\times10^6$ cm/s. Thus we find that the existing $d$-wave theory, largely untested until now, appears to give the proper *quantitative* description of low energy quasiparticle properties in the superconducting state.

# References

A. A. Abrikosov. JETP **5**, 1174 (1957).

S. Adenwalla *et al.*, Phys. Rev. Lett. **65**, 2298 (1990).

H. Akoh, C. Camerlingo and S. Takada, Appl. Phys. Lett. **56**, 1487 (1990).

A. Amato *et al.*, Z. Phys. B **86**, 159 (1992).

James F. Annett, Nigel Goldenfeld and S. R. Renn, in *Physical Properties of High Temperature Superconductors*, edited by Donald M. Ginsberg (World Scientific, Singapore, 1990) vol II, p. 571.

James F. Annett, Nigel Goldenfeld and S. R. Renn, Phys. Rev. B **43**, 2778 (1991).

N. W. Ashcroft and N. D. Mermin, *Solid State Physics* (Saunders College Publishing, Philadelphia, 1976).

W. A. Atkinson, Phys. Rev. B **59**, 3377 (1999).

Hervé Aubin *et al.*, Phys. Rev. Lett. **82**, 624 (1999).

A. V. Balatsky, A. Rosengren and B. L. Altshuler, Phys. Rev. Lett. **73**, 720 (1994).

J. Bardeen, L. N. Cooper, and J. R. Schrieffer, Phys. Rev. **108**, 1175 (1957).

J. Bardeen, G. Rickayzen and L. Tewordt, Phys. Rev. **113**, 982 (1959).

D. N. Basov *et al.*, Phys. Rev. Lett. **74**, 598 (1995).

J. G. Bednorz and K. A. Müller, Z. Phys. **B64**, 189 (1986).

K. Behnia *et al.*, Physica C **196**, 57 (1992).

K. Behnia *et al.*, Synthetic Metals **71**, 1611 (1995).

K. Behnia, private communication (1998).

D. A. Bonn *et al.*, Phys. Rev. B **50**, 4051 (1994).

D. A. Bonn *et al.*, Czech. J. Phys. **46**, 1941 (1995).

D. A. Bonn and W. N. Hardy, in *Physical Properties of High Temperature Superconductors*, edited by Donald M. Ginsberg (World scientific, Singapore, 1996) vol. IV, p. 1.

C. D. Bredl et al., Z. Phys. B **86**, 187 (1992).

B. Bucher *et al.*, Phys. Rev. Lett. **70**, 2012 (1993).

G. Burns, *High temperature superconductivity*, (Academic Press, New York, 1992).

C. Caroli, P. G. de Gennes and J. Matricon, Phys. Lett. **9**, 307 (1964).

R. Caspary *et al.*, Phys. Rev. Lett. **71**, 2146 (1993).

Daniel L. Cox and M. Brian Maple, Phys. Today, 32 (February 1995).

M. Cyrot and D. Pavuna, *Introduction to superconductivity and high-$T_c$ materials*, (World Scientific, London, 1992).

A. de Visser *et al.*, Physica B **179**, 84 (1992).

H. Ding *et al.*, Nature **382**, 51 (1996).

G. J. Dolan *et al.*, Phys. Rev. Lett. **62**, 2184 (1989); L. Vinnikov *et al.*, Zh. Eksp. Teor. Fiz. **49**, 83 (1989).

J. Dominec, Superconductor Science and Technology **6**, 153 (1993).

A. Erb, E. Walker and R. Flükiger, Physica C **245**, 245 (1995); A. Erb, Ph.D. Thesis, Universitat Karlsruhe, Germany, 1994.

D. Esteve *et al.*, Europhys. Lett. **3**, 1237 (1987).

R. Feyerherm *et al.*, Physica B **199&200**, 103 (1994).

R. A. Fisher *et al.*, Phys. Rev. Lett. **62**, 1411 (1989).

R. A. Fisher *et al.*, Physica C **252**, 237 (1995).

Z. Fisk *et al.*, Science **239**, 33 (1988).

M. Franz *et al.*, Phys. Rev. B **56**, 7882 (1997).

M. Franz, Phys. Rev. Lett. **82**, 1760 (1999).

Robert Gagnon *et al.*, Phys. Rev. B **50**, 3458 (1994).

Robert Gagnon *et al.*, Phys. Rev. Lett. **78**, 1976 (1997).

C. Geibel *et al.*, Z. Phys. B **84**, 1 (1991).

C. Geibel *et al.*, Conference Proceedings for $T^2$PFS, Hiroshima, Japan (1992).

V. L. Ginzburg and L. D. Landau, Zh. Eksp. Teor. Fiz. **20**, 1064 (1950).

Z. Gold, *et al.*, Physica C **235-240** 1485 (1994).

L. P. Gor'kov, Sov. Phys. JETP **9**, 1364 (1959).

C. E. Gough *et al.*, Nature **326**, 855 (1987).

M. J. Graf *et al.*, Phys. Rev. B **53**, 15147 (1996).

A. Grauel *et al.*, Phys. Rev. B **46**, 5818 (1992).

F. M. Grosche *et al.*, preprint (cond-mat/9812133).

F. Gross *et al.*, Z. Phys. B **64**, 175 (1986).

W. N. Hardy *et al.*, Phys. Rev. Lett. **70**, 3999 (1993).

S. M. Hayden *et al.*, Phys. Rev. B **46**, 8675 (1992).

Hikami *et al.*, Jpn. J. Appl. Phys. **26**, L314 (1987).

Hiroi *et al.*, J. Phys. Soc. Jpn. **66**, 1595 (1997).

P. J. Hirschfeld *et al.*, Solid State Commun. **59**, 111 (1986).

P. J. Hirschfeld and W. O. Putikka, Phys. Rev. Lett. **77**, 3909 (1996).

P. J. Hirschfeld, private communication

P. J. Hirschfeld, lecture notes on "Disorder and Unconventional Superconductivity in the Cuprates" presented at "Cohérence quantique dans les systemes très correlés",Aussois, France, 1998.

P. J. Hirschfeld, W. O. Putikka and D. J. Scalapino, Phys. Rev. B **50**, 10250 (1994).

C. C. Homes *et al.*, Phys. Rev. Lett. **71**, 1645 (1993).

A. Hosseini, private communication (1998).

A. Hosseini *et al.*, preprint (cond-mat/9811041).

Y. Inada *et al.*, Physica B **119&200**, 119 (1994).

K. Ishida *et al.*, J. Phys. Soc. Jpn. **62**, 2803 (1993).

T. Ito, K. Takenaka and S. Uchida, Phys. Rev. Lett. **70**, 3995 (1993).

B. D. Josephson, Phys. Lett. **1**, 251 (1962).

M. Jourdan, M. Huth and H. Adrian, Nature **398**, 47 (1999).

S. R. Julian *et al.*, J. Magn. Magn. Mat. **177-181**, 265 (1998).

Alain Junod, in *Physical Properties of High Temperature Superconductors*, edited by Donald M Ginsberg (World Scientific, Singapore, 1990) vol. II, p. 13.

Alain Junod *et al.*, Proceedings of the 22nd Int. Conf. on Low Temp. Phys., Aug. 4-11, 1999, Espoo and Helsinki, Finland, to be published in Physica B.

P. H. Kes *et al.*, J. Low Temp. Phys. **17**, 341 (1974).

Charles Kittel, *Introduction to Solid State Physics* (John Wiley & sons, New York 1986).

R. H. Koch *et al.*, Appl. Phys. Lett. **51**, 200 (1987).

N. B. Kopnin and G. E. Volovik, JETP Lett. **64**, 690 (1996).

K. Krishana *et al.*, Phys. Rev. Lett. **75**, 3529 (1995).

K. Krishana *et al.*, Science **277**, 83 (1997).

K. Krishana *et al.*, preprint (1998).

C. Kübert and P. J. Hirschfeld, Sol. St. Commun. **105**, 459 (1998).

C. Kübert and P. J. Hirschfeld. Phys. Rev. Lett. **80**, 4963 (1998).

M. Kyogaku *et al.*, Physica B **186-188**, 285 (1993).

M. Kyogaku *et al.*, J. Phys. Soc. Jpn. **62**, 4016 (1996).

Patrik Lambert. M.Sc. Thesis. McGill University (1998).

L. D. Landau. Zh. Eksp. Teor. Fiz. **35**, 97 (1958); Sov. Phys. JETP **8**, 70 (1959).

A. I. Larkin and Y. N. Ovchinnikov. Zh. Eksp. Teor. Fiz. **55**, 2262 (1968); Sov. Phys. JETP **28**, 1200 (1969).

R. B. Laughlin. Phys. Rev. Lett. **80**, 5188 (1998).

Patrick A. Lee. Phys. Rev. Lett. **71**, 1887 (1993).

Patrick A. Lee and Xiao-Gang Wen. Phys. Rev. Lett. **78**, 4111 (1997).

Patrick A. Lee, private communication (1998).

Ruixing Liang, D. A. Bonn and W. N. Hardy. Physica C **304**, 105 (1998).

H. London. Conf. on Temp. Phys., Oxford (1951); H. London, G. B. Clarke and E. Mendoza. Phys. Rev. **109**, 262 (1956).

J. W. Loram *et al.*, Phys. Rev. Lett. **71**, 1740 (1993).

J. Lowell and J. B. Sousa. J. Low Temp. Phys. **3**, 65 (1970).

Benoit Lussier *et al.*, Phys. Rev. B **53**, 5145 (1996).

Benoit Lussier, Ph.D. Thesis, Mcgill University (1997).

I. Maggio-Aprile *et al.*, Phys. Rev. Lett. **75**, 2754 (1995).

W. Mao and A. V. Balatsky, Phys. Rev. B **58**, 6024 (1999).

M. B. Maple, J. Magn. Magn. Mat. **177**, 18 (1998).

A. Mathai *et al.*, Phys. Rev. Lett. **74**, 4523 (1995).

N. D. Mathur *et al.*, Nature **394**, 39 (1998).

W. Meissner and R. Ochsenfeld, Naturwissenschaften **21**, 787 (1933).

J. Mesot *et al.*, preprint (cond-mat/9812377).

Naoto Metoki *et al.*, Phys. Rev. Lett. **80**, 5417 (1998).

A. J. Millis, S. Sachdev and C. M. Varma, Phys. Rev. B **37**, 4975 (1988).

A. J. Millis et al., J. Phys. Chem. Solids **59**, 1742 (1998).

R. Modler *et al.*, Physica B **186-188**, 294 (1993).

Kathryn A. Moler *et al.*, Phys. Rev. Lett. **73**, 2744 (1994); ibid. Phys. Rev. B **55**, 3954 (1997).

M.R. Norman and P.J. Hirschfeld, Phys. Rev. B **53**, 5706 (1996) .

M. R. Norman, private communication (1996).

C. O'Donovan and J. P. Carbotte, Phys. Rev. B **55**, 8520 (1997).

H. Kamerlingh Onnes, Leiden Comm. **120b, 122b, 124c** (1911).

T. T. M. Palstra *et al.*, Phys. Rev. Lett. **64**, 3090 (1990).

R. Pankaluoto *et al.*, Phys. Rev. B **50**, 6408 (1994).

S. D. Peacor, J. L. Cohn and C. Uher, Phys. Rev. B **43**, 8721 (1991).

C. H. Pennington and C. P. Slichter, in *Physical Properties of High Temperature Superconductors*, edited by Donald M. Ginsberg (World scientific, Singapore, 1990) vol. II, p. 269.

N. E. Phillips *et al.*, in *Progress in Low Temperature Physics*, edited by D. F. Brewer, (Elsevier Science, North Holland, 1992) vol. XIII, and references therein.

M. Prohammer and J. P. Carbotte, Phys. Rev. B **43**, 5370 (1991).

Song Pu, M.Sc. Thesis, McGill University (1997).

A. V. Puchkov, D. N. Basov and T. Timusk, J. Phys.: Condens. Matter **8**, 10049 (1996).

B. Revaz *et al.*, Czech. J. Phys. **46**, suppl., part S3, 1205 (1996).

J. Rossat-Mignod *et al.*, Physica C **153-155**, 1115 (1988).

D. Sanchez *et al.*, Physica B **204**, 167 (1995).

N. Sato *et al.*, J. Phys. Soc. Jpn. **61**, 32 (1992).

C. B. Satterthwaite, Phys. Rev. **125**, 873 (1962).

S. Schmitt-Rink, K. Miyake and C. M. Varma, Phys. Rev. Lett. **57**, 2575 (1986).

T. Senthil *et al.*, preprint (cond-mat/9808001).

Steven H. Simon and Patrick A. Lee, Phys. Rev. Lett. **78**, 1548 (1997).

J. E. Sonier *et al.*, preprint (cond-mat/9811420).

G. Sparn *et al.*, Physica C **162-164**, 508 (1989).

F. Steglich *et al.*, Phys. Rev. Lett. **43**, 1892 (1979).

H. Suderow *et al.*, J. Low Temp. Phys. **108**, 11 (1997).

H. Suderow *et al.*, preprint (1999).

Ye Sun and Kazumi Maki, Europhys. Lett. **32**, 355 (1995).

Ye Sun and Kazumi Maki, Phys. Rev. B **51**, 6059 (1995).

Louis Taillefer *et al.*, Physica B **169**, 257 (1991).

Louis Taillefer, Hyperfine Interactions **85**, 379 (1994).

Louis Taillefer *et al.*, Phys. Rev. Lett. **79**, 483 (1997).

M. Takigawa *et al.*, Phys. Rev. B **43**, 247 (1991).

T. Timusk, lecture notes on "Optical properties of superconductors" from the Canadian Institute for Advanced Research Superconductivity Summer School, Hamilton, 1995.

M. Tinkham, *Introduction to Superconductivity* (McGraw-Hill, New York, 1996).

C. C. Tsuei *et al.*, Phys. Rev. Lett. **73**, 593 (1994).

G. E. Volovik, JETP Lett. **58**, 469 (1993).

J. R. Waldram, *Superconductivity of metals and cuprates* (IoP Publishing, London 1996).

J. R. Waldram *et al.*, Phys. Rev. B **55**, 3222 (1997).

B. Wand *et al.*, J. Low Temp. Phys. **105**, 993 (1996).

W. W. Warren Jr. *et al.*, Phys. Rev. Lett. **62**, 1193 (1989).

Xiao-Gang Wen and Patrick A. Lee, Phys. Rev. Lett. **80**, 2193 (1998).

D. A. Wollman *et al.*, Phys. Rev. **71**, 2134 (1993).

D. A. Wright *et al.*, J. Low Temp. Phys. **105**, 897 (1996).

D. A. Wright *et al.*, Phys. Rev. Lett. **82**, 1550 (1999).

M. K. Wu *et al.*, Phys. Rev. Lett. **58**, 908 (1987).

W. C. Wu, D. Branch and J. P. Carbotte, preprint (1998).

W. C. Wu and J. P. Carbotte, preprint (1998).

D. Xu, S. K. Yip and J. A. Sauls, Phys. Rev. B **51**, 16233 (1995).

Kun Yang and S. L. Sondhi, Phys. Rev. B **57**, 8566 (1998).

Kuan Zhang *et al.*, Phys. Rev. Lett. **73**, 2484 (1994).

Shou-Chen Zhang, Science **275**, 1089 (1997).

Z. X. Zhao *et al.*, Kexue Tongbao **33**, 661 (1987).